Online ISSN: 2249-4596
Print ISSN: 0975-5861
DOI: 10.17406/GJRE

Global Journal of Researches in Engineering: J

General Engineering

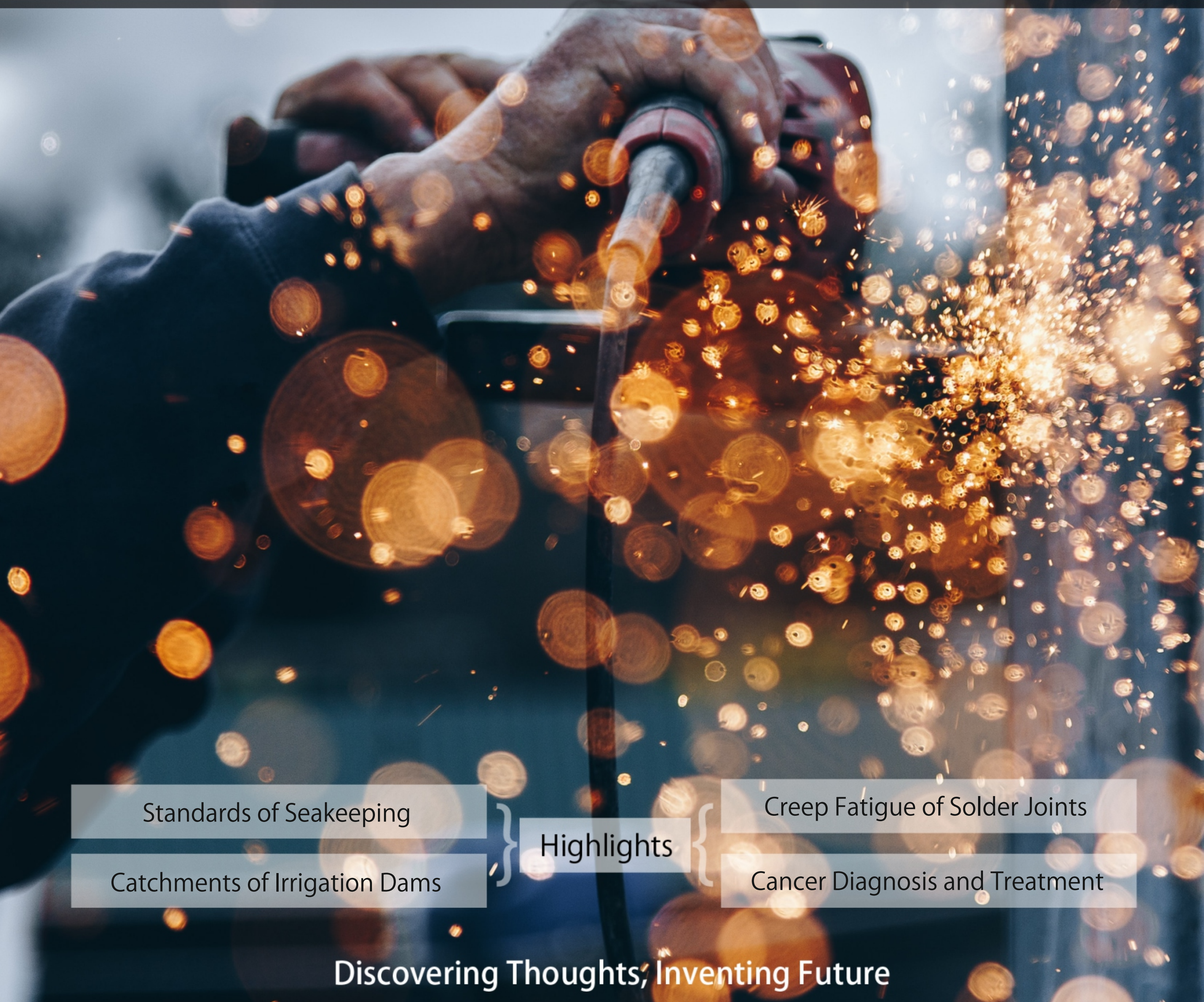

Standards of Seakeeping

Catchments of Irrigation Dams

Highlights

Creep Fatigue of Solder Joints

Cancer Diagnosis and Treatment

Discovering Thoughts, Inventing Future

VOLUME 23 ISSUE 4 VERSION 1.0

Global Journal of Researches in Engineering: J
General Engineering

Global Journal of Researches in Engineering: J
General Engineering

Volume 23 Issue 4 (Ver. 1.0)

Open Association of Research Society

Incorporation No.: 0423089
License No.: 42125/022010/1186
Registration No.: 430374
Import-Export Code: 1109007027
Employer Identification Number (EIN):
USA Tax ID: 98-0673427

Global Journals Inc.

*(A Delaware USA Incorporation with "Good Standing"; **Reg. Number: 0423089**)*

Sponsors: *Open Association of Research Society*
Open Scientific Standards

Publisher's Headquarters office

Global Journals® Headquarters
945th Concord Streets,
Framingham Massachusetts Pin: 01701,
United States of America
USA Toll Free: +001-888-839-7392
USA Toll Free Fax: +001-888-839-7392

Offset Typesetting

Global Journals Incorporated
2nd, Lansdowne, Lansdowne Rd., Croydon-Surrey,
Pin: CR9 2ER, United Kingdom

Packaging & Continental Dispatching

Global Journals Pvt Ltd
E-3130 Sudama Nagar, Near Gopur Square,
Indore, M.P., Pin:452009, India

Find a correspondence nodal officer near you

To find nodal officer of your country, please email us at *local@globaljournals.org*

eContacts

Press Inquiries: *press@globaljournals.org*
Investor Inquiries: *investors@globaljournals.org*
Technical Support: *technology@globaljournals.org*
Media & Releases: *media@globaljournals.org*

Pricing (Excluding Air Parcel Charges):

Yearly Subscription (Personal & Institutional)
250 USD (B/W) & 350 USD (Color)

Dr. Omid Gohardani

Ph.D. Senior Aerospace/Mechanical/ Aeronautical, Engineering professional M.Sc. Mechanical Engineering, M.Sc. Aeronautical Engineering B.Sc. Vehicle Engineering Orange County, California, US

Dr. Paolo Veronesi

Ph.D., Materials Engineering, Institute of Electronics, Italy President of the master Degree in Materials Engineering Dept. of Engineering, Italy

Contents of the Issue

i. Copyright Notice
ii. Editorial Board Members
iii. Chief Author and Dean
iv. Contents of the Issue

1. On Standards of Seakeeping. *1-5*
2. Creep Fatigue of Solder Joints in Electronic Assemblies. *7-20*
3. Landuse and Landcover Changes in Reservoir Catchments of Irrigation Dams in Northern Ghana. *21-34*
4. Evolution of the use of Nanoparticles in Cancer Diagnosis and Treatment. *35-42*
5. Effect of Interlayer Thickness on Mechanical Properties of Steel/Polymer/ Steel Laminates Fabricated by Roll Bonding Technique. *43-64*

v. Fellows
vi. Auxiliary Memberships
vii. Preferred Author Guidelines
viii. Index

Global Journal of Researches in Engineering: J
General Engineering
Volume 23 Issue 4 Version 1.0 Year 2023
Type: Double Blind Peer Reviewed International Research Journal
Publisher: Global Journals
Online ISSN: 2249-4596 & Print ISSN: 0975-5861

On Standards of Seakeeping

By Victor A. Dubrovsky

Abstract- One from the main characteristic of a sea-going ship is seaworthiness. It defines the safety of sailing, comfort of using and service at sea. The complete characteristic includes some partial ones, and some of them contradict to others. A lot of standards of seakeeping were proposed by various authors from the middle of the XX century, some propositions are shown by the table. It means the practical need for official standards of seakeeping. The proposed standards belong to higher habitability, restriction of external loads, ensuring a ship service.

The introduction of seakeeping standards to classification rules is proposed. For example, the shown dependencies of sailor workability can be used for restriction of the motion and acceleration amplitudes. The standards, which ensure strength of structures and equipments, can be various for ships of various purposes.

Formal standards of seakeeping can be used for based comparison of various ships of the same purpose by the previously proposed method of seakeeping estimation by one digit. It allows the simple definition of price of a time unit (a hour or a month, for example) of the ship service at sea.

Keywords: seakeeping, standards, classification, motions, slamming, wet deck.

GJRE-J Classification: UDC: 629.124

ONSTANDARDSOFSEAKEEPING

On Standards of Seakeeping

Victor A. Dubrovsky

Abstract- One from the main characteristic of a sea-going ship is seaworthiness. It defines the safety of sailing, comfort of using and service at sea. The complete characteristic includes some partial ones, and some of them contradict to others. A lot of standards of seakeeping were proposed by various authors from the middle of the XX century, some propositions are shown by the table. It means the practical need for official standards of seakeeping. The proposed standards belong to higher habitability, restriction of external loads, ensuring a ship service.

The introduction of seakeeping standards to classification rules is proposed. For example, the shown dependencies of sailor workability can be used for restriction of the motion and acceleration amplitudes. The standards, which ensure strength of structures and equipments, can be various for ships of various purposes.

Formal standards of seakeeping can be used for based comparison of various ships of the same purpose by the previously proposed method of seakeeping estimation by one digit. It allows the simple definition of price of a time unit (a hour or a month, for example) of the ship service at sea.

Keywords: seakeeping, standards, classification, motions, slamming, wet deck.

I. Introduction

One from the main characteristic of a sea-going ship is seaworthiness. It defines the safety of sailing, comfort of using and service at sea. The complete characteristic includes some partial ones, and some of them contradict to others. A lot of standards of seakeeping were proposed by various authors from the middle of the XX century, some propositions are shown by the table. The proposed standards belong to higher habitability, restriction of external loads, ensuring a ship service. The table contains some proposed standards.

Table 1: Some Proposed Standards of Seakeeping. [1]

№	Year, author, ship.	Wetness	Slamming	Acceleration	Pitch	Roll	Bare propeller
1	1972, Lipis, Kondrikov, «storm diagrams»	3 cases at 100 sec, Frame 20	1 case at 500 sec.	0.4g at Frame 20.			1 danger. case at 5 hours
2	1974, Aertssen, Container carrier	7 cases at 100 sec, Frame 20	3 cases at 100 sec, Fr. 17	0.4g Fr. 20			25 cases at 100 sec
3	1974, Ochi,			Possibility 0.4g at Fr. 20 – no more 7% for full load, no more. 3% - for ballast			
4	1975, Connoly, Frigate, destroyer.	1 case at 110 sec, Fr.20	1 case at 1360 sec, Fr. 16.	Less 1 at 673 sec, Fr. 16.			
5	1975, Tasaki, Takerava, Takaishi, cargo	Possib. Less 0.01	Possib. less 0.01	Possib. more 0.8g - 0.001 Ft. 20, Possib. more 0.6g – 0.01 at bridge		Possib. more 25 deg.- 0.001	Blade tip possib. – 0.1, 0.3 diam. – 0.1
6	1976, Moiseeva, fish-tech. base, Fishery ship					Ampl.3% -7 degr., Ampl.3% - 18degr.	
7	1979, Chilo, cargo	Possib. 7% at Fr. 20.	Possib.3% at 3 Fr.17	0.4g at Fr. 20			
8	1980, Comstock, Aircraft carrier::						
	• Crew			0.4g all, 0.2g- bridge			

Author: e-mail: multi-hulls@yandex.ru

	• Hull • Usual	30 cases at hour, Fr.20	20 cases at hour, Fr.17				
	• Hull • (Swath)	Bottom 5 cases at hour	Bow, 20 cases at hour				No more 25% of diameter
	• Elevator				Level displ. No more 7,65 m		
	• Flying Deck, SWATH	At bow, 5 cases at hour					
	• Usualaircraft				1 deg., vert. velocity 2 m/sec, stern	5 degrs.	
	• Vert.Fly-Off				3 degrs.	5 degrs.	
9	• 1982, • Landsburg, Tanker		6 cases at 100 sec, Fr.17	0.5g at Fr.20 0.4g – at bridge		30 degrs.	25 cases at 100 sec.
10	• 1983,Hosoda, Patrol Ship:						
	• Forhelic.			less 0.2g			
	• Radar					less 25 degrs	
	• Crew, Full Workab.			less 0.1g	3 degrs.	8 degrs.	
	• The Same, 50% Workability.			Vertical. 0.35g, horizont. 0.15g			
	• The Same, 10% • Workability.			Vert.0.5g, horiz. 0.2g	7.5 degrs.	20 degrs.	
11	1984, Gerritsme:						
	Level A	30 at hour	20 at hour	Vert. 0.4g, horiz. 0.2g, vert. speed 0. 2m/sec	3 degr.	5 degr.	
	Level **B**	30 at hour	20 at hour	0.4g & 0.2g	3 degr.	10 degr.	
	Level **C**	50 at hour	50 at hour	0.4g &0.4g	8 degr.	30 degr.	
12	1984, Petrie, Bongort	Free board at Fr.2012.8 m	Draft at Fr. 20 9.76 м, vert. speed 4.2 m/sec	Less, than 0.4g for upper raw of cont.		40 degr. For cargo	Axe deep 5.5м
13	1985, Creight, Stahl:						
	destroyer	30 at hour at Fr. 20	20 at hour at Fr.17.	0.4g at Fr. 14	3 degr.	5 degr.	
	• Frigate	same	same	At Fr. 15	same	same	
	• Swaship	30 at hour, Fr. 18	same	At Fr. 18	same	same	
14	1986, Kent, Battle ships	20 at hour, Fr.20	20 at hour				
15	1987, Karppinen, crew:						
	• Short Time			0.275g			
	• Light Profess. Work			0.2g			
	• - Hardwork			0.15g			
	• - Long Time Sailing			0.1g			

	• -Sea • Seakness, 10% Of Passengers			0.05g			
	• - Cruise Liners			0.02g			
16	1988, Kehoe	1 at minute	1 at min., Fr.17				
17	1988, Luis	10 at hour, Fr.20.	5 at hour			Subj, crit. 15.	Less 2 at hour
18	1988, Lloid	1 at 100 sec. Fr. 20		Shock accel. At island – less 0.05g			
19	1988, OTAN standards:						
	• USA			0.2g at bridge	5 deg.	8 deg.	
	• The • Netherlands			0.16g at Fr.16	The same	The same	
	• Germany			0.18g at Fr.20	The same	The same	
	• UK			0.14g at mass center	The same	The same	
	• Canada			0.2g at Fr.16	The same	The same	
20	1988, USSR, Fishery Ministry	Middle free boardmore 0.13 of overall beam; Bow free boardmore 0.3 of overall beam.		$K_1 = (\sigma^2 + x_\sigma{}^2 + \sigma 2)^{05}$ Y z $K_2 = (\sigma^2 + x\,\sigma^2)$, y	$K_3 = (\sigma pitch^2 + \sigma ro\, l^2)^{0.5}$ l σi – standard of i-th process		
	• At Not Noted Apartments			$K_1 = 0.08g$	K3 = 4.5		
	• At Bridge			$K_1 = 0.15g$, $K_2 = 0.2g$			
	• At Engine Room			$K_1 = 0.15g$, $K_2 = 0.2g$			
	• At Upper Deck			$K_2 = 0.12g$			
	• At Cook			$K_2 = 0.15g$			
	• At Passenger Apartments			$K_2 = 0.16g$			
	• At Process Apartment			$K_2 = 0.18$			
21	1992, Wilson	30 at hour	20 at hour	Vertical. 0.4g, Horiz. 0.2g for crew			

Let us note, the shown standards are proposed for displacement ships or for ships of the transient speed mode. And it must be noted, the horizontal accelerations decrease the labor productivity more strongly, than vertical acceleration. Then the restrictions of the firsts is twice bigger, than the seconds.

The table does not contain the standards of acceleration of planning boats, which are bigger, than shown, at about an order – and decreasing of the accelerations of planning boats can`t be decreased by any measurements.

It can be supposed, the shown values of standards correspond to 14-% repeatability, i.e. are so named “sufficient” values.

1. Establishment of seakeeping standards by classification societies.

It can be supposed, establishment of seakeeping standards can promote the seakeeping increasing, i.e. higher habitability and bigger safety of sea-going ships.

Today the contemporary level of science development (accessibility of the experimental method of seakeeping prediction and fast development of digital methods of prediction) allows introduction of such standards for most wide-spread types of ships, as a minimum.

It seems the standards must be divided by the aims of using for their wider applicability.

The standards, which are connected with labor productivity and rest conditions, and with ensuring of permissible conditions of structures and equipment exploitation, must be general ones for all types of ships.

Evidently, these standards will be applicable only for not combat ships, and for displacement or transient modes of speed regimes. Possible, such general standards will be established for ships, which are classified by corresponded societies, and by ship owners for the other ships.

2. Standards, which define the conditions of labor productivity.

These standards can be established, for example, on the base of special researching of Japan scientists,[1].

Figure 1 contains the dependence of various labor productivity from vertical accelerations of motion.

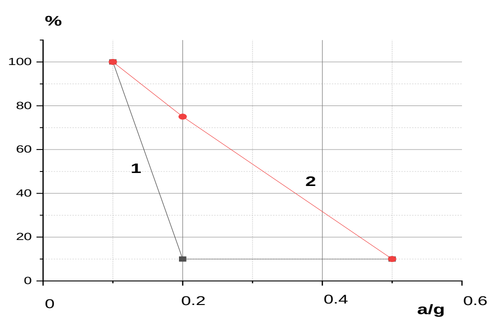

Fig. 1: Dependence of Labor Productivity from Motion Acceleration: 1 – Hard Manual Labor; 2 – Light Mental Labor

The comparison of Fig. 1 with previously presented standards (0.25g and 0.4g) shows the smaller value correspond to minimal productivity of hard manual labor, but affects on the mental labor not sufficiently.

Bigger value of acceleration leads to elimination of manual labop possibility, and to sufficient decreasing of mental labor, evidently – ship control too.

Figure 2 contains the dependence of labor productivity from pitch amplitudes.

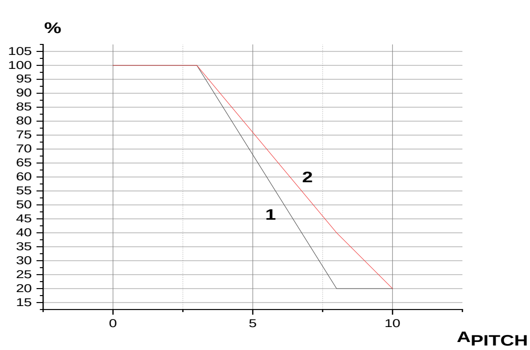

Fig. 2: Labor Productivity Versus Pitch Amplitudes: 1 – Hard Manual Labor; 2 – Light Mental Labor

The comparison the data of Fig. 2 with the proposed standards from the Table (3 and 5 degrees) shows the smaller restriction not changes the productivity of any labor. But the second restriction leads to labor productivity at about 30%.

Figure 3 contain the dependence of labor productivity from roll amplitudes.

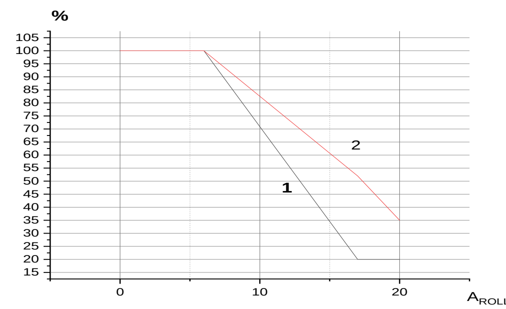

Fig. 3: Labor Productivity Versus Roll Amplitudes: 1 – Hard Manual Labor; 2 – Light Mental Labor

Evidently, the shown by the table restriction 5 degrees does not decrease the labor productivity, and even more strong the restriction (8 degrees) decreases the productivity not so notable.

It must be noted, most possible, the standards can`t be introduced for ships of any displacement: usually small enough ships of the traditional type, mono-hulls, can`t ensure the same level of seakeeping, as big enough ships.

3. Standards, which are connected with conditions of structures and equipment exploitation.

Such standards, firstly, include number (or frequency) of slamming of any structures. The characteristic ultimately defines the shock loads from slamming: bigger frequency of slamming usually means higher shock loads. Of course, straight measurement of shock loads gives most exact picture of such loads. But, unfortunately, the maximal load placement can`t be defined previously… Than limitation of shock number seems more simple and convenient method. For example, it can be no more, than 20 shocks per a hour, referring to practical experience.

If more danger of wet deck, than of slamming, will be taken into account, possible, number of wet deck cases must be no bigger, than 20 cases at a hour too.

It seems, the permissible frequency of propeller baring, must be connected with characteristics of the equipment, which restricts the frequency.

II. Conclusions, Recommendations

1. Permanently repeated propositions of seakeeping standards mean the practical need of official introduction them to classification rules of registers.

2. Introduction of seakeeping standards will stimulate wider examination of seakeeping characteristics by experiments and calculations and introduction of motion mitigation methods and ship types with higher seakeeping.
3. The method of seakeeping estimation by one digit [2] is recommended for wide using after introduction of corresponded standards. Some other restriction of seakeeping characteristics, which correspond to a ship purpose, can be used together with official standards.

References Références Referencias

1. Dubrovsky, V., "Specificity & designing of multi-hull ships & boats", *2016, Nova Science Publishers, ISBN 9781634846158, USA, 210 p.*
2. Dubrovsky, V., "Complex Comparison of Seakeeping: Method and Example" 2000, *Marine Technology and SNAME News, vol. 37, # 4, October, pp.223 – 229.*

This page is intentionally left blank

Global Journal of Researches in Engineering: J
General Engineering
Volume 23 Issue 4 Version 1.0 Year 2023
Type: Double Blind Peer Reviewed International Research Journal
Publisher: Global Journals
Online ISSN: 2249-4596 & Print ISSN: 0975-5861

Creep Fatigue of Solder Joints in Electronic Assemblies

By E. H. Wong

Abstract- Electronic assembly is formed by mechanically joining, and hence electrically interconnecting, integrated circuit components onto printed circuit board using arrays of solder joints. Differential thermal expansion between the integrated circuit component and the printed circuit board leads to failure of solder joints through the combined mechanisms of creep and fatigue. This manuscript condenses the recent advances in creep fatigue analysis of solder joints in electronic assemblies into two major analyses: thermomechanical analysis and creep fatigue life modelling. The analytical thermomechanical analysis models an electronic assembly as a sandwich structure. By modelling the actual geometry of solder joints, it has found stout hourglass to be the ideal shape for solder joints that could reduce the magnitude of stress by 80% compared to the standard barrel-shape solder joints. The new creep integrated fatigue equation integrates the fundamental equation of creep into fatigue life equation and has been shown to model very well the creep fatigue of solder alloy.

Keywords: thermomechanical analysis, environmental fatigue, optimum shape, life prediction, shear compliance.

GJRE-J Classification: LCC: TK7871

CREEPFATIGUEOFSOLDERJOINTSINELECTRONICASSEMBLIES

Strictly as per the compliance and regulations of:

Creep Fatigue of Solder Joints in Electronic Assemblies

E. H. Wong

Abstract- Electronic assembly is formed by mechanically joining, and hence electrically interconnecting, integrated circuit components onto printed circuit board using arrays of solder joints. Differential thermal expansion between the integrated circuit component and the printed circuit board leads to failure of solder joints through the combined mechanisms of creep and fatigue. This manuscript condenses the recent advances in creep fatigue analysis of solder joints in electronic assemblies into two major analyses: thermomechanical analysis and creep fatigue life modelling. The analytical thermomechanical analysis models an electronic assembly as a sandwich structure. By modelling the actual geometry of solder joints, it has found stout hourglass to be the ideal shape for solder joints that could reduce the magnitude of stress by 80% compared to the standard barrel-shape solder joints. The new creep integrated fatigue equation integrates the fundamental equation of creep into fatigue life equation and has been shown to model very well the creep fatigue of solder alloy. More valuably, this methodology can be generalised to integrate general aggravating forces into fatigue life equation. It can be further generalised to integrate multiple aggravating forces into fatigue equation.

Keywords: thermomechanical analysis, environmental fatigue, optimum shape, life prediction, shear compliance.

I. Introduction

The mother board assembly constitutes morphologically the brain of an engineering device. The integrated circuits that are photolithographically etched onto silicon chips constitutes morphologically the brain cells. However, the brain cells on individual silicon chip are isolated from other chips; and they need to be electrically interconnected. The brain cells are very delicate and even the interconnects are mechanically fragile; and they need to be mechanically protected. Lastly, the brain cells generate high intensity of heat when running, and the heat needs to be dissipated before the brain cells would be burned. The jobs of electrical interconnection, mechanical protection, and thermal dissipation rest on the design and engineering of electronic and microelectronic assemblies [1].

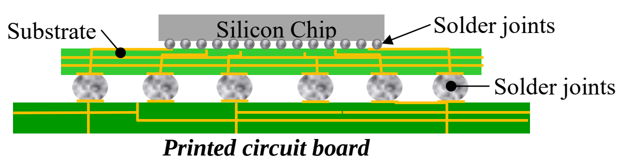

Figure 1: Schematic of the Cross-Section of an IC Component and a PCB

Figure 1 shows the schematic of a silicon chip that is electrically interconnected to a substrate, which is in turn interconnected to a printed circuit board, through arrays of solder joints. The former assembly is frequently referred to as an integrated circuit component/assembly while the latter is frequently referred to as a printed circuit board assembly. We shall refer to both assemblies as simply electronic assemblies. The solder joints are formed by melting solder balls/paste to form metallurgical bonds with the metal pads on the chip and the substrate, and with the metal pads on the substrate and the printed circuit board.

Electronic assemblies are susceptible to undue stress during manufacturing and while in service resulting in functional failure. In general, electronic assemblies may experience three main physics of damage: the violent vaporisation of the ingress moisture in the integrated circuit assembly during the solder joint forming process leading to cracking and/or delamination of the assembly [2][3]; fracturing of interconnection caused by drop-shock of mobile electronic products [2][4]; and lastly, creep-fatigue damage of interconnecting solder joints after repeated cycles of powering on/off of engineering devices [2][5]. The last is especially critical and has attracted maximum interest in

Author: e-mail: eehuawong@gmail.com

Global Journal of Researches in Engineering (J) Volume XXIII Issue IV Version I Year 2023

electronic assemblies. In essence, the differential thermal expansions between the silicon chip and the substrate and between the integrated circuit assembly and the printed circuit board give rise to cyclical deformation of the solder joints at temperature above their homologous temperature, driving them towards failure by the mechanism of creep fatigue. The propensity for creep fatigue failure of solder joints is aggravated by the trend towards increasing functionality of consumer electronic products, which is driving increase size of integrated circuit assembly and reduce size of solder joints.

The failure of a nuclear plant or a commercial aircraft is accompanied by unacceptable catastrophic consequences. The structural integrity and reliability of such products are therefore the paramount design considerations. In contrast, the two paramount design considerations for electronic assemblies are electrical performance and space. The former to support the ever-increasing performance of electronic products and the latter to support the increasing functionality of electronic products. Failure of consumer electronic products in service though annoyable is acceptable to most users. This has encouraged a relatively relax attitude towards the structural integrity of electronic assemblies; and this is further encouraged by the relatively short life cycle of consumer electronic products. Nevertheless, there is a positive aspect of this more relax attitude towards structural analysis. The structural design of electronic assemblies is not bounded by a design protocol or a design code. Electronic assembly engineers are free to use any analysis method so long as the designed electronic assemblies will meet the integrity and reliability test requirements. It is inherently easy to monitor the structural integrity of an electronic assembly through monitoring the electrical connectivity of the assembly [6]. If necessary, the growth of damage in an electronic assembly can be tracked in real time through monitoring the changing electrical impedance of the assembly [6][7]. The absence of a strict design protocol and the ease of validating an analysis with tests has encouraged the exploration and adoption of new analysis methods, notwithstanding some of these methods may not be robust.

This manuscript gives a condensed presentation of the recent advances in the creep fatigue analysis of solder joints in electronic assemblies. This comprises two major analyses: thermomechanical analysis of solder joints in electronic assemblies; and creep fatigue life modelling of solder joints. It is believed that these advanced analyse techniques are fundamentally robust and they can be adopted to similar applications in other engineering field.

II. Thermomechanical Analysis of Solder Joints

Electronic assembly engineers routinely performed thermomechanical analysis of electronic assemblies using finite element analysis software in which the solder joints are modelled using solid finite elements. This has inadvertently led to singularity of stress/strain at discontinuities of geometry and materials giving rise to inconsistent analysis - because the magnitude of the stress/strain is dependent on the size and shape of the finite element at the site of singularity. To circumvent such singularity, electronic assembly engineers have adopted the practice of volume-averaging the stress/strain over a selected volume of solder joints [8][9]. Unfortunately, such arbitrary volume averaging act is equivalent to smearing the geometry of solder joints, effectively denying the engineers the ability to analyse the geometrical effects of solder joints on the magnitude of stress/strain. The issue of stress/strain singularity can be addressed by modeling the components of electronic assemblies as shells and beams. Maximum insights into the mechanics of the subject matter can be achieved through analytical modeling.

Analytical models of varied sophistication have been reported in the electronic assembling community [10][11][12][13]. In essence, an electronic assembly is treated as a sandwich structure constituting of array of solder joints sandwiched between two outer members. The simplest model treats the outer members as being infinitely rigid and the solder joints as being infinitely compliant such that the solder joints experience only shear strain whose magnitude increases linearly with distance from the neutral plane of an electronic assembly and is given by $\gamma = \Delta\alpha T.x/h$ (*Figure 2a*) [10], where $\Delta\alpha T$ is the differential thermal strain between the two outer members, x is the distance of a discrete joint from the neutral plane of the assembly, and h is the height of the discrete joint. This unrealistic model would grossly overestimate the magnitude of shear strain. The more sophisticated models treat the outer members as rectangular beams; and the solder joints as linear springs [11], or as cylindrical beams that are capable of shearing, flexing, and stretching [12][13]. The inclusion of elasticity of the outer members in the model have led to the vital understanding that shear strain in the solder joints does not increase linearly but exponentially with distance from the neutral plane of an electronic assembly. It takes the form $\gamma = \gamma_o e^{\beta(x-l)}$ (*Figure 2b*), where γ_o is approximately the shear strain at the outmost solder joint, β is a compliance parameter of the assembly, l is the half-length of the assembly.

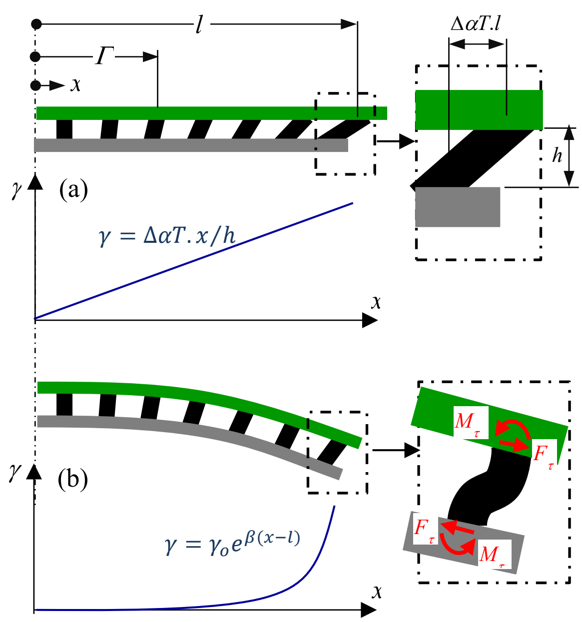

Figure 2: Analytical Models with Closed-Form Solution: (a) Infinitely Rigid Outer Members; (b) Outer Members as and Solder Joints as Elastic Beams

a) *Analytical Modelling*

Evaluating the stresses in the discrete joints of an assembly involves four steps of analysis, starting with smearing the discrete joints into a continuously bonded joint and then evaluating the compliances of the smeared assembly. This is followed by evaluating the smeared stresses in the smeared joints. The third step integrates the stresses into boundary forces and moments acting on individual discrete joint. The last step evaluates the stresses in the discrete joint due to the boundary forces and moments.

The discrete joints are assumed to be of identical shape and size and are distributed at uniform spacing. *Figure 3* shows the schematic of discrete joints with a height h_d and spacing at pitches p_x and p_y along the x and the y coordinates, respectively. In the case that individual discrete joint is not of cylindrical shape but one with non-uniform sections along its height, it is represented by a pseudo cylindrical joints with a representative shear area, $A_{d,rep}$, and a representative second moment of area, $I_{d,rep}$, that would return identical shear and flexural stiffnesses as the original discrete joints [14]. Theses representative parameters are given by

Global Journal of Researches in Engineering (J) Volume XXIII Issue IV Version I Year 2023

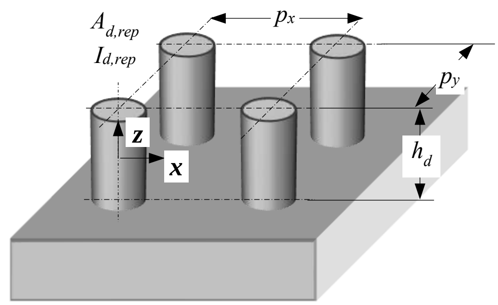

Figure 3: Schematic of Solder Joints

$$A_{d,rep} = \frac{1}{\int_{-h_d/2}^{h_d/2} \frac{dz}{A_Z(z)}}$$
$$I_{d,rep} = \frac{1}{12 \int_{-h_d/2}^{h_d/2} \int_{-h_d/2}^{z} \frac{\xi d\xi}{I_Z(\xi)} dz} \tag{1}$$

Referring to the outer members as member #1 and member #2, and the discrete joint as member #*d*, the height, the stretch modulus, the shear modulus, and the flexural stiffness of member #*i* are denoted as h_i, E_i, G_i, and D_i, respectively; the shear and the in-plane stretch compliances of the assembly are denoted as κ_s and λ_x respectively. For ease of reference, we shall refer to the moduli of the smeared joints as smeared moduli and the compliances as smeared compliances. Those characteristics that are associated with the smeared joints will be marked with an asterisk.

b) Compliances of a Smeared Assembly

The in-plane stretch compliance of the assembly is a function of the outer members and, for the case of plane stress, is given by [12][13]

$$\lambda_x = \sum_{i=1}^{2} \left(\frac{1}{E_i h_i} + \frac{{h_i}^2}{4D_i} \right), \tag{2}$$

where in $D_i = E_i h_i^3/12$ for plane stress. The smeared shear compliance of the assembly, κ_s^*, is given by [12][13]

$$\kappa_s^* = \sum_{i=1}^{2} \kappa_{si} + \kappa_{sd}^* + \kappa_{sd\varphi}, \tag{3}$$

where
$$\kappa_{si} = \frac{h_i}{8G_i},\ \kappa_{sd}^* = \frac{h_d}{G_d^*},\ \kappa_{sd\varphi} = \frac{{h_d}^3}{12D_d^*}. \tag{4}$$

wherein κ_{si} is associated with the shear compliance of member #*i*; κ_{sd}^* is associated with the shear deformation of the smeared joints; while $\kappa_{sd\varphi}$ is associated with the flexural deformation of the discrete joints – referring to *Figure 2b*. The smeared shear modulus, G_d^*, and the smeared flexural rigidity, D_d^*, are given by $G_d^* = G_d A_{d,rep}/(p_x p_y)$ and $D_d^* = E_d I_{d,rep}/(p_x p_y)$.

c) Stresses in Smeared Joints

The shear stress in the smeared joints along the bonded length of a balanced assembly is given by [12][13][15][16]

$$\tau^*(x) = A_c^* e^{\beta^*(x-l)},\ x>0, \tag{5}$$

where
$$A_c^* = \frac{\varepsilon_T}{\sqrt{\lambda_x \kappa_s^*}}, \tag{6}$$

$\beta^* = \sqrt{\lambda_x/\kappa_s^*}$; ε_T=$\Delta\alpha T$ is the differential thermal strain between the outer members.

d) Sectional Force and Moment in a Discrete Joint

The magnitude of the sectional shear force on a discrete joint that is at a distance Γ from the mid plane of the assembly may be evaluated approximately as

$$F_\tau(\Gamma) \approx \tau^*(\Gamma)p_x p_y, \tag{7}$$

The sectional shear force does not vary along the height of the discrete joint. On the other hand, and referring to *Figure 4*, rotational equilibrium dictates that the sectional moment varies linearly along the height of the discrete joint and is given by

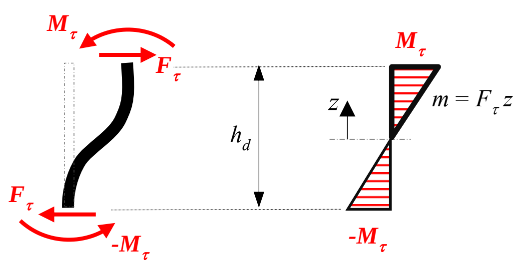

Figure 4: Bending Moment Distribution Along a Discrete Joint

$$m(\Gamma, z) = F_\tau(\Gamma)z, \tag{8}$$

where z is the local coordinate of a solder joint as shown in *Figure 3*.

e) Shearing and Bending Stresses in a Discrete Joint

The distribution of shear stress and bending stress along the height of a discrete joint, assuming it being an Euler beam, are simply [12][13]:

$$\begin{aligned} \tau_d(\Gamma, z) &= \frac{F_\tau(\Gamma)}{A_d(z)} \\ \sigma_b(\Gamma, z) &= m_\tau(\Gamma, z)\frac{r_d(z)}{I_d(z)} \end{aligned} \tag{9}$$

where $A_d(z)$, $I_d(z)$, and $r_d(z)$ are the local cross-sectional area, the local second moment of area, and the local outer fibre of the discrete joint. Assuming circular cross-section, as in the case of solder joints, the ratio r_d/I_d is reduced to $4/(\pi r_d^3)$. The largest magnitudes of shear force and bending moment, and hence shearing and the bending stresses, occur at the discrete joint furthest from the mid-plane of the assembly. Assuming $\Gamma_{\max}=l$, these stresses are given by

$$\begin{aligned} \tau_{d,max} &= \frac{F_{\tau,max}}{A_{d,min}} \\ \sigma_b(l, z) &= \frac{4F_{\tau,max}z}{\pi r_d^3(z)}, \end{aligned} \tag{10}$$

where $$F_{\tau,max} = \frac{\varepsilon_T p_x p_y}{\sqrt{\lambda_x \kappa_s^*}}, \tag{11}$$

and $A_{d,min}$ is the minimum cross-sectional area of the discrete joint.

f) Optimum Shape of Solder Joints

The solder joints are formed through controlled heating of solder into liquid form followed by controlled cooling the assembly to room temperature, forming metallurgical bonds with metal pads at its two ends. A solder joint will take up the natural shape of a spherical barrel, as shown in *Figure 5a*, that has the minimum surface energy. It is clear from Eq. (10) that a standard solder joint will experience the maximum magnitude of shear stress, $\tau_{d,max}$, and the maximum magnitude of bending stress, $\tau_{b,max}$, at its ends joining the outer members; and

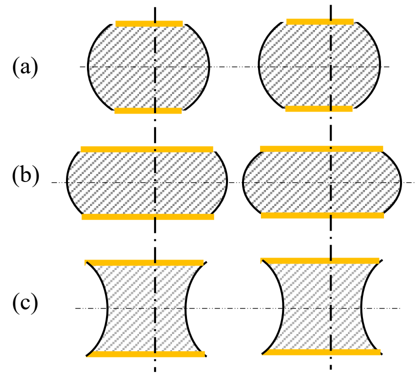

Figure 5: Geometries of Solder Joints (a) Barrel Shape, (b) Flatten Barrel Shape, (c) Stout Hourglass

$$\frac{\sigma_{b,max}}{\tau_{d,max}} = \frac{2h_d}{r_{d,end}} \tag{12}$$

where $r_{d,end}$ is the radius of the solder joint joining the outer member. In a standard barrel-shape solder joint, the magnitude of h_d is much larger than that of $r_{d,end}$. In other words, $\sigma_{b,max}$ is a far dominant stress in a standard barrel-shape solder joint. On paper, the magnitude of the dominant stress, $\sigma_{b,max}$, can be lowered by increasing the end radius of barrel-shape solder joints, which for the same volume of solder joint, will result in flatten barrel-shape solder joints leading to very significant reduction in the magnitude of $\sigma_{b,max}$. In practice, such a manipulation would inevitably raise the risk of bridging between adjacent solder joints, as is illustrated in *Figure 5b*.

It is clear from the linear distribution of bending moment in solder joints, as depicted in *Figure 4*, that solder joints should ideally have the shape of an hourglass. Solder joints of progressive hourglass shape can be designed into electronic assembly [14]. Modeling the curvature of an hourglass-shape solder joint as a hyperbolic sine curve and evaluating its representative shear area, $A_{d,rep}$, and representative second moment of area, $I_{d,rep}$, using Eq. (1), a stout hourglass-shape solder joint – similar to that illustrated in *Figure 5c* – has been found to return the minimum magnitude of stress for the same volume of solder as a standard barrel-shape solder joint. The maximum magnitude of bending stress, $\sigma_{b,max}$, in the stout hourglass solder joints is less than 15% that in a standard barrel-shape solder joints [14]. It is also worth noting that the use of stout hourglass solder joints does not increase the risk of bridging between solder joints.

III. Creep Fatigue Modeling

The fatigue life of a metal experiencing pure low cycle fatigue – that is, in the absence of aggravating element – and under a constant amplitude of cyclic stressing has been found to be satisfactorily modelled using the Coffin-Manson equation:

$$\varepsilon_p = C_o N_f^{-\beta_o}, \tag{13}$$

where ε_p is the amplitude of the incremental plastic strain in a cycle; N_f is the number of cycles to failure; C_o and β_o are material dependent fitting constants. While it is tempting to extend the equation to creep fatigue modelling by replacing the plastic strain amplitude, ε_p, with inelastic strain amplitude, $\varepsilon_{in} = \varepsilon_p + \varepsilon_c$, wherein ε_c is the incremental creep strain in a single cycle, this simplicity approach of lumping creep strain with fatigue strain contradicts with the different macrostructural damages of creep and fatigue in metals [17][18] and has been convincingly disproved by abundant experimental data [19].

a) A Brief Review of Practising Creep Fatigue Life Prediction Models

The power generation community and the aerospace engineering community have vast knowledge and experience in modelling creep fatigue life of metals. Both the power generation and the aerospace communities have subscribed to the idea that creep fatigue damage can be evaluated by summing independently the damages due to creep, due to fatigue, and due to interaction of these two damages. The summative creep fatigue damage in a single creep fatigue cycle may be expressed mathematically as

$$d = d_f + d_c + d_{cf}. \tag{14}$$

Interestingly, the two communities have subscribed to different idea of defining the respective damages, d_f, d_c, and d_{cf}.

The aerospace community characterises the three cyclic damage indices from the hysteresis loop of a tension-compression creep fatigue experiment. Three components of inelastic strain: ε_{pp}, ε_{cc}, ε_{cp} (or ε_{pc}) are partitioned and extracted from the hysteresis loop, wherein the first letter of the subscript (c for creep and p for plastic strain) refers to the type of strain imposed in the tensile portion of the cycle, and the second letter refers to the type of strain imposed during the compressive portion of the cycle. Individual strain component is assumed to follow a power-law relation with the number of hysteresis cycles to failure. That is,

$$\varepsilon_{jk} = C_{jk} N_{jk}^{-\beta_{jk}}. \tag{15}$$

The damage per creep-fatigue cycle due to individual component is then simply

$$d_{jk} = \frac{1}{N_{jk}} = \left(\frac{\varepsilon_{jk}}{C_{jk}}\right)^{1/\beta_{jk}}. \tag{16}$$

This is known as the strain range partitioning model [19]. While this noble model has served the aerospace community well, its characterisation is inherently challenging.

The power generation community conveniently treats the cyclic fatigue damage, d_f, as that due to pure fatigue, which can be evaluated using the Coffin-Manson equation; that is,

$$d_f = \frac{1}{N_f} = \left(\frac{\varepsilon_p}{C_o}\right)^{1/\beta_o}; \tag{17}$$

and the cyclic creep damage, d_c, as that due to pure creep, which may be evaluated using the creep strain exhaustion rule:

$$d_c = \frac{1}{\varepsilon_R}\int_0^{t_c} \dot{\varepsilon}_c(t)dt, \tag{18}$$

wherein $\dot{\varepsilon}_c(t)$ is the instantaneous creep strain rate and t_c the cyclic period. However, the cyclic creep-fatigue interaction damage, d_{cf}, is a fitting index, which can only be established through extensive experimental characterisation [20][21][22].

The electronic packaging professionals have fallen for the creep fatigue equation of Darveaux [9],

$$N_{cf} = K_1 {w_{in}}^{K_2} \tag{19}$$

where $w_{in}=w_p+w_c$ is the sum of the cumulative plastic work density and the cumulative creep work density in a single creep fatigue cycle. Just like the failed idea of substituting plastic strain with inelastic strain in Eq. (13), the act of lumping the two work densities is clearly against the macrostructural evidence of the two damages. Consequently, and unsurprisingly, the fitting constants, K_1 and K_2, are found to be dependent on the size and shape of individual electronic assembly [9], in other words, on the magnitude of the inelastic work density, w_{in}. Nevertheless, the electronic packaging community have stubbornly stuck with the model.

b) *Creep Integrated Fatigue Equation*

In the case of fatigue being the dominant mechanism in creep fatigue failure, the role of creep may be treated as one to lower the material capacity in fatigue. This has led to the idea of creep integrated fatigue equation [23][24][25]:

$$\varepsilon_p = C_o c(\varepsilon_p, T, t_c) {N_{cf}}^{-\beta_o}; \tag{20}$$

where $c(\varepsilon_p,T,t_c)$ is a function. Expressing the fatigue capacity in Eq. (13) for the case of pure fatigue as $\varepsilon_{p,ref}$ and it becomes clear that $c(\varepsilon_p, T, t_c) = \varepsilon_p/\varepsilon_{p,ref}$ describes the fractional fatigue capacity of a subject in the presence of creep. Its magnitude ranges from zero to unity - a zero magnitude corresponds to the case of pure creep while a magnitude of unity corresponds to the case of pure fatigue. The function 1- $c(\varepsilon_p,T,t_c)$ describes the fractional creep damage acting on the subject.

i. *The Fundamental Equations of Pure Creep In Metals*

The strain rate in a uniaxial steady-stress creep rupture experiment may be described in the form of Sherby-Dorn equation, $\dot{\varepsilon}_{SD}$, or Larson-Miller equation, $\dot{\varepsilon}_{LM}$, or Manson-Haferd equation, $\dot{\varepsilon}_{MH}$:

$$\begin{aligned} \dot{\varepsilon}_{SD} &= f(\sigma_s)e^{-H/kT}, T\geq 0 \\ \dot{\varepsilon}_{LM} &= Be^{-H(\sigma_s)/kT}, T\geq 0 \\ \dot{\varepsilon}_{MH} &= De^{(T-T_{ref})r(\sigma_s)}, T\geq T_{ref} \end{aligned} \quad , \tag{21}$$

wherein $f(\sigma_s)$, $H(\sigma_s)$, and $r(\sigma_s)$ are functions of the applied tensile stress, σ_s; k is the Boltzmann's constant; H, B, and D are material dependent constants; and T_{ref} is the temperature below which the mechanism of creep is assumed to be dormant. Assuming the dominance of the secondary stage of creep, the eventual creep rupture strain, ε_R, is given by

$$\varepsilon_R = \dot{\varepsilon}_{II} t_R \, , \tag{22}$$

where t_R is the time to creep rupture. Assuming ε_R to be independent of the applied stress and temperature, Eq. (21) may be rearranged into:

$$\begin{aligned} P_{SD}(\sigma_s) &= \frac{\varepsilon_R}{f(\sigma_s)} = \frac{t_R}{e^{H/kT}} \\ P_{LM}(\sigma_s) &= \frac{H(\sigma_s)}{k} = \frac{\ln t_R + \ln B_R}{1/T} \\ P_{MH}(\sigma_s) &= -\frac{1}{r(\sigma_s)} = \frac{T-T_{ref}}{\ln(t_R/t_\infty)} \end{aligned} \, , \tag{23}$$

wherein $B_R=B/\varepsilon_R$ and $t_\infty=\varepsilon_R/D$. These functions are known respectively as the Sherby-Dorn parameter, the Larson-Miller parameter, and the Manson-Haferd parameter. These parameters describe the relations between the applied stress, σ_s, and the gradient of the respective time-temperature function. These relations can be readily characterized and are used extensively in the creep rupture design of metal structures.

The corresponding stress parameter for a single stressing cycle may be expressed as [25]:

$$\begin{aligned} P_{c\_SD}(\sigma) &= t_c e^{-H/kT} \\ P_{c\_LM}(\sigma) &= T(\ln t_c + \ln B_c), \\ P_{c\_MH}(\sigma) &= \frac{T-T_{ref}}{\ln(t_c/t_{c\infty})} \end{aligned} \tag{24}$$

where σ is the amplitude of the cyclic stress; and $B_c=B/\varepsilon_c$, $t_{c\infty}=\varepsilon_c/D$, and ε_c is the cumulative creep strain in a single cycle. Assuming (i) identical creep damage due to tensile and compressive stresses, and (ii) linear cumulation of creep strain over varied magnitudes of stress, then the cumulative creep strain in a single cycle may be expressed as $\varepsilon_c = \int_0^{t_c} k(|\sigma(t)|, T)dt$, where the function $k(|\sigma(t)|, T)$ represents one of the rate equations of the *SD*, *LM* and *MH*; and $|\sigma(t)|$ is the instantaneous magnitude of the cyclic stress. The cyclic stress parameter function may then be evaluated mathematically from the steady-stress parameter function as [25]

$$\begin{aligned} P_{c\_SD}(\sigma) &= \frac{\phi_\varepsilon t_c}{\int_0^{t_c} \frac{dt}{P_{SD}(|\sigma(t)|)}} \\ P_{c\_LM}(\sigma) &= \frac{\int_0^{t_c} P_{LM}(|\sigma(t)|)dt}{t_c}, \\ P_{c\_MH}(\sigma) &= \frac{t_c}{\int_0^{t_c} \frac{dt}{P_{MH}(|\sigma(t)|)}} \end{aligned} \tag{25}$$

where $\phi_\varepsilon=\varepsilon_c/\varepsilon_R$.

ii. *Fractional Fatigue Capacity Function*

Let the fractional fatigue capacity function $c(\varepsilon_p,T,t_c)$ takes the form:

$$c(\varepsilon_p, T, t_c) = 1 - \chi(\varepsilon_p)\eta(T, t_c). \tag{26}$$

Herein $\chi(\varepsilon_p)\eta(T,t_c)$= is the fractional creep damage function. It is intuitive that the function $\eta(T,t_c)$ shall take the form of the rate equation of creep; that is,

$$\begin{aligned} \eta_{SD}(T, t_c) &= t_c e^{-H/kT} \\ \eta_{LM}(T, t_c) &= T(\ln t_c + \ln B_c). \\ \eta_{MH}(T, t_c) &= \frac{T-T_{ref}}{\ln(t_c/t_{c\infty})} \end{aligned} \tag{27}$$

It is worth noting that $\eta(T,t_c)$ vanishes at $T\leq 0$ for η_{SD} and η_{LM} and at $T\leq T_{ref}$ for η_{MH} when the mechanism of creep becomes dormant; the condition of pure fatigue prevails and the fractional fatigue capacity function $c(\varepsilon_p,T,t_c)$ acquires the maximum magnitude of unity. Similarly, the condition of pure creep requires that the magnitude of fractional fatigue capacity function vanishes to nil. This implies, from Eq. (24), that

$$X_k(\varepsilon_p) = \frac{1}{P_{c\_k}(\sigma)}, \tag{28}$$

wherein the subscript k signifies *SD*, *LM*, and *MH*, respectively. The cyclic parameter function, $P_{c\_k}(\sigma)$, can be evaluated from the steady-stress parameter function, $P_k(\sigma_s)$, using Eq. (25). Using the Ramberg–Osgood relation, $\sigma =$

$\bar{K}\varepsilon_p{}^{\bar{n}}$, where $\bar{K}$ and $\bar{n}$ are assumed to be the representative material constants over the range of temperature of interest, the cyclic parameters may then be expressed as a function of plastic strain; that is,

$$P_{c\_k}(\sigma) \rightarrow P_{c\_k}(\varepsilon_p). \tag{29}$$

The material dependent fitting constants, C_o, β_o, $\bar{K}$, $\bar{n}$, and ϕ_ε (the constant H may be evaluated from the steady-stress creep rupture test data) or B_c or $t_{c\infty}$, may be established through regressing the experimental creep fatigue data with Eq.(20). It is worth mentioning that the constants $\bar{K}$, $\bar{n}$, and ϕ_ε or B_c or $t_{c\infty}$ represent the damages due to pure creep and also creep fatigue interaction.

In practice, one can do away with the experimental characterisation of the steady-stress parameter function, $P_k(\sigma_s)$, and the subsequent mathematical evaluation of the cyclic parameter function, $P_{c\_k}(\sigma)$. By expressing the steady stress parameter function as a power law in the form $P_k(\sigma_s) = p\sigma_s{}^q$, where p and q are fitting constants, it can be shown that the cyclic stress parameter function will be reduced to a power law function, $P_{c\_k}(\sigma) = \hat{p}\sigma^{\hat{q}}$, where $\hat{p}$ and $\hat{q}$ are constants, for the sinusoidal and the triangular stress-time profile. This could then be transformed to $P_{c\_k}(\varepsilon_p)$ using the Ramberg–Osgood relation. In other words, the function $\chi(\varepsilon_p)$ may simply be assumed to be a power-law function,

$$\chi(\varepsilon_p) = a\varepsilon_p{}^b, \tag{30}$$

where a and b are arbitrary constants. These two arbitrary constants can be established together with three material dependent fitting constants C_o, β_o, and H or B_c or $t_{c\infty}$, through regressing the experimental creep fatigue data with Eq. (20). This shall be illustrated in the following section.

iii. *Illustration and Validation*

The experimental creep fatigue data of Sn37Pb under cyclic triangular stress-time stressing generated by Shi et al. [26] has been analysed and the fitting constants, C_b and β_b, for nine sets of (ε_p, N_{cf}) data have been extracted and these are tabulated in ***Table 1*** [23]. Using these fitting constants, the (ε_p, N_{cf}) data were regenerated and these are depicted in *Figure 6*.

Table 1: Sn37Pb: Extracted Creep Fatigue Fitting Constants [23]

Creep-fatigue coefficients	Temperature (K) at t_c = 1 sec				
	233K	298K	348K	398K	423K
C_b	2.76	2.22	1.70	1.43	0.97
β_b	0.775	0.755	0.745	0.75	0.715
Creep-fatigue coefficients	Cycle time, t_c (s) at T=298 K				
	10^0 s	10^1 s	10^2 s	10^3 s	10^4 s
C_b	2.22	1.92	1.67	1.23	0.60
β_b	0.755	0.735	0.715	0.715	0.670

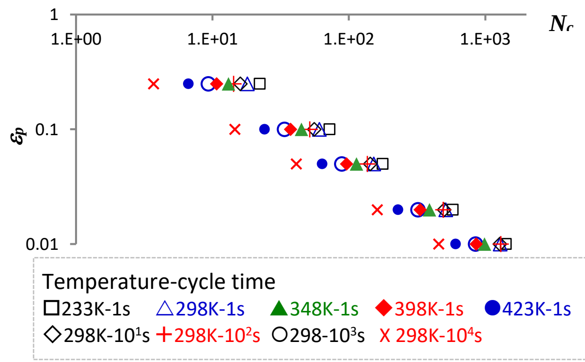

Figure 6: Sn37Pb: Regenerated Experimental Creep Fatigue Data

It is clear from Eq. (20) that a set of creep fatigue data, (ε_p, N_{cf}), can be transformed into a set of pure fatigue data, ($\varepsilon_{p,ref}$, N_f), by transforming the magnitude of ε_p into $\varepsilon_{p,ref}$ using the relation,

$$\varepsilon_{p,ref} = \frac{\varepsilon_p}{c(\varepsilon_p,T,t_c)}. \qquad (31)$$

Let $c(\varepsilon_p,T,t_c) = 1 - X_k(\varepsilon_p)\eta_k(T,t_c)$, where $X_k(\varepsilon_p) = a_k\varepsilon_p{}^{b_k}$, the optimum values of C_o, β_o, a_k, b_k, and H/k, B_c, $t_{c\infty}$ corresponding to the three cyclic parameter functions have been established through regressing the transformed fatigue data ($\varepsilon_{p,ref}$, N_f) with the pure fatigue equation, $\varepsilon_{p,ref} = C_o N_f{}^{-\beta_o}$. The optimum values are tabulated in ***Table 2*** completes with the relative magnitude of regression difference. The collapsed data of ($\varepsilon_{p,ref}$, N_f) corresponding to the three cyclic parameter functions are depicted in *Figure 7*.

Table 2: Sn37Pb: Fitting Constants for Creep Integrated Fatigue Equation Based on the Rate Equations of Sherby-Dorn, Larson-Miller, and Manson-Haferd

Rate equations	Fatigue coefficients		$\chi=a\varepsilon_p{}^b$		Fitting constant for $\eta(T,t_c)$	Relative magnitude of regression residue
	C_o	β_o	a	b		
Sherby-Dorn	1.85	0.740	8.40×10^{8}	6.93×10^{-2}	$H/k= 8.98\times10^{3}$	3.4
Larson-Miller	6.58	0.806	1.17×10^{-4}	4.43×10^{-2}	$B_c= 4.39\times10^{7}$	2.8
Manson-Haferd	3.75	0.773	-2.00×10^{-2}	5.00×10^{-2}	$t_{c\infty}= 2.34\times10^{7}$	1

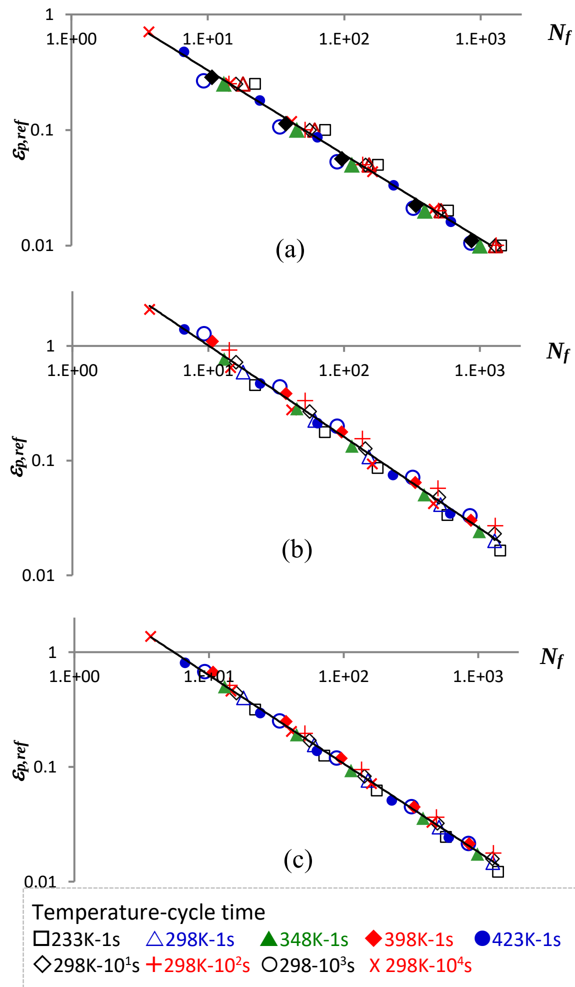

Figure 7: Sn37Pb: Transformed Pure Fatigue Data using the Rate Equations of (a) Sherby-Dorn, (b) Larson-Miller and (c) Manson-Haferd

It is noted that the fractional fatigue capability function that is based on the Manson-Hafred parameter returns a much smaller magnitude of regression residue than the other two parameter functions. This is consistent with the reported superior description of creep rupture of metal alloys for the Manson-Hafred parameter over the other two parameters [17]. Indeed, the magnitude of the fatigue capacity, C_o, given by the Sherby-Dorn parameter function was impossibly low – lower than the magnitude of C_b – while that given by the Larson-Miller parameter function appears to be unrealistically high.

IV. Discussions

The creep integrated fatigue equation integrates seamlessly the damages of creep and fatigue over the range from pure creep to pure fatigue. Comparing to the approach of the damage summation method, the creep integrated equation offers a more cohesive account for the combined damages of creep and fatigue. It does away with the challenging characterisation experiment that is required for the strain range partitioning method.

More valuably, the method can be generalised to model metal fatigue that is aggravated by a generalised damage driving force, X, whose rate of growth of damage may be expressed in the form

$$\dot{x} = g(\mu)h(T,t), \tag{32}$$

where $g(\mu)$ is a function of the magnitude of the damage driving parameter (for example, $\mu \rightarrow \sigma$ in the case of creep being the damage driving force) while $h(T, t)$ is a function of temperature and time. The rate function, Eq. (32), shall then be expressed into the form:

$$\hat{g}(\mu)\hat{h}(T,t) = 1 \quad (33)$$

such as that shown in Eq. (23). The function $\hat{g}(\mu)\hat{h}(T,t)$ is the damage function for the damage driving force X. The damage force integrated fatigue equation is then given by

$$\varepsilon_p = C_o c(\mu, T, t_c) N_{xf}{}^{-\beta_o}, \quad (34)$$

wherein

$$c(\mu, T, t_c) = 1 - \hat{g}(\mu)\hat{h}(T, t_c). \quad (35)$$

The magnitude of $c(\mu, T, t_c)$ ranges from nil to unity corresponding to the case of pure fatigue and pure X damage, respectively. Let the damage function, $\hat{g}(\mu)$, takes the form $\hat{g}(\mu) = a\mu^b$, the fitting constants, C_o, β_o, a, b, and that associated with $\hat{h}(T, t_c)$ may be extracted through regression as illustrated in the previous section.

In case of a metal fatigue that is aggravated by n damage driving forces, Eq. (34) may be further generalised to integrate these damage forces, X_1, $X_2 \ldots X_n$, into the fatigue equation:

$$\varepsilon_p = C_o c_1(\mu_1, T, t_c) c_2(\mu_2, T, t_c) \ldots c_n(\mu_n, T, t_c) N_{xf}{}^{-\beta_o}, \quad (36)$$

where
$$c_j(\mu_j, T, t_c) = 1 - \hat{g}_j(\mu_j)\hat{h}_j(T, t_c), \quad j=1,2,\ldots.n, \quad (37)$$

and $\hat{g}_j(\mu_j)$ may be conveniently assumed to be a power law relation, $a_j \mu_j{}^{b_j}$. In the absence of interaction between the damage forces, the coefficients, a_j and b_j, of individual damaging force may be established individually by holding off other damaging forces.

It is worth mentioning that the Basquin equation, $\sigma = C_\sigma N_f{}^{-\beta_\sigma}$, may be substituted for the Coffin-Manson equation in Eq. (34) in the case of an environmentally aggravated high cycle fatigue situation.

V. Conclusions

Creep fatigue analysis of solder joints in electronic assemblies has been presented. The condensed presentation comprised two major analyses: thermomechanical analysis and creep fatigue life modelling. The advanced analytical analysis can optimize the geometry of solder joints to minimise the magnitude of stresses in solder joints. This has led to the ideal geometry of stout hourglass for solder joints. The creep integrated fatigue equation integrates cohesively the damages of creep and fatigue over the range from pure creep to pure fatigue. The methodology can be generalised to model metal fatigue that is aggravated by multiple damaging forces.

References Références Referencias

1. Tummala RR (2001). Fundamentals of Microsystems Packaging, 1st edition, McGraw-Hill Education.
2. Wong EH & Mai Yiu-Wing, "Robust Design of Microelectronics Assemblies against Mechanical Shock, Temperature and Moisture, 1st Edition, Woodhead publishing, June 2015.
3. IPC/JEDEC-J-STD-020F (2023), Moisture/Reflow Sensitivity Classification for Non-hermetic Surface Mount Devices (SMDs)
4. JEDEC STANDARD JESD22-B111A (2016) Board Level Drop Test Method of Components for handheld electronic products.

5. JEDEC standard JESD22-A104-B (2000) Temperature Cycling.
6. Lamb MJ, Rouillard V, Sek MA, Monitoring the Evolution of Damage in Packaging Systems under Sustained Random Loads, Packaging technology and science, Volume25, Issue1 January/February 2012 Pages 39-51.
7. Kwon D, Azarian MH, Pecht M, Early Detection of Interconnect Degradation by Continuous Monitoring of RF Impedance, IEEE Trans. Device and Materials Reliability, Vol. 9, No. 2, June 2009.
8. Akay, HU; Paydar, NH; Bilgic, A. (1997). Fatigue life predictions for thermally loaded solder joints using a volume-weighted averaging technique. Journal of electronic packaging, 119, 228-235.
9. Darveaux, R. (2002). Effects of simulation methodology on solder joint crack growth correlation and faituge life prediction. Trans. ASME J. Electron. Packag., 124, 147.
10. Engelmaier, W. (1983). Fatigue life of leadless chip carrier solder joint during power cycling. IEEE Trans on Components, Hybrids and Manufacturing Technology, 6, 232-237
11. Suhir E, "On a paradoxical phenomenon related to beams on elastic foundation: Could external compliant leads reduce the strength of a surface-mounted device?", J. Applied Mechanics, 55:818, 1988.
12. Wong EH & Wong CK (2008). Tri-Layer Structures Subjected to Combined Temperature and Mechanical Loadings. IEEE Trans. Comp. Packag. Techno., 31(4), 790-800.
13. Wong EH, Thermal stresses in the discrete joints of sandwiched structures, Comp Struct 2015;125:72-80.
14. Wong EH. Stout hourglass - the ideal shape for solder joints. Microelectronics Reliability 145 (2023) 114978.
15. Bigwood DA, Crocombe AD (1989). Elastic analysis and engineering design formulae for bonded joints. Int J Adhes Adhes, 9, 229.
16. Silva LFM et al. (2009). Analytical models of adhesively bonded joints—Part I: Literature survey, Int. J. Adhes. Adhes., 29, 319–330.
17. Penny, R. & Marriott, D. (1995). Design for creep (2nd ed.). Chapman & Hall.
18. Wong EH, Driel W. van, Dasgupta A., Pecht M., "Creep Fatigue of Solder Joints: A Critical Review", Microelectron. Reliab. 2016;59:1-12.
19. Manson, SS, Halford, GR, Hirschberg, MH (1971). Creep-fatigue analysis by strain range partitioning. Symposium on design for elevated temperature environment (pp. 12-28). New York: ASME.
20. AFCEN (1986). Design and construction rules for mechanical components of FBR nuclear island.
21. ASME (1988). Code Case N47-29, Class I components in elevated temperature service, Section III, Division 1. ASME.
22. British. (1991). The R5 procedures. Nuclear electric plc.
23. Wong EH & Mai Yiu-Wing, "A unified equation for creep fatigue", Int J Fatigue 2014;68:186-194.
24. Liu D., Pons D. & Wong EH, Creep-Integrated Fatigue Equation for Metals, Int. J. Fatigue 2016; doi.org/10.1016/j.ijfatigue.2016.11.030.
25. Wong EH. Derivation of novel creep-integrated fatigue equations. Int J Fatigue 128 (2019) 105184.
26. Shi XQ, Pang HLJ, Zhou W & Wang ZP (2000). Low cycle fatigue analysis of temperature and frequency effects in eutectic solder alloy. Int J Fatigue, 22, 217-228.

Global Journal of Researches in Engineering (J) Volume XXIII Issue IV Version I Year 2023

Global Journal of Researches in Engineering: J
General Engineering
Volume 23 Issue 4 Version 1.0 Year 2023
Type: Double Blind Peer Reviewed International Research Journal
Publisher: Global Journals
Online ISSN: 2249-4596 & Print ISSN: 0975-5861

Landuse and Landcover Changes in Reservoir Catchments of Irrigation Dams in Northern Ghana

By Thomas Apusiga Adongo & Felix K. Abagale
University for Development Studies

Abstract- An assessment of landuse and landcover (LULC) patterns and changes at catchment level is crucial to planning and management of dam reservoirs. LULC changes over a 30-year period for 9 reservoir catchments in northern Ghana were assessed using a mixed-method approach involving GIS/remote sensing technique and key informant interviews. Four major LULC namely; cropland, water bodies, built-up land and open savannah woodlands were identified and classified from 1986, 1996, 2006 and 2016 LandSat TM images of the reservoir catchments. Substantial changes in LULC were observed in the reservoir catchments from 1986 to 2016, mainly through the conversion of large areas of closed and open savannah woodlands to cropland and built-up areas. Across all the catchments, cropland and built-up land increased significantly whilst water bodies, open savannah woodland and closed savannah woodland experienced a declined over the past 30-years.

Keywords: landuse and landcover changes, reservoir catchments, croplands, waterbodies, built-up areas, closed and open savannah woodlands.

GJRE-J Classification: LCC: GB980-2998

LANDUSEANDLANDCOVERCHANGESINRESERVOIRCATCHMENTSOFIRRIGATIONDAMSINNORTHERNGHANA

Strictly as per the compliance and regulations of:

Research | Diversity | Ethics

Landuse and Landcover Changes in Reservoir Catchments of Irrigation Dams in Northern Ghana

Thomas Apusiga Adongo [α] & Felix K. Abagale [σ]

Abstract- An assessment of landuse and landcover (LULC) patterns and changes at catchment level is crucial to planning and management of dam reservoirs. LULC changes over a 30-year period for 9 reservoir catchments in northern Ghana were assessed using a mixed-method approach involving GIS/remote sensing technique and key informant interviews. Four major LULC namely; cropland, water bodies, built-up land and open savannah woodlands were identified and classified from 1986, 1996, 2006 and 2016 LandSat TM images of the reservoir catchments. Substantial changes in LULC were observed in the reservoir catchments from 1986 to 2016, mainly through the conversion of large areas of closed and open savannah woodlands to cropland and built-up areas. Across all the catchments, cropland and built-up land increased significantly whilst water bodies, open savannah woodland and closed savannah woodland experienced a declined over the past 30-years. Between the years 1986 and 2016, cropland and built-up areas increased by 13.80 to 58.88% and 3.17 to 18.82% respectively, whereas water bodies and open savannah woodland decreased by 14.28 to 46.03% and 0.17 to 5.29% respectively. The driving factors of these changes have been noted as human population, farmland expansion, deforestation, lack of community involvement in the management of the catchments and lack of proper education on catchment management. The changes in LULC in the catchments could lead to dramatic changes in the catchment peak flows, increase in soil erosion, high sediment loads and sedimentation of the reservoirs. Good agricultural practices are necessary in the catchment management.

Keywords: landuse and landcover changes, reservoir catchments, croplands, waterbodies, built-up areas, closed and open savannah woodlands.

I. Introduction

Landuse and landcover (LULC) changes in reservoir catchments around the globe have significant environmental implications and consequences, which may include distresses in hydrological cycles, loss of biodiversity, increase in soil erosion, sediment loads and reservoir sedimentation (Lambin and Geist, 2006). Changes in LULC in a reservoir catchment can be categorized by the complex interaction of structural and behavioral factors associated with technological capacity, demand and social relations that affect both environmental capacity and the demand, along with the nature of the environment of interest (Verburg et al., 2004). Changes in LULC are primarily associated with anthropogenic activities such as deforestation, bush burning, urbanization, construction of dams and agriculture (Yigzaw and Hossain, 2016). Anthropogenic activities have been identified as the main cause of landuse/landcover changes and sedimentation in the Shiyang Reservoir in China with 43% of woodland areas converted into agricultural land (Zhou, 2002). Mzuza *et al.* (2017) reported that the Nkula Dam in the Middle Shire River Catchment in Malawi had been threatened with massive sedimentation and this was attributed to increased human population and agricultural activities in the reservoir catchment. In Ghana, a similar study conducted by Boakye et al. (2008) to assess the impact of landuse changes in the Barekese catchment on its associated reservoir revealed a loss in reservoir storage capacity of 45% due to sedimentation over a period of six years. The causes for the rapid rate of sedimentation of the reservoir were attributed to deforestation, population growth and lack of proper education of the communities in catchment management.

Increased demands on available resources mainly due to expanding population globally have led to the clearing of marginal lands for agricultural production and for settlement purposes. This has resulted in increased erosion, more rapid rates of sediment loading in reservoirs and reduced socio-economic benefits which they were constructed for (Mavima et al., 2011). In northern Ghana, the estimated mean annual soil loss in reservoir catchments ranged from 3.71 – 8.17 t/ha/yr and this could potentially contribute to sedimentation of their associated reservoirs (Adongo et al., 2019a). Spatial and temporal data on landuse and landcover changes is required to arrive at informed decisions in integrated water management (Mavima et al., 2011). LULC Change detection involves applying multi-temporal remote sensing information to analyze the historical effects of an occurrence quantitatively and thus helps in determining the changes associated with land cover and landuse properties with reference to the multi-temporal datasets (Ahmad, 2012; Seif and Mokarram, 2012).

Author α: Department of Agricultural Mechanisation & Irrigation Technology, University for Development Studies, Tamale, Ghana.
e-mail: aapusiga@uds.edu.gh
Author σ: Department of Agricultural Engineering, University for Development Studies, Tamale, Ghana.

Global Journal of Researches in Engineering (J) Volume XXIII Issue IV Version I Year 2023

In recent years, a variety of LULC change detection techniques and algorithms have been developed that make use of remotely sensed images. The most commonly used techniques include; Unsupervised classification, Supervised classification, Principal Component Analysis, Hybrid classification, Fuzzy classification, image overlay, classification comparisons of land cover statistics, change vector analysis, image rationing and the differencing of Normalized Difference Vegetation Index (NDVI) (Duadze, 2004). With proper understanding of the spatial and temporal variations occurring in a reservoir catchment over time and the interaction of the hydrological components of a reservoir catchment with each other, better water conservation strategies can be formulated (Ashraf, 2013). The question regarding information on landuse and landcover changes over time, and their driving forces in the reservoir catchments in northern Ghana are not known. Such knowledge is critical to the development of policies and action plans necessary for controlling sediment accumulation in reservoirs. Therefore, this study was carried out using GIS and Remote Sensing applications to analyze the extent of changes in nine (9) reservoir catchments over a period of 30 years in northern Ghana.

II. Materials and Methods

a) Study Area

The study was carried out in nine (9) reservoir catchments in northern Ghana as presented in Table 1 which also contains their principal characteristics and with Fig. 1 being the maps of the study sites.

Table 1: Study Reservoirs and Their Principal Characteristics

Region		Northern			Upper East			Upper West		
Reservoir		Bontanga	Golinga	Libga	Gambibgo	Tono	Vea	Daffiama	Karni	Sankana
District/ Municipality		Kumbungu	Tolon	Savelugu	Bolgatanga	Kassena-Nankana	Bongo	Daffiama-Bussie-Issa	Lambussie-Karni	Nadowli-Kaleo
Location Coordinates		9° 57'N 1° 02'W	9° 22'N 0° 57'W	9°59'N 0° 85'W	10° 45'N 0° 50'W	10° 52'N 1° 08'W	10°52'N 0° 51'W	10° 27'N 02° 34'W	10° 40'N 02° 38'W	10° 11'N 02° 36'W
Catchment Area (km^2)		165	53	31	1.70	650	136	21	35	141
Rainfall System	Type	Uni-modal			Uni-modal			Uni-modal		
	Annual Mean (mm)	1,000 – 1,300			700 – 1,010			800 – 1,100		
	Duration (months)	5 – 6			5 – 6			5 – 6		
Temperature (°C)	Day	33 – 39			20 – 22			29.0		
	Night	35 – 45			23 – 28			32.2		
	Mean	33 – 45			36 – 55			35 - 50		
Relative Humidity (%)	Dry Season	50			10			20		
	Wet Season	80			65			70		
Agro-ecological Zone		Guinea Savannah			Guinea/Sudan Savannah			Guinea Savannah		
Geology		Precambrian basement rocks and Paleozoic rocks from the voltaian sedimentary basin			Metamorphic and igneous rocks with gneisss, granodiorite and sandstone			Precambrian, granite and metamorphic rocks		
Soil Classes		Acrisols, plinthosols, planosols, luvisols, gleysols and fluvisols			Plinthosols, luvisols, vertisols, leptosols, lixisols, and fluvisols			Lixisols, fluvisols, leptosols, vertisols, acrisols and plinthosols		

Adapted from Adongo et al. (2019a)

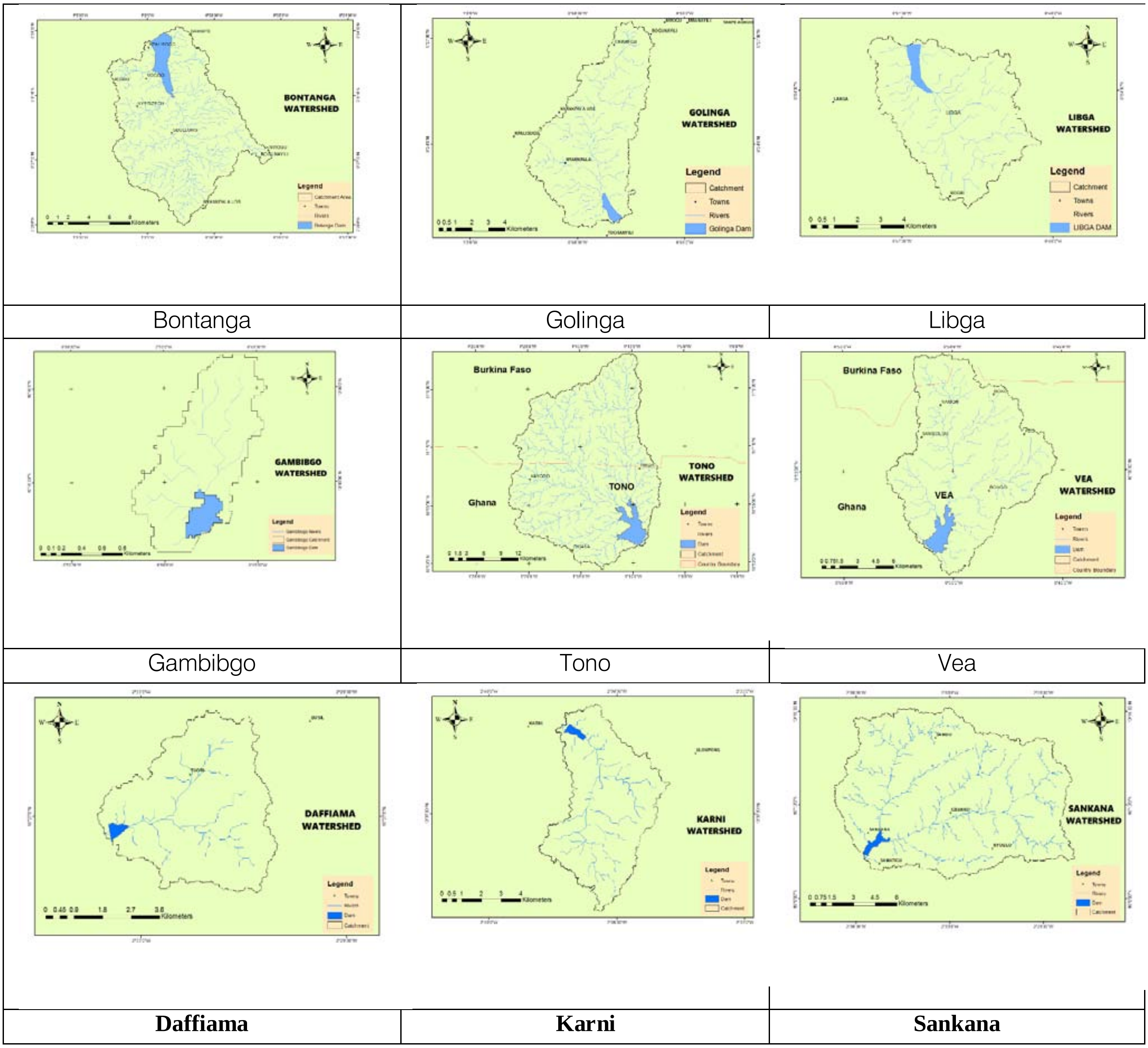

Fig. 1: Maps of the Study Reservoir Catchments

b) Methodology

The study used multi-temporal and multi-sensor Landsat satellite imageries to establish the landuse and landcover (LULC) changes in the study reservoir catchments for the years of 1986, 1996, 2006 and 2016. A summary of the flow chart of the methodology of LULC change detection analysis of the reservoir catchments is presented in Fig. 2.

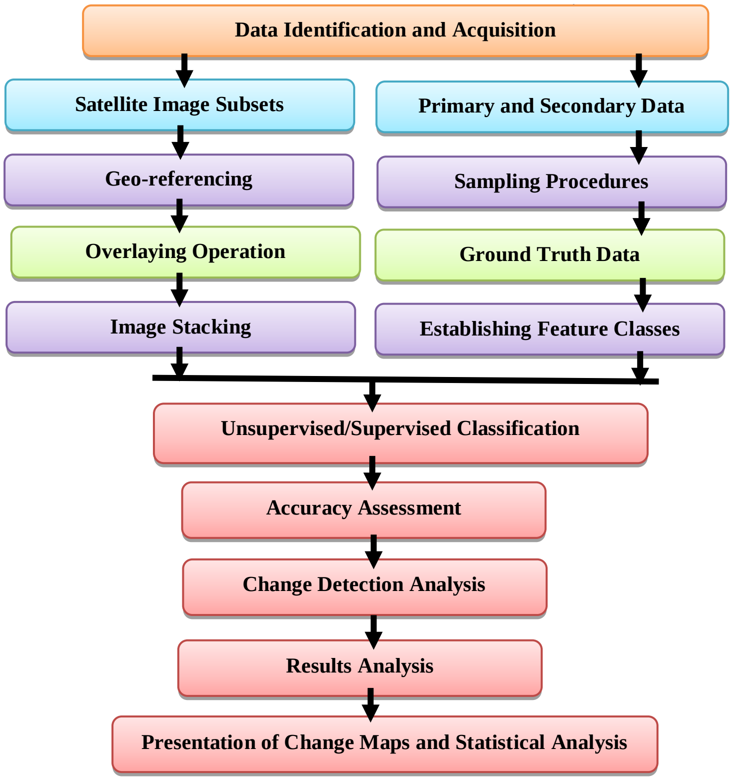

Adapted from Luca (2013)

Fig. 2: Methodology flow chart for LULC Change Analysis

The satellite images were derived from an open source Satellite Imagery Database from the United States Geological Survey (USGS) website. Detailed characteristics of the Landsat images of the various catchments is presented in Table 2.

Table 2: Characteristics of Landsat Images of the Reservoir Catchments

Catchment	Sensors	Date of Acquisition	Spatial Resolution (m)	Spectral Bands	Path/ Row	Source
Gambibgo, Tono	Landsat TM	05/10/1986	30 x 30	4,3,2	195/52	USGS GloVis
	Landsat TM	05/10/1996	30 x 30	4,3,2	195/52	
	Landsat TM	05/10/2006	30 x 30	4,3,2	195/52	
	Landsat 8 OLI	05/10/2016	30 x 30	5,4,3	195/52	
Vea	Landsat TM	05/10/1986	30 x 30	4,3,2	194/52	USGS GloVis
	Landsat TM	05/10/1996	30 x 30	4,3,2	194/53	
	Landsat TM	05/10/2006	30 x 30	4,3,2	194/53	
	Landsat 8 OLI	05/10/2016	30 x 30	5,4,3	194/52	
Bontanga, Golinga, Libga	Landsat TM	05/10/1986	30 x 30	4,3,2	194/53	USGS GloVis
	Landsat TM	05/10/1996	30 x 30	4,3,2	194/53	
	Landsat TM	05/10/2006	30 x 30	4,3,2	194/53	
	Landsat 8 OLI	05/10/ 2016	30 x 30	5,4,3	195/53	
Daffiama, Karni, Sankana	Landsat TM	05/10/1986	30 x 30	4,3,2	195/53	USGS GloVis
	Landsat TM	05/10/1996	30 x 30	4,3,2	195/53	
	Landsat TM	05/10/2006	30 x 30	4,3,2	195/53	
	Landsat 8 OLI	05/10/ 2016	30 x 30	5,4,3	195/53	

TM – Thematic Mapper; OLI – Operational Land Image; USGS GloVis – United States Global Visualization Viewer

Two software; ERDAS Imagine version 10.4 and ArcGIS version 10.4 were used to process the satellite images for layer stacking, mosaicking, geo-referencing, subsetting and training of the images according to the Area of Interest (AOI). In ERDAS Imagine, image band combinations were manipulated from the default natural colour band combination in the image drape viewer to effectively identify different land use types in the study area, and the findings were later verified by ground truthing (gathered information/image material related to real features on the ground) to generate an appropriate training sample dataset for supervised classification. To improve the visual interpretability of the satellite data for a particular application, image enhancement was performed on all the acquired scenes. A classification scheme was then developed of which the following five (5) landuse and landcover classes were distinguished; cropland, water body, built-up land/bare land/rocky ground, closed savannah woodland and open savannah woodland. Description of the various LULC classification schemes used in this study is presented in Table 3.

Table 3: Description of Delineated Landuse and Landcover Classes of the Catchments

Serial Number	Landuse/Landcover Class	Description
1	Cropland	Lands used for the cultivation of crops, i.e, crop fields.
2	Waterbodies	Waterbodies in the catchment area that empty into the reservoirs. These include; streams, lakes, ponds and rivers.
3	Built-up land/rocky ground/ bare land	Areas with intense infrastructural developments and exposed surfaces due to human activities or natural factors. These include; residential areas, industrial areas, commercial areas, recreational grounds, farmsteads, schools, lorry parks, roads and rocks. Bare land is land covered with sand or gravel. It has limited ability to support life and therefore uncultivated.
4	Closed savannah woodland	Thick forest lands, groves, thick plantations.
5	Open savannah woodland	Shrublands, grasslands and fallow lands.

Enhancement techniques were used together with classification techniques to extract features for the study reservoir catchments, locating areas and objects on the ground and deriving useful information from the images. Furthermore, use of enhancement techniques to visually interpret the images helped optimise the complementary capabilities of the processing. Classification was done for 1986, 1996, 2006 and 2016 images to identify the various LULC types and changes occurring over the years. Accuracy assessment of the classified imagery was performed to establish the level of accuracy of the classification. A non-parametric Cohen's Kappa test was performed to measure the extent of classification accuracy. Cohen's Kappa tries to measure the agreement between predefined producer-ratings and user assigned-ratings (Butt et al., 2015). It is computed using Equation 1 developed by Viera and Garrett (2005):

$$K = \frac{P\,(A) - P(E)}{1 - P(E)} \ldots\ldots\ldots\ldots\ldots\ldots\ldots\ldots \quad (1)$$

Where: P (A) – Number of times the k raters agree and P (E) – Number of times the k raters are expected to agree only by chance. The P(A) and P(E) were generated in ArcGIS using the ground coordinates of the ground truth samples.

The classification comparison of LULC statistics method was used for the change detection analysis. This method was adapted because the study sought to determine quantitative changes in the areas of the various LULC categories. Using the post-classification procedure, the area statistics for each of the LULC classes was derived from the classifications of the images for each date (1986, 1996, 2006 and 2016) separately, using functions in the ERDAS-Imagine-Software 10.4. The areas covered by each LULC type for the various time intervals were compared. The percentage landuse and landcover change (% LULCC) at the catchments was computed using the formula developed by Lambin(2001) and presented in Equation 2.

$$\%\,LULCC = \frac{Observed\;\;Area\;Change}{Total\;\;Area\;\;of\;Catchment} \times 100 \ldots\ldots\ldots\ldots\ldots \quad (2)$$

ArcGIS 10.4 was used for map composition as it increases the level of accuracy of the LULC change determined from the image.

c) Key-Informant Interviews

Key-informant interviews were conducted with key stakeholders such as local traditional leaders in the communities of the catchments and the management of the irrigation dams from January to March, 2018. The key-informant interviews were conducted so as to augment the data that was obtained from Landsat images and field measurements. A total of 81 respondents (9 from each catchment) were interviewed. To ensure the acquisition of comprehensive information, the respondents were people of age 45 to 60 years, who are longtime residents (i.e > 25 years) of the selected communities. They were selected based on their experience and knowledge on landuse and landcover changes in the catchments.

III. Results and Discussion

a) Areal Extent of Landuse and Landcover Classes in the Reservoir Catchments

Four (4) major landuse/landcover (LULC) categories namely; cropland, waterbodies, built-up land and open savannah woodland were identified and classified in the reservoir catchments, except Tono catchment where closed savannah woodland was identified as the fifth (5^{th}) major LULC class (Figure 3 and Table 4). The LULC maps of the catchments clearly showed that there were variations in the LULC types in the last 30 years (1986-2016).

In 1986, except the Tono catchment, open savannah woodland was the predominant LULC class, occupying an area of 45.99% at Bontanga to 80.72 %at Golinga. At Tono catchment, the predominant LULC was closed savannah woodland with a coverage area of 233.89 ha (35.98%), followed by open savannah woodland with area occupancy of 30.56%. Except Tono catchment, the second most predominant class was cropland with coverage area of 15.57% at Golinga to 45.57% at Bontanga, followed by built-up area with a coverage of 1.7% at Bontanga to 8.24% at Gambibgo. Across all the catchments, water body occupied the least area with values ranging from 0.44% at Sankana to 6.75% at Vea (Table 4).

The 1996 Landsat images of the catchments showed a reduction of LULC change compared with 1986 for the different LULC classes, except cropland and built-up areas. Open savannah woodland occupied a significant portion of the catchments with an area coverage of 32.94% at Gambibgo to 66.55% at Golinga, followed by cropland which was randomly distributed within the catchments with an area of 27.74% at Tono to 52.78% at Bontanga. Built-up area occupied a minor area of 2.39% at Bontanga to 15.29% at Gambibgo. Water bodies occupied the least area of 0.40% at Sankana to 5.85% at Vea (Table 4).

From the 2006 image classification it was noted that both water bodies and open savannah woodland were reduced from their coverage in 1996 (Table 4). Water bodies were reduced by 0.05% at Sankana to 2.35% at Gambibgo whilst open savannah woodland reduced by 5.75% at Vea to 18.94% at Golinga. Closed savannah woodland also reduced by 8.37% at Tono. On the other hand, cropland coverage increased by 3.11% at Tono to 18.72% at Golinga, and built-up areas coverage also increased by 0.36% at Golinga to 9.41% at Gambibgo catchment.

The 2016 Landsat map showed substantial changes relative to the previous 20-year period with croplands occupying the greatest area of the catchments with values ranging from 37.82% at Tono to 74.45% at Golinga, followed by open savannah woodland with 17.68% at Golinga to 33.63% at Tono catchment. However, at the Libga and Gambibgo catchments, built-up areas were noted to be the second largest LULC class occupying 22.87% and 37.06% of their areas respectively. Patches of closed savannah woodland with a total area coverage of 13.84% were found in the northern zone of the Tono catchment. Except Libga and Gambibgo catchments, built-up areas occupied an area of 4.99% at Bontanga to 18.62% at Daffiama catchment. The remaining parts of the catchments were composed of water bodies with the least area of 0.27% at Sankana to 4.49% at Bontanga (Table 4).

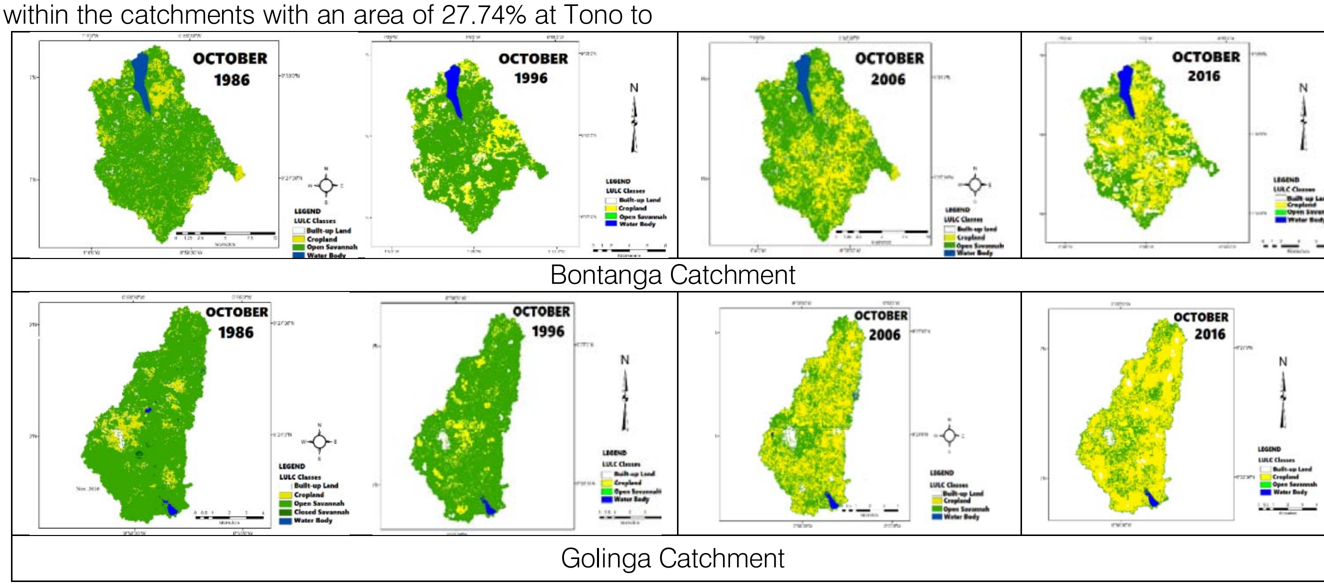

Bontanga Catchment

Golinga Catchment

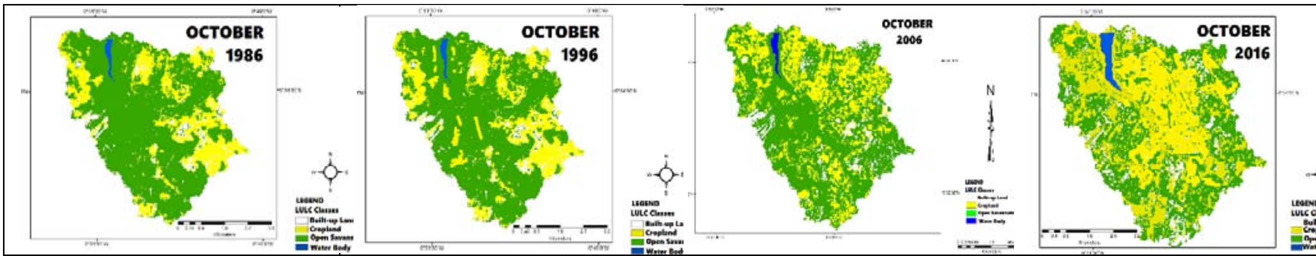

Libga Catchment

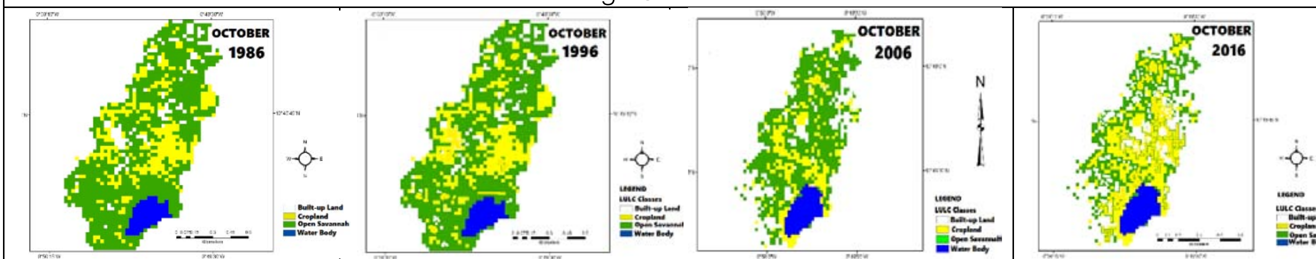

Gambibgo Catchment

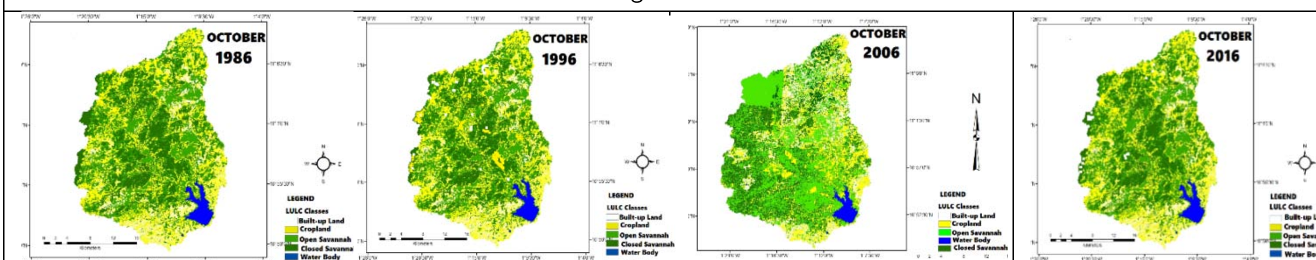

Tono Catchment

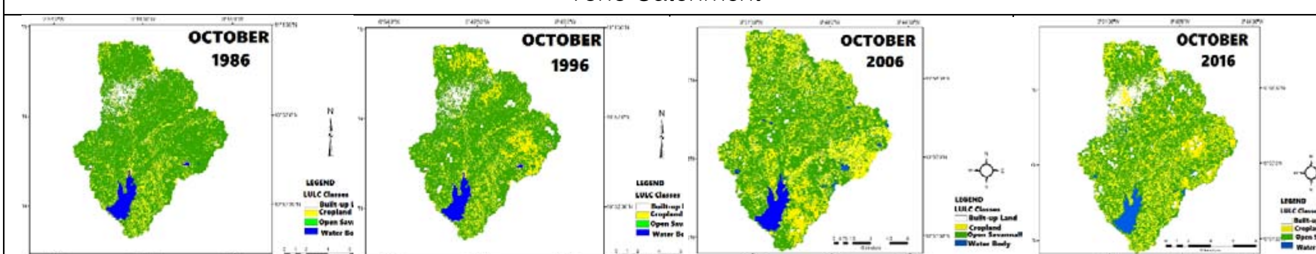

Vea Catchment

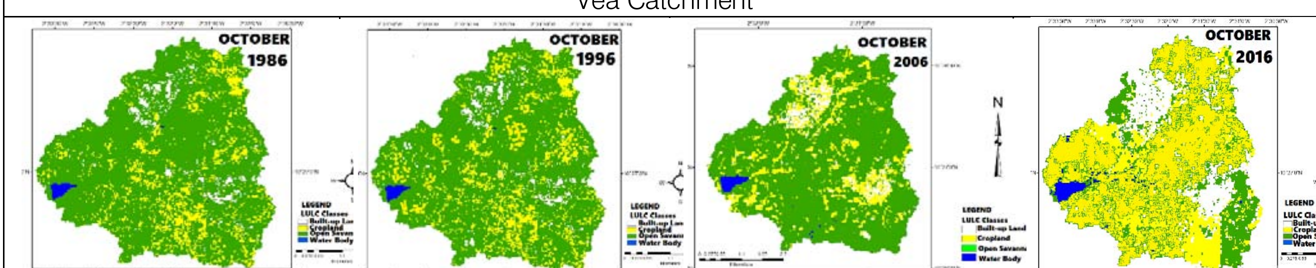

Daffiama Catchment

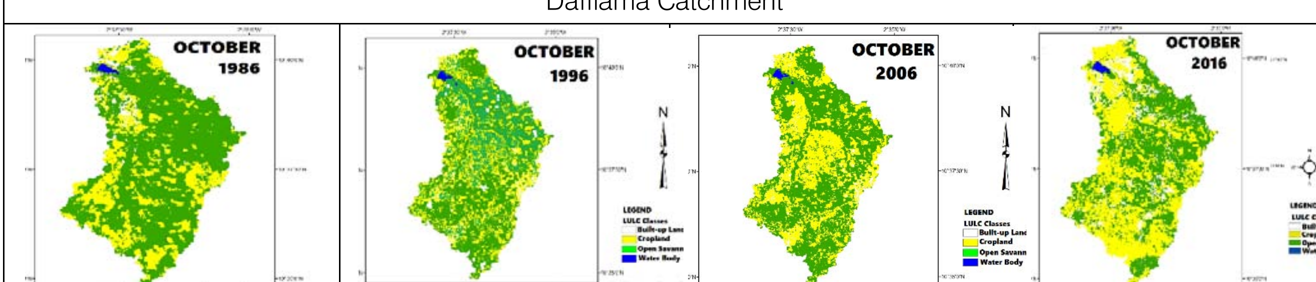

Karni Catchment

Global Journal of Researches in Engineering (J) Volume XXIII Issue IV Version I Year 2023

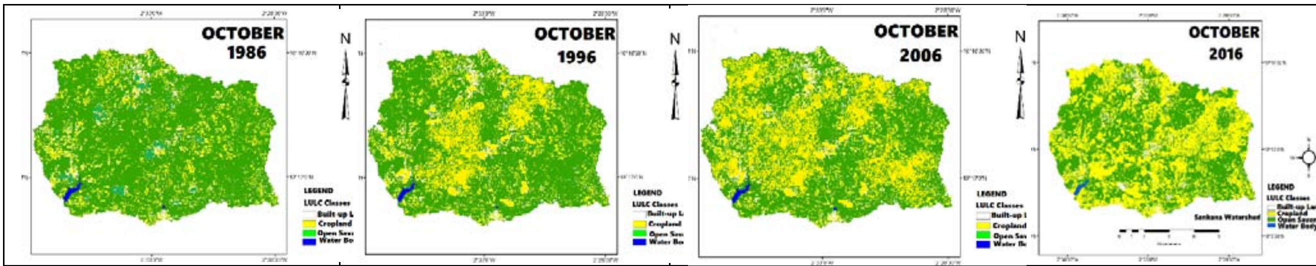

Sankana Catchment

Fig. 3: Landuse/Landcover Landsat Images of Study Reservoir Catchments for 1986, 1996, 2006 and 2016

Table 4: Areal Extent of Different Landuse/Landcover Classes in the Study Reservoir Catchments from the Year 1986 to 2016

Bontanga Catchment								
Landuse/ Landcover Class	1986		1996		2006		2016	
	km^2	%	km^2	%	km^2	%	km^2	%
Cropland	75.19	45.57	87.09	52.78	97.67	59.19	111	67.27
Built-up land	2.80	1.70	3.94	2.39	5.86	3.55	8.23	4.99
Water body	11.13	6.75	9.67	5.86	8.76	5.31	7.41	4.49
Open SW	75.88	45.99	64.30	38.97	52.71	31.95	38.36	23.25
Closed SW	0.0	0.0	0.0	0.0	0.0	0.0	0.0	0.0
Total	165	100	165	100	165	100	165	100
Golinga Catchment								
Landuse/ Landcover	1986		1996		2006		2016	
	km^2	%	km^2	%	km^2	%	km^2	%
Cropland	8.25	15.57	15.45	29.15	25.37	47.87	39.46	74.45
Built-up land	1.12	2.11	1.77	3.34	1.96	3.70	3.77	7.11
Water body	0.59	1.11	0.51	0.96	0.44	0.83	0.40	0.75
Open SW	42.78	80.72	35.27	66.55	25.23	47.60	9.37	17.68
Closed SW	0.26	0.49	0.0	0.0	0.0	0.0	0.0	0.0
Total	53	100	53	100	53	100	53	100
Libga Catchment								
Landuse/ Landcover	1986		1996		2006		2016	
	km^2	%	km^2	%	km^2	%	km^2	%
Cropland	10.37	33.45	14.53	46.87	16.15	52.10	16.95	54.68
Built-up land	1.96	6.32	3.08	9.94	4.92	15.87	7.04	22.71
Water body	0.52	1.68	0.35	1.13	0.28	0.90	0.23	0.74
Open SW	18.15	58.55	13.04	42.06	9.65	31.13	6.78	21.87
Closed SW	0.0	0.0	0.0	0.0	0.0	0.0	0.0	0.0
Total	31	100	31	100	31	100	31	100
Gambibgo Catchment								
Landuse/ Landcover	1986		1996		2006		2016	
	km^2	%	km^2	%	km^2	%	km^2	%
Cropland	0.35	20.59	0.66	38.82	0.8	47.06	0.70	41.18
Built-up land	0.14	8.24	0.26	15.29	0.42	24.71	0.63	37.06
Water body	0.37	21.76	0.22	2.94	0.18	1.59	0.11	0.47
Open SW	0.84	49.41	0.56	32.94	0.30	17.65	0.26	15.29
Closed SW	0.0	0.0	0.0	0.0	0.0	0.0	0.0	0.0
Total	1.7	100	1.7	100	1.7	100	1.7	100
Tono Catchment								
Landuse/ Landcover	1986		1996		2006		2016	
	km^2	%	km^2	%	km^2	%	km^2	%
Cropland	156.17	24.03	180.32	27.74	200.55	30.85	245.86	37.82
Built-up land	41.54	6.39	50.75	7.81	65.86	10.13	79.43	12.22
Water body	19.78	3.04	18.82	2.90	17.81	2.74	16.19	2.49
Open SW	198.62	30.56	234.94	36.14	255.02	39.23	218.60	33.63

Closed SW	233.89	35.98	165.17	25.41	110.76	17.05	89.92	13.84
Total	**650**	**100**	**650**	**100**	**650**	**100**	**650**	**100**
Vea Catchment								
Landuse/ Landcover	1986		1996		2006		2016	
	km^2	%	km^2	%	km^2	%	km^2	%
Cropland	53.46	39.31	59.33	43.63	65.74	48.34	74.86	55.04
Built-up land	4.17	3.07	5.71	4.20	7.92	5.82	10.38	7.63
Water body	8.71	6.40	7.95	5.85	7.15	5.26	5.59	4.11
Open SW	69.66	51.22	63.01	46.33	55.19	40.58	45.17	33.21
Closed SW	0.0	0.0	0.0	0.0	0.0	0.0	0.0	0.0
Total	**136**	**100**	**136**	**100**	**136**	**100**	**136**	**100**
Daffiama Catchment								
Landuse/ Landcover	1986		1996		2006		2016	
	km^2	%	km^2	%	km^2	%	km^2	%
Cropland	4.08	19.43	6.95	33.10	8.51	39.10	10.58	50.38
Built-up land	0.68	3.24	1.16	5.52	2.74	13.05	3.91	18.62
Water body	0.43	2.05	0.35	1.67	0.26	1.24	0.11	0.52
Open SW	15.81	75.29	12.54	59.71	9.79	46.62	6.40	30.48
Closed SW	0.0	0.0	0.0	0.0	0.0	0.0	0.0	0.0
Total	**21**	**100**	**21**	**100**	**21**	**100**	**21**	**100**
Karni Catchment								
Landuse/ Landcover	1986		1996		2006		2016	
	km^2	%	km^2	%		km^2	%	km^2
Cropland	10.99	31.40	14.26	40.74	17.84	50.97	23.25	66.43
Built-up land	1.46	4.17	1.75	5.0	2.22	6.34	3.01	8.60
Water body	0.46	1.31	0.42	1.20	0.33	0.94	0.20	0.57
Open SW	22.09	63.11	18.57	53.06	14.61	41.74	8.54	24.40
Closed SW	0.0	0.0	0.0	0.0	0.0	0.0	0.0	0.0
Total	**35**	**100**	**35**	**100**	**35**	**100**	**35**	**100**
Sankana Catchment								
Landuse/ Landcover	1986		1996		2006		2016	
	km^2	%	km^2	%		km^2	%	km^2
Cropland	41.18	29.21	57.63	40.87	76.64	54.35	96.52	68.45
Built-up land	4.34	3.08	5.11	3.62	6.43	4.56	8.80	6.24
Water body	0.62	0.44	0.56	0.40	0.49	0.35	0.38	0.27
Open SW	94.86	67.28	77.70	55.11	57.44	40.74	35.30	25.04
Closed SW	0.0	0.0	0.0	0.0	0.0	0.0	0.0	0.0
Total	**141**	**100**	**141**	**100**	**141**	**100**	**141**	**100**

SW = Savannah woodland

b) Landuse and Landcover Classification Accuracy Assessment for 2016

According to Owojori and Xie (2005), it is crucial to perform accuracy assessment for LULC classification if the classification data are to be used for change detection analysis. Accuracy assessment establishes the level of accuracy of the classfication . Coppin and Bauer (1996) reported that a classification accuracy of 0 - 69% indicates low accuracy whereas 70 – 100% indicates high accuracy, and a kappa coefficient < 0.5 and > 0.5 indicates low and high accuracies respectively. As presented in Table 5, an accuracy assessment elaborated for the 2016 image classification revealed an overall classification accuracy of 80% and overall Kappa coefficient (statistic) of 0.75. The highest user accuracy of all the LULC classes was obtained for water bodies of 92.5% whilst cropland recorded the lowest user accuracy of 72.2%. Also, for producer accuracies, water bodies and cropland recorded the highest and lowest values of 100% and 64.4% respectively. Based on the assertion of Coppin and Bauer (1996), the classification accuracy for the study was high. In a similar study in Ghana, Antwi-Agyei et al. (2019) obtained high overall classification accuracy of 77.56% and overall Kappa statistic of 0.77 in Owabi reservoir catchment.

Table 5: Classification Accuracy Assessment for the Year 2016

LULC Class	Reference Totals	Classified Totals	Correct Number	Producer's Accuracy (%)	User's Accuracy (%)	Kappa Coefficient
Cropland	45	40	29	64.4	72.2	0.68
Built-up land	34	40	30	88.2	75.0	0.71
Water body	37	40	37	100.0	92.5	0.87
Open SW	43	40	35	81.4	87.5	0.82
Closed SW	41	40	29	70.7	72.5	0.68
Total	**200**	**200**	**160**	-	-	-
Overall classification accuracy = 80.0 % and overall kappa coefficient (statistic) = 0.75						

LULC = Landuse and Landcover; SW = Savannah woodland

c) *Landuse and Landcover Changes Detection Analysis with the Reservoir Catchments from 1986 to 2016*

Substantial changes in LULC categories were observed to have taken place in the reservoir catchments from 1986 to 2016, mainly through the conversion of large areas of closed and open savannah woodlands to cropland and built-up areas. Across all the catchments, cropland and built-up land saw a consistent and significant increased whilst water bodies, open savannah woodland and closed savannah woodland experienced a declined over the past 30-years (Table 6). Between 1986 and 1996, cropland increased by 3.58% at Karni to 18.24% at Gambibgo. Also, built-up land increased by 0.47% at Karni to 7.06% at Gambibgo. Water bodies decreased by 0.04% at Sankana to 8.82% at Gambibgo whilst open savannah woodland declined by 5.75% at Vea to 16.48% at Libga. At Tono catchment, however, open savannah woodland increased by 5.59% and closed savannah woodland saw a decrease of 10.57% to other LULC classes.

The study also found that between 1996 and 2006, cropland increased by 3.11% at Tono catchment to 18.72% at Golinga catchment, whilst built-up land increased by 0.36% at Golinga to 9.41% at Gambibgo catchment. However, water bodies recorded a marginal declined by 0.05% at Sankana catchment to 2.35% at Gambibgo catchment. Open savannah woodland experienced a declined by 5.75% at Vea catchment to 18.94% at Golinga catchment as presented in Table 6.

Between 2006 and 2016, cropland significantly increased by 2.58% at Libga catchment to 26.59% at Golinga catchment, whilst at Gambibgo catchment, it decreased by 5.88% probably to settlement built-up areas. Also, built-up land increased by 1.44% at Sankana catchment to 12.35% at Gambibgo catchment. However, water bodies decreased marginally by 0.08% at Golinga and Sankana catchments to very high of 4.12% at Gambibgo catchment. Open savannah woodland also saw a decline of 2.21% at Tono catchment to 29.92% at Golinga catchment (Table 6). It was also noted that the closed savannah woodland at Tono catchment decreased by 5.60% to probably other LULC categories such as cropland and built-up land.

Table 6: Landuse and Landcover Changes of the Study Reservoir Catchments

Catchment	Bontanga						Golinga					
Landuse/ Landcover Change	1986-1996		1996-2006		2006-2016		1986-1996		1996-2006		2006-2016	
	km^2	%	km^2	%	km^2	%	km^2	%	km^2	%	km^2	%
Cropland	11.21	6.79	10.58	6.41	13.33	8.08	7.20	13.58	9.92	18.72	14.09	26.59
Built-up land	1.14	0.69	1.92	1.16	2.37	1.68	0.65	1.23	0.19	0.36	1.81	3.42
Water body	-1.46	-0.88	-0.91	-0.55	-1.35	-0.82	-0.08	-0.15	-0.07	-0.13	-0.04	-0.08
Open SW	-10.89	-6.60	-11.59	-7.02	-14.35	-8.70	-7.51	-14.17	-10.04	-18.94	-15.86	-29.92
Closed SW	0.0	0.0	0.0	0.0	0.0	0.0	-0.26	-0.49	0.0	0.0	0.0	0.0
Catchment	Libga						Gambibgo					
Cropland	4.16	13.42	1.62	5.23	0.8	2.58	0.31	18.24	0.14	8.24	-0.1	-5.88
Built-up land	1.12	3.61	1.84	5.94	2.12	6.84	0.12	7.06	0.16	9.41	0.21	12.35
Water body	-0.17	-0.55	-0.07	-0.23	-0.05	-0.16	-0.15	-8.82	-0.04	-2.35	-0.07	-4.12
Open SW	-5.11	-16.48	-3.39	-10.94	-2.87	-9.26	-0.28	-16.41	-0.26	-15.29	-0.04	-3.35
Closed SW	0.0	0.0	0.0	0.0	0.0	0.0	0.0	0.0	0.0	0.0	0.0	0.0
Catchment	Tono						Vea					
Cropland	24.15	3.72	20.23	3.11	45.31	6.97	5.87	4.32	6.41	4.71	9.12	6.71

Built-up land	9.21	1.42	15.11	2.32	13.57	2.09	1.54	1.13	2.21	1.63	2.46	1.81
Water body	-0.96	-0.15	-1.01	-0.16	-1.62	-0.25	-0.76	-0.56	-0.80	-0.59	-1.56	-1.15
Open SW	36.32	5.59	20.08	3.09	-36.42	-2.21	-6.65	-4.89	-7.82	-5.75	-10.02	-7.37
Closed SW	-68.72	-10.57	-54.41	-8.37	-20.84	-5.60	0.0	0.0	0.0	0.0	0.0	0.0
Catchment	Daffiama						Karni					
Cropland	2.87	13.67	1.56	7.43	2.07	9.86	3.27	9.34	3.58	10.23	5.41	15.46
Built-up land	0.48	2.29	1.58	7.52	.01.17	5.57	0.29	0.83	0.47	1.34	0.79	2.26
Water body	-0.08	-0.38	-0.09	-0.43	-0.15	-0.71	-0.04	-0.11	-0.09	-0.26	-0.13	-0.37
Open SW	-3.27	-15.57	-2.75	-13.10	-3.39	-16.14	-3.52	-10.06	-3.96	-11.31	-6.07	-17.34
Closed SW	0.0	0.0	0.0	0.0	0.0	0.0	0.0	0.0	0.0	0.0	0.0	0.0
Catchment	Sankana											
Cropland	16.45	11.67	19.01	13.48	19.88	14.10						
Built-up land	0.77	0.55	1.32	0.94	2.37	1.44						
Water body	-0.06	-0.04	-0.07	-0.05	-0.11	-0.08						
Open SW	-17.16	-12.17	-20.26	-14.37	-22.14	-15.70						
Closed SW	0.0	0.0	0.0	0.0	0.0	0.0						

SW = Savannah woodland;
+ indicates increase; and
- indicates decrease

d) Causes of the Landuse and Landcover Changes in Reservoir Catchments

The driving forces for LULC changes in the study reservoir catchments resulted from direct and indirect causes. The direct causes constituted human activities that originated from intended landuse and directly affect LULC. The results from key informant interviews in communities located in the catchments during the study indicated that there is a significant evidence of LULC change resulting from farmland expansion (37%); clearing trees for fuelwood and charcoal for domestic consumption and for sale (24%); clearing of forest for human settlement development (20%); wildfires (15%) and illegal harvesting of forests for timber production (4%) (Fig. 4). The most significant indirect drivers behind the LULC changes noticed on the catchments were related to human population increase (demographic factors) (43%); economic, technological and cultural factors among the land ownership (27%); climate variability in the catchment (19%) and institutional factors (11%) (Fig. 5).

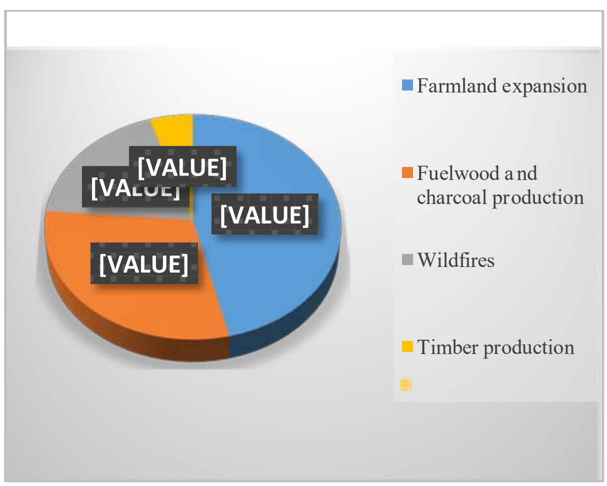

Fig. 4: Direct Causes of LULC Changes in Reservoir Catchments

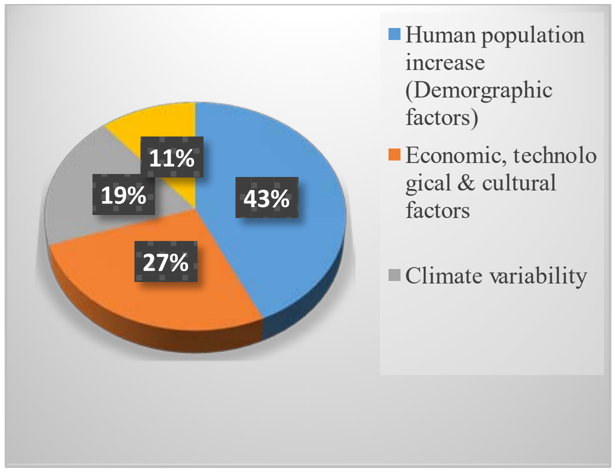

Fig. 5: Indirect Causes of LULC Changes in the Reservoir Catchments

The increased in human population in the catchments over the years has accelerated the demand for agricultural land and settlement development which had led to deforestation and thus reduced the forest cover. The results of the study showed a massive reduction in forested areas in the Tono catchment which was noted to correspond to the results of other studies suggesting that forest areas in Ghana have undergone massive reduction (Adade and Oppelt, 2019). Census data showed that between 1986 and 2016, human population in the five (5) regions of northern Ghana increased with an average growth rate of 2.1% per annum (GSS, 2014), implying an expansion of agricultural land and built-up areas to meet demand. According to Attua and Fisher (2011) and Antwi et al. (2014), human population growth is widely recognized as a main driver of environmental and LULC change, especially in developing countries. The changes observed in the study reservoir catchments are consistent with those observed in many studies conducted at national and regional levels in Ghana such as Antwi et al. (2014), Kleeman et al. (2017) Asubonteng et al. (2018), Shoyama et al. (2018), Adade and Oppelt (2019) and Antwi-Agyei et al. (2019). For example, using a mixed-method approach, Kleeman et al. (2017) identified population growth as a major driver of LULC changes in Ghana's Upper East Region. Various anthropogenic activities, including agriculture, have led to encroachment of human settlements on forest lands, with devastating consequences for biodiversity (Antwi et al., 2014). In Namibia and Kenya, studies have identified agricultural expansion, human population growth increase and illegal logging as the key drivers of landuse and landcover changes in catchments, with serious debilitating effects on their associated reservoirs and peoples' livelihood activities (Ogechi and Waithaka, 2017). Overall, a large population entails a higher demand for fuelwood and conversion of more agricultural land to human settlements to meet the growing feeding needs (Kassa et al., 2017). With the projected steady increase of the global human population at a rate of 1.1% per annum (UN-DESA, 2017), the fragile reservoir catchments of northern Ghana will without doubt continue to suffer from anthropogenic pressures.

e) Potential Consequences of the Landuse and Landcover Changes in the Study Catchments

The trend of landuse and landcover changes detected in the study has shown general conversion of the closed and open savannah woodland to cropland and built-up and open areas. These conversions have potential consequences on the catchments' characteristics and hydrology. According to Weiss and Milich (1997), landcover is a function of rainfall regime, soil conditions and geomorphology. This indicates that the conversion of the closed and open savannah woodlands to croplands, grasslands and settlements would definitely lead to changes in the soil conditions and the geomorphology of the catchments.

Similarly, Costa et al. (2003) reported that the conversion of forest to grassland disrupts the hydrological cycle of the catchment by altering the balance between rainfall and evaporation and, consequently, the runoff response of the area. With less litter due to wildfires and clear/burn practices in the catchments, the capacity of surface detention is decreased, and a greater proportion of the rainfall runs off as overland flow. The shift from sub-surface flow to overland storm flows accompanying deforestation, expansion of croplands and built-up areas may produce dramatic changes in the catchment peak flows as well and make the land more vulnerable to erosion leading to sedimentation of the reservoirs. Adongo et al. (2019b) reported that the estimated mean annual soil loss in the reservoir catchments ranged from 3.71 to 8.17 t/ha/yr. Lack of enforcement of environmental by-laws by the local rural district council regarding deforestation has led to uncontrolled cutting down of trees within the catchment and much of the woodland has now become grassland area.

Also, Boakye et al. (2008) noted that practices relating to farming and urbanization such as construction and soil compaction during logging can reduce the infiltration capacity of the soil and in turn the flow of water through the soil profile in Barekese catchment in Ghana. Moreover, the increase in farming activities in the catchments coupled with increasing runoff could also increase erosion and sedimentation of the reservoirs thus, transporting more sediment into the river leading to the gradual sedimentation of the reservoirs. Therefore, these LULC changes detected could be the cause of the sedimentation in the reservoirs at a rate of 0.26 to 0.91%/yr, as reported by Adongo et al*.* (2019b). A similar study conducted in Ghana noted a similar trend whereby sedimentation of reservoirs was mainly attributed to deforestation and lack of proper education of the communities in catchment management (Boakye et al., 2008).

IV. Conclusions

The study identified and classified cropland, water bodies, built-up land, open savannah woodland and closed savannah woodland as the five major landuse and landcover categories in the various sites. Over the 30 year period, substantial areas of closed and open savannah woodlands were noted to have been converted into croplands and built-up areas with water bodies declining mainly due to anthropogenic activities. Closed savannah woodland was only identified in the Tono reservoir catchment although its area decreased overtime.

Farmland expansion, domestic and commercial fuelwood and charcoal production, construction activities, wildfires/bushfires, and illegal harvesting of forests for timber production were observed as casual factors for these changes. These factors were influenced by human population increase, economic, climate variability in the catchment, etc. These changes observed in the various catchments have an effect on catchment hydrological characteristics thus affecting water flows and increasing the level of vulnerability to erosion and its attendant effect on reservoir sedimentation. Strategies such as afforestation, ban on illegal harvesting of forest products, etc and involving local communities for effective and sustainable management of the catchments to reduce the effect of landuse and landcover change on catchment characteristics are recommended.

References Références Referencias

1. Adade, B. and Oppelt, N., 2019. Landuse/landcover change analysis and urban growth modelling in the Greater Accra Metropolitan Area (GAMA). Ghana. *Urban Sci.* 2019, 3, 26.
2. Adongo, T. A., Agyare, W. A., Abagale, F. K. and Kyei-Baffour, N., 2019a. Spatial soil loss estimation using an integrated GIS-based revised universal soil loss equation (RUSLE) in selected watersheds in northern Ghana. International Journal of Engineering, Science and Technology, 11(4):58-71, MultiCraft. http://dx.doi.org/10.4314/ijest.v11i4.6
3. Adongo, T. A., Kyei-Baffour, N. Abagale, F. K. and Agyare, W. A., 2019b. Assessment of reservoir sedimentation of irrigation dams in northern Ghana. *Lake and Reservoir Management*, 36(1): 87-105, Taylor and Francis. ISSN: 1040-2381 (Print) 2151-5530 (Online), https://doi.org/10.1080/10402381.2019.1659461
4. Ahmad, F., 2012. Detection of Change in Vegetation Cover using Multi-spectral and Multi-Temporal Information for District Sargodha, Pakistan. *Sociedade and Natureza*, *24*(3): 557-571.
5. Antwi, E. K., Boakye-Danquah, J., Asabere, S. B., Yiran, G. A., Loh, S. K., Awere, K. G., Owusu, A. B., 2014. Landuse and Landscape Structural Changes in the Ecoregions of Ghana. *J. Dis. Res*. 9, 452–467.
6. Antwi-Agyei, P., Kpenekuu, F., Hogarh, J. N., Obiri-Danso, K., Abaidoo, R. C. Jeppesen, E., and Andersen, M. N., 2019. Land use and land cover changes in the owabi reservoir catchment, Ghana: Implications for livelihoods and management. *Geosciences*, 9(7), 286.
7. Ashraf, A., 2013. Changing Hydrology of the Himalayan Catchment. *Current Perspectives in Contaminant Hydrology and Water Resources Sustainability*, Intech, 9(1): 221-241. http://dx.doi.org/10.5772/54492.
8. Asubonteng, K., Pfeffer, K., Ros-Tonen, M., Verbesselt, J., Baud, I., 2018. Effects of tree-crop farming on land-cover transitions in a mosaic landscape in the eastern region of Ghana. *Environ. Manag.* 62, 529–547.
9. Attua, E. M., and Fisher, J. B., 2011. Historical and future land-cover change in a municipality of Ghana. *Earth Interact.* 15, 1–26.
10. Boakye, E., Odai, S. N., Adjei, K. A., and Annor, F. O., 2008. Landsat images for assessment of the impact of landuse and landcover changes on the Barekese catchment in Ghana. *European Journal of Scientific Research*, *22*(2), 269-278.
11. Butt, A., Shabbir, R., Sheikh Saeed Ahmad, S. S. and Aziz, N., 2015. Land Use Change Mapping and Analysis using Remote Sensing and GIS: A Case study of Simly Catchment, Islamabad, Pakistan. *The Egyptian Journal of Remote Sensing and Space Sciences,* 18(2): 251-259, http://dx.doi.org/10.1016/j.ejrs.2015.07.003
12. Coppin, P. and Bauer, M., 1996. Digital Change Detection in Forest Ecosystems with Remote Sensing Imagery. *Remote Sens*. Rev. 13, 207–234.
13. Costa, M. H., Botta, A., and Cardille, J. A., 2003. Effects of large-scale changes in land cover on the

discharge of the Tocantins River, Southeastern Amazonia. *Journal of Hydrology*, *283*(1-4), 206-217.
14. Duadze, S. E. K., 2004. Landuse and Landcover Study of the Savannah Ecosystem in the Upper West Region (Ghana) using Remote Sensing. ZEF Bonn, University of Bonn, Germany.
15. GSS, 2014. 2010 Population and Housing Census, Regional Analytical Report. Ghana Statistical Service. October, 2014.
16. Kassa, H., Dondeyne, S., Poesen, J., Frankl, A., and Nyssen, J., 2017. Transition from forest-based to cereal-based agricultural systems: A review of the drivers of land use change and degradation in Southwest Ethiopia. *Land Degrad. Dev.* 2017, 28, 431–449.
17. Kleeman, J., Baysal, G., Bulley, H. N. N., Furst, C., 2017. Assessing Driving Forces of Landuse and Landcover Change by a Mixed-method Approach in North-Eastern Ghana, West Africa. *J. Environ. Manag.* 196, 411-442.
18. Lambin, E. F., 2001. The causes of land-use and land-cover change: moving beyond the myths. *Global environmental change*, *11*(4), 261-269.
19. Lambin, E. F., and Geist, H. J., 2006. Landuse and landcover change: Local processes and global impacts. Environmental Sciences. 1:1-8
20. Luca, M., 2013. Change Detection in Landuse/landcover using Remote Sensing and GIS Techniques: A Case Study of Mahananda Catchment. *West Bengal International Journal of Research in Management Studies*, 2(2): 91-101.
21. Mavima, G., Soropa, G., Makurira, H. and Dzvairo, W., 2011.Sedimentation Impacts on Reservoir as a Result of Land Use on a Selected Catchment in Zimbabwe. *International Journal of Engineering Science and Technology*, *3*(8):6599-6608.
22. Mzuza, M. K., Weiguo, Z., Chapola, L. S., Tembo, M., Kapute, F., 2017. Determining sources of sediments at Nkula Dam in the Middle Shire River, Malawi, using mineral magnetic approach. *Journal of African Earth Sciences*. 2017; 126:23-32. DOI: 10.1016/j.jafrearsci.2016.11.023
23. Ogechi, B. A. and Waithaka, E. H., 2017. Landuse landcover changes and implications for food production: A case study of Keumbu Region Kisii County, Kenya. In Proceedings of the Scientific Conference Proceedings, Washington, DC, USA, 19 May 2017.
24. Owojori, A. and Xie, H., 2005. Landsat Image-based LULC Changes of San Antonio, Texas using Advanced Atmospheric Correction and Object-oriented Image Analysis Approaches. Paper Presented at the 5th International Symposium on Remote Sensing of Urban Areas, Tempe, AZ. https://www.researchgate.net/profile/Hongjie_Xie/publication/253839686_LANDSAT_IMAG.
25. Seif, A., and Mokarram, M., 2012. Change Detection of Gil Playa in the Northeast of Fars Province. *Iran Am. J. Sci. Res*, *86*, 122-130.
26. Shoyama, K., Braimoh, A. K., Avtar, R., Saito, O., 2018. Land Transition and Intensity Analysis of Cropland Expansion in Northern Ghana. *Environ. Manag.*2018, 62, 892–905.
27. UN-DESA, 2017. World Population Prospects: The 2017 Revision, Key Findings and Advance Tables. Working Paper No. ESA/P/WP/248. New York: United Nations. Accessed on 29th August, 2017 at *https://esa.un.org/unpd/wpp/publications/files/wpp2017_keyfindings.pdf*
28. Verburg, P. H., van Eck, J. R., de Hijs, T. C., Dijst, M. J., and Schot, P., 2004. Determination of land use change patterns in the Netherlands. *Environment and Planning B: Planning and Design,* 31(1): 125-150.
29. Viera, A. J. and Garrett, J. M., 2005. Understanding Inter-observer Agreement: The Kappa Statistic. *Family Med.,* 37(5), 360-363.
30. Weiss, E., and Milich, L., 1997. Errors in a standard method for generating interannual NDVI coefficient of variation (CoV) images. *International Journal of Remote Sensing*, *18*(18), 3743-3748.
31. Yigzaw, W., and Hossain, F., 2016. Landuse and landcover impact on probable maximum flood and sedimentation for artificial reservoirs: Case study in the Western United States. *Journal of Hydrologic Engineering*, *21*(2), 05015022.
32. Zhou, L., 2002. Impact of Land-use Changes on soil erosion in Upper reaches of Shiyang River in Arid Northwest China. In *IGARSS IEEE International Geoscience and Remote Sensing Symposium* (Vol. 4, pp. IV-639). IEEE.

Global Journal of Researches in Engineering: J
General Engineering
Volume 23 Issue 4 Version 1.0 Year 2023
Type: Double Blind Peer Reviewed International Research Journal
Publisher: Global Journals
Online ISSN: 2249-4596 & Print ISSN: 0975-5861

Evolution of the use of Nanoparticles in Cancer Diagnosis and Treatment

By Camila Andrea Gualdría Sandoval, Esperanza del Pilar Infante Luna & Luz Helena Camargo Casallas

Abstract- The use of nanoparticles in the health area is a research topic that has been increasing in recent years, from that perspective this work focused on making a characterization of nanoparticles, their evolution and interaction with blood, aspect addressed through the description of the biomagnetic fluid, focusing on characteristics such as viscosity and geometry. Also, the evolution of the applications or techniques in which nanoparticles have been used is presented, focusing the review on cancer treatments, for which the four progressive generations of this research field were considered, as well as the use of nanoparticles in diagnostic imaging. Finally, some fields of implementation and study in Colombia were identified. The review carried out allows concluding that the evolution of the use of nanoparticles.

Keywords: biomagnetic fluid, nanoparticles, magnetic nanoparticles, SPIONs

GJRE-J Classification: FOR Code: 0903

EVOLUTIONOFTHEUSEOFNANOPARTICLESINCANCERDIAGNOSISANDTREATMENT

Strictly as per the compliance and regulations of:

Evolution of the use of Nanoparticles in Cancer Diagnosis and Treatment

Camila Andrea Gualdría Sandoval [α], Esperanza del Pilar Infante Luna [σ] & Luz Helena Camargo Casallas [ρ]

Abstract- The use of nanoparticles in the health area is a research topic that has been increasing in recent years, from that perspective this work focused on making a characterization of nanoparticles, their evolution and interaction with blood, aspect addressed through the description of the biomagnetic fluid, focusing on characteristics such as viscosity and geometry. Also, the evolution of the applications or techniques in which nanoparticles have been used is presented, focusing the review on cancer treatments, for which the four progressive generations of this research field were considered, as well as the use of nanoparticles in diagnostic imaging. Finally, some fields of implementation and study in Colombia were identified. The review carried out allows concluding that the evolution of the use of nanoparticles.

Keywords: biomagnetic fluid, nanoparticles, magnetic nanoparticles, SPIONs.

I. Introduction

The term nanotechnology refers to a multidisciplinary field that deals with the research, design, synthesis, application of materials and functional systems by controlling substances at the nanometer level. The interest of nanotechnology is not only to manipulate matter on a small scale, but also to study the unique physical and chemical properties of nanostructures (e.g., surface properties, electrical conductivity and magnetic properties). In recent years, nanotechnology has had a major impact in areas such as biology and medicine (Rojas, Aguado, & González, 2016). With the aim of advancing in this field, a bibliographic review was carried out, oriented towards three topics: characterizing nanoparticles (np) and their evolution; describing the medium in which they move and therefore their interaction with it, and identifying the applications or techniques of nanotechnology in health sciences, specifically in cancer treatments (tumors), and the obtaining of diagnostic images through methods that use nanoscopic contrast agents or markers.

II. Characterization, Description and Evolution of the NP

The np are particles with dimensions of the order of 1 nm = 1x10^-9 m, which facilitates their application to different fields of nanotechnology, in medicine for example, they are used for the purpose of monitoring, control, construction or repair, defending or improving the human biological system at the molecular level (Wakaskar, 2018). Some of the np used in cancer treatments have been dentrimers, being np with three-dimensional tree-like structures in the range of 1-100 nm, they can host a variety of carrier molecules, both hydrophobic and hydrophilic and are useful delivery agents for genes, drugs and anticancer agents; thanks to their size and geometry they can be specifically controlled in groups, in order to possess pre-designed and specific physical and chemical properties (Alfonso & Casado, 2016).

On the other hand, micelles are hydrophobic spherical structures that are grouped to form the central core of the sphere in a liquid environment (Haley & Frenkel, 2008), so they are useful for the administration of water-insoluble drugs with sizes in the range of 10 - 50 nm (Urrejola et al., 2018). Nanospheres, on the other hand, are spherical structures composed of a matrix system where the surface can be modified by adding polymers and also biological materials, have a size in the range of 10 - 100 nm (Haley & Frenkel, 2008). From the perspective of their use as carriers, nanocapsules are vesicular systems with a central cavity or core to which it is possible to confine a drug, their size is in the range of 10 - 500 nm (Chávez, Olvera, Ganem, & Quintanar, 2002). Finally, we find the magnetic ones, on which we will go deeper, because their characteristics have made possible advances in the transport through the blood as a biomagnetic fluid.

a) *Magnetic Nanoparticles (MNP)*

They are np that are iron-based, therefore they can be manipulated by employing an external magnetic field (B) (Avval et al., 2020). Magnetite (Fe_3O_4) is a black ferromagnetic iron oxide of Fe(II) and Fe(III), which has been the most studied, due to the potential to act as an electron donor (Mohammed, Gomaa, Ragab, & Zhu, 2017).

b) *Ferrofluids*

When talking about ferrofluids, we refer to a colloidal dispersion made by a special multidomain particles based on iron oxide and iron hydroxide by a wet chemical method, which facilitates the steering capability under the influence of a B (Lübbe, Bergemann, Riess, et al., 1996). Additionally, these colloidal magnetic np have unique surface properties

Author α σ ρ: e-mails: cagualdrias@correo.udistrital.edu.co, epinfantel@udistrital.edu.co, lhcamargoc@udistrital.edu.co

that allow biocompatibility and biodegradability in addition to having minimal toxicity, they are suitable as drug-delivery vehicles that have excellent magnetic saturation (Liu, Xu, Wang, & Ke, 2008).

c) *Superparamagnetic*

They are a unique type of MNP, because they have many desirable properties, from the point of view of biomedical applications, such as: biocompatibility, biodegradability and ease of synthesis, to which we must add their superparamagnetic nature. On the other hand, they do not produce hysteresis, since they leave a zero residual magnetization after an external B is removed, this feature helps to prevent coagulation, so compared to other MNP, it reduces the possibility of agglomeration in the body (Mohammed, Gomaa, Ragab, & Zhu, 2017).

The size of these particles influences both their physicochemical and pharmacokinetic properties, so two groups are classified: Spions: (superparamagnetic iron oxides) are np that in particular are generally based on inorganic iron oxide coated with hydrophilic polymers, whose size is larger than 50 nm (including the coating). USpions: (ultra-small superparamagnetic iron oxides) are np that have a size smaller than 50 nm, being blood pooling agents they could be used for perfusion imaging enabling the diagnosis of cerebral or myocardial ischemic diseases (Zhang et al., 2020).

III. Characterization and Interaction of the Environment

Currently there is a field of research associated with the interaction of B with living beings, and in particular it has gained relevance in nanomedicine, from this perspective we can consider two basic areas: magnetobiology and biomagnetism. The former deals with the effects produced by magnetic fields on organisms, ranging from the orientation capacity of some animals, to the controversial damage to health caused by exposure to low-frequency electromagnetic waves. Biomagnetism, on the other hand, focuses on the study of the B associated to the organism itself, in particular, we refer to the biomagnetic fluid, which is found in organisms and reacts to the presence of a B. The results of these experimental fields are useful to obtain information that does not allow us to understand biophysical systems, to implement new clinical diagnostic techniques and to create new therapies centered on the use of np (Sosa, Alvarado, & Gonz, 2002).

a) *Blood as a Transport Medium for Nanoparticle*

The various applications of np as a means of transporting drugs or contrast chemicals, have led researchers to deepen both the knowledge of the blood, as the fluid through which these particles move, the interaction with the components thereof, and the incidence of external magnetic fields applied, in this sense, Bose & Banerjee, (2015) mention measurements made to estimate the magnetic susceptibility of blood and reported that this is between 3.5 X 10 ^-6 and 6.6 X 10 ^-7 for venous and arterial blood, respectively, also Bartoszek & Drzazga, (1999) show an experimental study of the magnetic anisotropy of blood cells at a B of up to 1.8 T for a temperature range between 75 - 295 K, employing torsional magnetometry.

Ichioka & Ueno, (2000) conducted in vivo experiments using rats as subjects, which were subjected to magnetic fields of 8 T, showing a reduction in blood flow and temperature of the animal. In the same direction, the in vitro experiments conducted by Haik, Pai & Chen (1999), in which they used human blood samples subjected locally to a B of the same intensity, reduced by 30%, additionally established that as the biofluid enters and exits the gradient of B, In relation to the biomagnetic flux in narrow channels, Tzirtzilakis in 2005 found that these are affected by a constant and local B (Bose & Banerjee, 2015).

b) *Simulating Biomagnetic Fluid (Blood)*

Liu, Zhu, Rao, Clausen & Aidun, (2018) simulate the biotransport of np under a complex cell flow environment using a multiscale method based on the Lattice Boltzmann method (LBM), the basic components of which include liquid-phase LBM processing, the red blood cell spectrum linkage method (SLM), and the Langevin dynamics (LD) method to capture pauses of np motion. In addition, extensive bidirectional coupling schemes are established to capture precise interactions between each component and thus simulate np transport in cellular blood flow with high efficiency.

In turn, Lee, Ferrari & Decuzzi, (2009) present a general mathematical model to predict the transport behavior of particles with different physical properties: size (nano-microparticles) and shape, as well as the material in which they are immersed, considering a linear laminar flow. Their results show that non-spherical particles, under the concurrent action of inertial and hydrodynamic forces, can deflect laterally, an effect known as hydrodynamic margination, increasing the probability of interaction with the wall surface. Thus, in blood, np will periodically oscillate around their trajectory, thus reducing their distance from the vessel wall, while the particles may actually separate with a net lateral deflection.

On the other hand, Duncan & Bevan, (2015) generated a Monte Carlo simulation, measuring the net interactions between np "decorated" by ligands, which possess distinct chemical structures, providing multiple interactions in self-assembly, and membrane proteins on the surfaces of healthy and diseased cells. From their analysis, they identify that these ligand-functionalized np are able to selectively bind to populations of diseased cells rather than healthy cells, proving attractive for improving the efficacy of drug therapies by using lower affinity ligands to target cancer cells with targeted membrane proteins.

Along the same lines, Müller, Fedosov & Gompper, (2014) performed simulations and attempted to study the marginal characteristics of carriers of different shapes and sizes using mesoscopic hydrodynamic simulations to explain the related physical mechanisms, finding that the properties of particle edges increase with increasing carrier size. The above results lead to the conclusion that addressing the various problems associated with drug delivery is a complex issue; its solution requires an interdisciplinary effort, including in vitro and in vivo experiments and realistic numerical simulations.

c) *Viscosity*

Blood viscosity and plasma viscosity are the best known parameters characterizing the properties of blood flow. Haik, Pai & Chen, (2001) conduct an investigation on the behavior of viscosity due to magnetic discharges in human blood, for which they carried out flow experiments on oxygenated blood in vitro and which is subjected to a B of up to 10 T. Additionally, they use a mathematical model to simulate biomagnetic fluid dynamics under similar conditions, which allows them to identify that the magnetization action will introduce a rotational motion to orient the magnetic fluid particles with the B (Afkhami & Renardy, 2017); however, the behavior and characteristics of the blood are unique to each patient. As a complement to the aforementioned computational experiments, Rukshin, Mohrenweiser, Yue & Afkhami, (2017) proposed a mathematical model describing the behavior of equations to visualize particle trajectories and calculate capture rates to assess the impact of various physical conditions on the success of magnetic drug targeting.

d) *Geometry of the Medium*

Another element to take into account in the characterization of the medium is the geometry, muscle arteries have three major geometrical differences with capillaries, for example in microvessels, the anti-slip boundary condition reduces the velocity of blood near the wall relative to the centerline and improves the ability to trap particles by weaker magnetic force due to lower resistance compared to millimeter vessels (Avilés et al., 2005). In this case, the force required is well below the maximum allowable exposure, however, due to the higher blood flow rate in muscles and blood vessels, the particles require a higher magnetic force to resist the "tenacity" that occurs in the opposite direction of particle motion.

IV. Evolution of Applications in Cancer Treatments, using NP

Cancer is a disease in which the cells of the human body acquire the ability to divide and multiply uncontrollably a (Sharma, Sharma, Punj, & Priya, 2019), this condition acquired by the diseased cells through mutations of the genome, as the cancer cells divide, leads to the fact that the new cells will inherit the same growth capacity and increase the number of cancer cells (Miller, 2018). The treatments for this disease are diverse and in any case, side effects must be considered, therefore, targeted treatments are an important option for patients. In this sense, the evolution in the use of np is presented, which is approached through four generations, identifying the main investigations and their results.

a) *First Generation*

The first experiment was performed "in vivo" by Lübbe et al, (1996), who developed a magnetic fluid to which drugs, cytokines and other molecules can chemically bind to allow these agents to be directed into an organism by an external high-energy B. They used male rats and mice, kept in a controlled environment. For which they used male rats and mice, kept in a controlled environment. For the design of the external B, using high-energy permanent magnets made of rare earths (neodymium), they consisted of disks or blocks with variable thickness, configured in the shape of a column or a block (see Figure 1). In this way, the magnets could be arranged more closely around the individual tumor configuration, with a B between 0.2 - 0.5 T (depending on tumor size). They tested two forms of therapy with the magnetic fluid: treatment of tumors by mechanical occlusion with the ferrofluid in high concentrations; and magnetic therapy, using small amounts of the ferrofluid as a drug carrier vehicle, which allowed epirubicin to be concentrated locally in the tumors.

The first part of the study focused on tolerance to ferrofluid and magnetically bound epirubicin. The results show that hematological and blood chemistry values did not change from baseline after injection of different amounts of ferrofluid. On the other hand, epirubicin caused changes in hematological parameters. Histological data showed that the magnetic particles accumulated in the liver and spleen, without causing significant hepatosplenomegaly, the latter two results were within predicted. After the sixth week of observation, one animal in each high-dose group died, possibly due to cardiovascular failure caused by sepsis. In those groups in which the highdose epirubicin was administered, the animals died quickly; in the low-dose groups, they died somewhat later, around 4 - 6 weeks. In all other groups, including those receiving low levels of epirubicin, the animals survived the observation

Global Journal of Researches in Engineering (J) Volume XXIII Issue IV Version I Year 2023

period (Lübbe, Bergemann, Huhnt, Fricke, & Riess, 1996).

The second part of this investigation focused on the mechanical embolization by the ferrofluid after its injection and concentration in the tumor by means of an external B, regardless of the type of tumor, there was a rapid and constant decrease in tumor volume within 14 days after treatment. It was impossible to reproduce this tumor response in the animals given only epirubicin, although the tumors responded to the high dose of this drug, this was only for a brief period and most of the animals in this group died shortly thereafter.

Subsequent experiments by Lübbe led to the conclusion that magnetic fluid is a good agent to decrease tumor volume and with further studies, it can be used in different forms of local cancer treatment in conjunction with high-energy magnetic fields, avoiding mortality of the subject (Lübbe., Bergemann, Brock, & McClure, 1999).

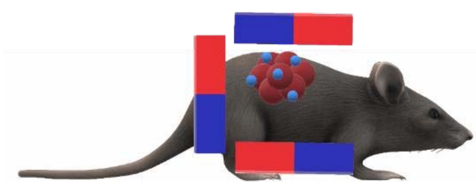

Source: own

Fig. 1: Graphic Illustration of Placement of Rare Earth Magnets in Block form on the Tumor to be Treated

Thus, in the second experiment, Lübbe et al., (1999) chose their subjects with an eligibility criterion among them, seven patients with breast cancer, two with chondrosarcoma, two with parotid squamous cell carcinoma, one with Ewing's sarcoma and two with malignant tumor; with a life expectancy of at least three months and renal preservation. Continuing their line of research, they employed anticancer drugs that would reversibly bind to magnetic fluids, which were focused on locally advanced tumors through a B disposed on the tumor surface outside the body.

They tested for magnetite concentration in the tumor, and 10 of the 14 patients, had intact skin covering the tumors, the other four showed wound healing and open superficial wounds. In the first four cases, since the B will obscure the shape of the magnetic block attached to the tumor, it is easy to observe magnetite absorption into the tumor, this discoloration lasted for 24 - 36 hours and then disappeared completely, these areas were not locally toxic and ensured that the discoloration could not be removed to rule out the possibility of iron deposition from the magnetic lumps in the superficial layer of the skin. So the targeted magnetic drug with epirubicin was well tolerated and mild tumor reductions were achieved at day 10 and some small responses at day 40 (Lübbe. et al., 1999) (Lübbe, Bergemann, Riess, et al., 1996).

b) Second Generation

Based on the results described above, Alexiou et al. (2000) used mitoxantrone-linked ferrofluid (FF-MTX) to treat rabbits with squamous cell carcinoma and concentrated it under a B. When the tumor reaches a volume of 3500 mm^3, FF-MTX is injected intra-arterially or intravenously. When an external B is focused on the tumor, it is activated by an electromagnet with a maximum flux density of 1.7 T, producing a non-uniform B, both in direction and magnitude, a feature that is crucial for the use of magnetic drugs. Magnetic drug targeting is a means of keeping the chemotherapeutic agent at the desired site of activity, thus increasing efficacy and decreasing systemic toxicity.

Only when the MTX dose was increased to 75% and 100%, tumor remission was observed, but this resulted in severe side effects (hair loss, ulcers and leukopenia). However, this "magnetically targeted drug" provides a unique opportunity to locally treat malignant tumors without systemic toxicity. In addition, it is possible to use these magnetic particles as "carrier systems" for various anticancer agents such as radionuclides, antibodies and cancer-specific genes (Alexiou et al., 2002).

c) Third Generation

Under another line of research, Gitter & Odenbac (2011) presented experimental results based on systematic "in vitro" quantitative measurements of a tube model simulating a Y-branched artery, in which they conclude that the success of particle orientation towards branching depends largely on the crossing point and the magnetic force at the site, elements that as previously mentioned must be evaluated.

For their part, Krukemeyer, Krenn, Jakobs & Wagner, (2011) performed a verification method on the effectiveness of cytostatic drugs coupled to ferromagnetic np and extracorporeal magnets, using 42 adult rats that were transfected with rhabdomyosarcoma. In the biodistribution assay, concentrations of mitoxantrone iron oxide and conventional mitoxantrone with and without 0.6 T magnets were measured in vitro in plasma and tumor tissue for one and two doses. During magnetic drug treatment, iron particles are rapidly removed and remain in the area where the tumor remained.

d) Fourth Generation

From the perspective of assessing patient safety, Attar et al., (2016) propose a configuration which investigates the thermal effect of superparamagnetic np on human cells, present a study considering general details on the design and construction of the configuration needed to generate a safe B to examine the thermal effect of superparamagnetic np on human cancer cells, then performed a series of experimental tests to study the effect of B on the cells for 30 minutes, which allowed them to calculate the temperature rise and specific absorption. While it is true, hyperthermia treatment (Eivazzadeh-Keihan et al., 2019) is a mechanism to destroy malignant cells by increasing tissue temperature up to a range of 42 - 45°C, temperatures above 45 - 56°C, can cause necrotizing damage and subsequent tissue inflammation (Shabestari Khiabani, Farshbaf, Akbarzadeh, & Davaran, 2017). In this regard, ferromagnetic materials are commonly used to treat hyperthermia and the general procedure involves the allocation of magnetic particles of various sizes depending on the type of treatment to the tissue, then, when the particles generate heat through two mechanisms (including hysteresis and eddy currents), the tissue is exposed to an alternating B.

Among the advances in this fourth generation, it is important to mention the work of Al-Jamal et al., (2018), who performed in vivo experimentation based on a solid theoretical foundation for the design of a magnetic nanocarrier, capable of magnetizing uptake after intravenous administration, in order to elucidate the parameters necessary for the detection of magnetic tumors. Because long-circulating polymeric magnetic nanocarriers are capable of encapsulating increasing amounts of superparamagnetic iron oxide np (SPIONs) in a biocompatible oil carrier, they were able to study the effects of SPION loading and applied B intensity on magnetic tumor targeting in tumor-bearing mice.

Another important element is the fact that the high loading of SPIONs eliminates the need to use highly magnetized np and the oil core promotes high hydrophobic drug loading, compared to polymer-coated SPIONs. The objective of this experiment was to evaluate the key factors influencing magnetic targeting efficiency, including the loadings of SPIONs on m-NC (polymeric oil-core magnetic nanocapsules) and the magnitude of the magnetic force applied at a distance. Under controlled conditions, they quantified magnetic targeting in vivo and found that it was directly proportional to SPIONs loading and B intensity, however, higher SPIONs loading resulted in reduced blood circulation time and stabilization of magnetic targeting.

V. Diagnostic Imaging with NP

Due to the physicochemical properties presented by nanomaterials, the development of nanodevices as contrast agents in medical imaging has clear advantages over traditional agents used in the diagnosis of diseases, among which we can mention: better optical dispersion (absorption of light in the material, with a clearer visual spectrum), increased biocompatibility, decreased probability of denaturation and especially, their ability to bind to ligands, which turns them into devices with multiple functions that bind to cells, simultaneously allowing imaging for diagnosis and transport of drugs to specific sites, thus, achieving targeted and efficient treatment (Minbashi, Kordbacheh, Ghobadi, & Tuchin, 2020).

Nan, Suciu, Ardelean, Senila & Turcu (2020), report a simple reaction strategy for the synthesis of magnetic iron oxide np's stabilized with ethylenediaminetetraacetic acid (EDTA) followed by the chelation reaction of gadolinium (Gd) ions. These results show that these magnetic nanosystems represent a promising dual-mode contrast in agents for MRI applications with biomedical applications in mind.

Another type of contrast agent used for feature detection are SPIONs, due to their long half-life and small diameter, they provide a variety of possibilities to visualize intracellular targets, they can also be coupled with fluorescent dyes so that these particles can be detected in vitro and in vivo by optical fluorescence methods.

In this technique, SPIONs are inhibited by the binding of polyethylene glycol (PEG) chains that are anchored by peptide substrates shed by proteases, in diagnostic imaging, dextran-coated SPIONs provide stability for imaging, such as magnetic resonance imaging, computed tomography and optical fluorescence (Cicha, Lyer, Alexiou, & Garlichs, 2013).

In this direction, Nahrendorf et al., (2014) performed a study, where single-crystalline fluorochromelabeled SPIONs in the infrared were chelated with DTPA (diethylenetriaminepentaacetic acid) to allow binding of the PET radiotracer 64 Cu. While the iron oxide core provided the MRI contrast, the fluorochrome served for fluorescence imaging (fluorescence microscopy, flow cytometry and fluorescence mediated tomography), and the 64Cu radiotracer allowed PET (positron emission tomography) imaging, while the iron oxide core provided the MRI contrast.

The reported results show a trend towards the increasing use of SPIONs in various biomendicine applications.

VI. Implementation in Colombia

Jaimez, Gonzales, Granados, Álvarez & Espitia, (2012) of the Pontificia Universidad Javeriana carried out a review article to see what advances and expectations there are in surgery to date, explaining what nanotechnology consists, its basic principles and some utilities in the field of surgery. On the other hand, Mendez and Muñoz [43] of the National University of Colombia wrote an article describing the clinical and molecular characteristics of premalignant lesions and oral cancer, as well as diagnostic methods using nanotechnology (nanochips, nanosensors, etc.) as an effective method for the early detection of cancer. Rodriguez, Moyano and Roa [44] from the Universidad Distrital Francisco Jose de Caldas, obtained a mathematical model and a computational simulation

Global Journal of Researches in Engineering (J) Volume XXIII Issue IV Version I Year 2023

describing the trajectory of magnetic np injected near the target tissue. The magnetic np propagate along the blood vessel in the Z-direction and point to the target area through a cylindrical magnet located outside the body generating a constant B.

Likewise, Gallo and Ossa [45] from the University of Antioquia carried out a study where they evaluated two silver np synthesis processes, using, in addition, a biofunctionalization process with polyethylene glycol (PEG) to improve the anchoring properties and biocompatibility of the np, for possible treatments against skin cancer.

In the master's thesis in engineering of Pantoja, (2020) of the Universidad Distrital Francisco José de Caldas, he has focused on proposing a mathematical model that can estimate the trajectory of NPM through the action of an external B and the blood flow is obtained through computational simulation. The model includes forces that significantly affect NPM dynamics, including magnetic fields generated by magnets, scattering forces, and drag. Molecular dynamics results show that NPM under the action of a B will be captured and attracted by it, so that they can be directed to the proposed target.

The reported results show that although there is no defined line of research on the use of np in Colombia, they nevertheless highlight the possibility of joining efforts to strengthen this field of knowledge.

VII. Conclusion

The np seen as drug nanocarriers play a leading role and it is in this direction in which research has been carried out, from this perspective to characterize the np and evaluate its evolution, it is identified that currently the work is focused on superparamagnetic np. The review carried out provides clarity regarding the evolution of np, as well as the importance of understanding how their kinematics are through the blood, seen as a biomagnetic fluid, a characteristic that has allowed the evaluation of strategies for directing nanoparticles that move through this medium, in this direction the main advances are associated with SPIONs for their biomedical application. There are many challenges from the treatment of diseases, starting from an accurate diagnosis to achieve an effective treatment, which involves a reduction of the adverse effects that these may have on the organism of the treated subject, in this sense the np offer a viable possibility both in diagnosis and therapy with low adverse effects, due to the possibility of targeting the treatment.

References Références Referencias

1. Afkhami, S., & Renardy, Y. (2017). Ferrofluids and magnetically guided superparamagnetic particles in flows: a review of simulations and modeling. *Journal of Engineering Mathematics*, *107*(1), 231–251. https://doi.org/10.1007/s10665-017-9931-9
2. Al-Jamal, K. T., Bai, J., Wang, J. T. W., Protti, A., Southern, P., Bogart, L., … Pankhurst, Q. A. (2018). Magnetic Drug Targeting: Preclinical in Vivo Studies, Mathematical Modeling, and Extrapolation to Humans. *Nano Letters*, *16*(9), 5652–5660. https://doi.org/10.1021/acs.nanolett.6b02261
3. Alexiou, C., Arnold, W., Klein, R. J., Parak, F. G., Hulin, P., Bergemann, C., … Lubbe, A. S. (2000). Locoregional cancer treatment with magnetic drug targeting. *Cancer Research*, *60*(23), 6641–6648.
4. Alexiou, Ch, Schmidt, A., Klein, R., Hulin, P., Bergemann, C., & Arnold, W. (2002). Magnetic drug targeting: Biodistribution and dependency on magnetic field strength. *Journal of Magnetism and Magnetic Materials*, *252*(1-3 SPEC. ISS.), 363–366. https://doi.org/10.1016/S0304-8853(02)00605-4
5. Alfonso, B., & Casado, C. (2016). DENDRÍMEROS: MACROMOLÉCULAS VERSÁTILES CON INTERÉS INTERDISCIPLINAR. *Journal of Chemical Information and Modeling*, *01*(01), 1689–1699.
6. Attar, M. M., Amanpour, S., Haghpanahi, M., Haddadi, M., Rezaei, G., Muhammadnejad, S., … Javadi, S. (2016). Thermal analysis of magnetic nanoparticle in alternating magnetic field on human HCT-116 colon cancer cell line. *International Journal of Hyperthermia*, *32*(8), 858–867. https://doi.org/10.1080/02656736.2016.1204667
7. Avilés, M. O., Ebner, A. D., Chen, H., Rosengart, A. J., Kaminski, M. D., & Ritter, J. A. (2005). Theoretical analysis of a transdermal ferromagnetic implant for retention of magnetic drug carrier particles. *Journal of Magnetism and Magnetic Materials*, *293*(1), 605–615. https://doi.org/10.1016/j.jmmm.2005.01.089
8. Avval, Z. M., Malekpour, L., Raeisi, F., Babapoor, A., Mousavi, S. M., Hashemi, S. A., & Salari, M. (2020). Introduction of magnetic and supermagnetic nanoparticles in new approach of targeting drug delivery and cancer therapy application. *Drug Metabolism Reviews*, *52*(1), 157–184. https://doi.org/10.1080/03602532.2019.1697282
9. Bartoszek, M., & Drzazga, Z. (1999).; *A study of magnetic anisotropy of blood cells*. *197*, 573–575.
10. Bose, S., & Banerjee, M. (2015). Magnetic particle capture for biomagnetic fluid flow in stenosed aortic bifurcation considering particle-fluid coupling. *Journal of Magnetism and Magnetic Materials*, *385*, 32–46. https://doi.org/10.1016/j.jmmm.2015.02.060
11. Chávez, F., Olvera, B. I., Ganem, A., & Quintanar, D. (2002). Liberación de sustancias lipofílicas a partir de nanocápsulas poliméricas. *Journal of the Mexican Chemical Society*, *46*(4), 349–356.
12. Cicha, I., Lyer, S., Alexiou, C., & Garlichs, C. D. (2013). Nanomedicine in diagnostics and therapy of cardiovascular diseases: Beyond atherosclerotic

Global Journal of Researches in Engineering (J) Volume XXIII Issue IV Version I Year 2023

plaque imaging. *Nanotechnology Reviews*, *2*(4), 449–472. https://doi.org/10.1515/ntrev-2013-0009
13. Duncan, G. A., & Bevan, M. A. (2015). Computational design of nanoparticle drug delivery systems for selective targeting. *Nanoscale*, *7*(37), 15332–15340. https://doi.org/10.1039/c5nr03691g
14. Eivazzadeh-Keihan, R., Radinekiyan, F., Maleki, A., Salimi Bani, M., Hajizadeh, Z., & Asgharnasl, S. (2019). A novel biocompatible core-shell magnetic nanocomposite based on cross-linked chitosan hydrogels for in vitro hyperthermia of cancer therapy. *International Journal of Biological Macromolecules*, *140*, 407–414. https://doi.org/10.1016/j.ijbiomac.2019.08.031
15. Gallo, J., & Ossa, C. (2019). Fabricación y caracterización de nanopartículas de plata con potencial uso en el tratamiento del cáncer de piel. *Ingeniería y Desarrollo*, *37*(1), 88–104. https://doi.org/10.14482/inde.37.1.6201
16. Gitter, K., & Odenbach, S. (2011). Experimental investigations on a branched tube model in magnetic drug targeting. *Journal of Magnetism and Magnetic Materials*, *323*(10), 1413–1416. https://doi.org/10.1016/j.jmmm.2010.11.061
17. Haik, Y., Pai, V., & Chen, C. J. (1999). Development of magnetic device for cell separation. *Journal of Magnetism and Magnetic Materials*, *194*(1), 254–261. https://doi.org/10.1016/S0304-8853(98)00559-9
18. Hajiaghajani, A., Hashemi, S., & Abdolali, A. (2017). Adaptable setups for magnetic drug targeting in human muscular arteries: Design and implementation. *Journal of Magnetism and Magnetic Materials*, *438*, 173–180. https://doi.org/10.1016/j.jmmm.2017.04.058
19. Haley, B., & Frenkel, E. (2008). Nanoparticles for drug delivery in cancer treatment. *Urologic Oncology: Seminars and Original Investigations*, *26*(1), 57–64. https://doi.org/10.1016/j.urolonc.2007.03.015
20. Jaimes, S., Gonzáles, A., Granados, C., Álvarez, D., & Espitia, E. (2012). Redalyc.Nanotecnología: avances y expectativas en cirugía. *Revista Colombiana de Cirugía*, *27*, 158–166.
21. Krukemeyer, M. G., Krenn, V., Jakobs, M., & Wagner, W. (2012). Mitoxantrone-iron oxide biodistribution in blood, tumor, spleen, and liver - Magnetic nanoparticles in cancer treatment. *Journal of Surgical Research*, *175*(1), 35–43. https://doi.org/10.1016/j.jss.2011.01.060
22. Lee, S. Y., Ferrari, M., & Decuzzi, P. (2009). Shaping nano-/micro-particles for enhanced vascular interaction in laminar flows. *Nanotechnology*, *20*(49). https://doi.org/10.1088/0957-4484/20/49/495101
23. Liu, H. D., Xu, W., Wang, S. G., & Ke, Z. J. (2008). Hydrodynamic modeling of ferrofluid flow in magnetic targeting drug delivery. *Applied Mathematics and Mechanics (English Edition)*, *29*(10), 1341–1349. https://doi.org/10.1007/s10483-008-1009-y
24. Liu, Zhu, Y., Rao, R. R., Clausen, J. R., & Aidun, C. K. (2018). Nanoparticle transport in cellular blood flow. *Computers and Fluids*, *172*, 609–620. https://doi.org/10.1016/j.compfluid.2018.03.022
25. Lübbe., Bergemann, C., Brock, J., & McClure, D. G. (1999). Physiological aspects in magnetic drug-targeting. *Journal of Magnetism and Magnetic Materials*, *194*(1), 149–155. https://doi.org/10.1016/S0304-8853(98)00574-5
26. Lübbe, A. S., Bergemann, C., Huhnt, W., Fricke, T., & Riess, H. (1996). *Lübbe1996_Preclinical*. 4694–4701.
27. Lübbe, A. S., Bergemann, C., Riess, H., Schriever, F., Reichardt, P., Possinger, K., … Huhn, D. (1996). Clinical experiences with magnetic drug targeting: A phase I study with 4'-epidoxorubicin in 14 patients with advanced solid tumors. *Cancer Research*, *56*(20), 4686–4693.
28. Méndez, B., & Muñoz, C. (2012). *Nanochips y nanosensores para eldiagnóstico temprano de cáncer oral: una revisión*. (67), 131–147.
29. Miller, M. E. (2018). *Human Diseases and Yeast.Pdf* (First edit). New York: Momentum Press Health.
30. Mohammed, L., Gomaa, H. G., Ragab, D., & Zhu, J. (2017). Magnetic nanoparticles for environmental and biomedical applications: A review. *Particuology*, *30*, 1–14. https://doi.org/10.1016/j.partic.2016.06.001
31. Müller, K., Fedosov, D. A., & Gompper, G. (2014). Margination of micro- and nano-particles in blood flow and its effect on drug delivery. *Scientific Reports*, *4*, 1–8. https://doi.org/10.1038/srep04871
32. Nahrendorf, M., Zhang, H., Hembrador, S., Panizzi, P., Sosnovik, D. E., Aikawa, E., … Weissleder, R. (2008). Nanoparticle PET-CT imaging of macrophages in inflammatory atherosclerosis. *Circulation*, *117*(3), 379–387. https://doi.org/10.1161/CIRCULATIONAHA.107.741181
33. Nan, A., Suciu, M., Ardelean, I., Şenilă, M., & Turcu, R. (2020). Characterization of the Nuclear Magnetic Resonance Relaxivity of Gadolinium Functionalized Magnetic Nanoparticles. *Analytical Letters*, *0*(0), 1–16. https://doi.org/10.1080/00032719.2020.1731522
34. Pantoja, J. (2020). *nanopartículas magnéticas en flujo sanguíneo para tratamiento de cáncer*. Universidad Distrital Francisco José de Caldas.
35. Rodriguez, D., Moyano, J., & Roa, L. (2018). Estudio por dinámica molecular browniana de nanopartículas bajo efectos de campo magnéticos externos. *INGENIEROS MILITARES*, *13*(9), 90–98.
36. Rojas, Y., Aguado, K., & Gonz´alez, I. (2016). La nanomedicina y los sistemas de liberación de fármacos: ¿la revolución de la terapia contra el

cáncer? Educación Química, 27 (4), 286–291. https://doi.org/10.1016/j.eq.2016.07.002

37. Rukshin, I., Mohrenweiser, J., Yue, P., & Afkhami, S. (2017). Modeling superparamagnetic particles in blood flow for applications in magnetic drug targeting. *Fluids*, *2*(2), 1–12. https://doi.org/10.3390/fluids2020029
38. Shabestari Khiabani, S., Farshbaf, M., Akbarzadeh, A., & Davaran, S. (2017). Magnetic nanoparticles: preparation methods, applications in cancer diagnosis and cancer therapy. *Artificial Cells, Nanomedicine and Biotechnology*, *45*(1), 6–17. https://doi.org/10.3109/21691401.2016.1167704
39. Sharma, V. R., Sharma, A. K., Punj, V., & Priya, P. (2019). Recent nanotechnological interventions targeting PI3K/Akt/mTOR pathway: A focus on breast cancer. *Seminars in Cancer Biology*, *59*(July 2019), 133–146. https://doi.org/10.1016/j.semcancer.2019.08.005
40. Sosa, M., Alvarado, J. J. B., & Gonz, J. L. (2002). *Tecnicas biomagneticas y su comparacion con los metodos bioelectricos*. *48*(5), 490–500.
41. Tong, S., Zhu, H., & Bao, G. (2019). Magnetic iron oxide nanoparticles for disease detection and therapy. *Materials Today*, *31*(December), 86–99. https://doi.org/10.1016/j.mattod.2019.06.003
42. Urrejola, M. C., Soto, L. V, Zumarán, C. C., Peñaloza, J. P., Álvarez, B., Fuentevilla, I., & Haidar, Z. S. (2018). Sistemas de Nanopartículas Poliméricas II: Estructura, Métodos de Elaboración, Características, Propiedades, Biofuncionalización y Tecnologías de Auto-Ensamblaje Capa por Capa (Layer-by-Layer Self-Assembly). *International Journal of Morphology*, *36*(4), 1463–1471. https://doi.org/10.4067/s0717-95022018000401463
43. Wakaskar, R. R. (2018). General overview of lipid–polymer hybrid nanoparticles, dendrimers, micelles, liposomes, spongosomes and cubosomes. *Journal of Drug Targeting*, *26*(4), 311–318. https://doi.org/10.1080/1061186X.2017.1367006
44. Zhang, G., Zhang, L., Si, Y., Li, Q., Xiao, J., Wang, B., Tian, G. (2020). Oxygen-enriched Fe3O4/Gd2O3 nanopeanuts for tumor-targeting MRI and ROS-triggered dual-modal cancer therapy through platinum (IV) prodrugs delivery. *Chemical Engineering Journal*, *388*(February), 124269. https://doi.org/10.1016/j.cej.2020.124269

Global Journal of Researches in Engineering: J
General Engineering
Volume 23 Issue 4 Version 1.0 Year 2023
Type: Double Blind Peer Reviewed International Research Journal
Publisher: Global Journals
Online ISSN: 2249-4596 & Print ISSN: 0975-5861

Effect of Interlayer Thickness on Mechanical Properties of Steel/Polymer/Steel Laminates Fabricated by Roll Bonding Technique

By Payam Maleki, Abbas Akbarzadeh & Mahdi Damghani
University of the West of England (UWE)

Abstract- Nowadays, metal/polymer/metal laminates are extensively used in various industries due to their unparalleled properties. In this study, the roll bonding process was employed for lamination of low carbon steel (St14) and semi-melted thermoplastic polyurethane sheets. The T-peel and Single Lap Shear (SLS) tests were conducted to determine the optimal rolling speed to achieve the highest bond strength between the polymer core and the steel skins. Then, with the goal of investigation of the effect of polymer volume fraction on the mechanical properties of laminates, the lamination process was performed at the optimal rolling speed and various thickness reductions. The uniaxial tensile tests were conducted at three directions of 0°, 45°, and 90° with respect to rolling direction for the skin sheet and four different laminates. The results of both T-peel and SLS tests recommend the lowest rolling speed (25 rpm) to acquire maximum bond strength. The results of tensile tests show that the mechanical properties of the laminates depend on the sample direction.

Keywords: metal/polymer/metal laminate sheet, roll bonding, thermoplastic polyurethane, low carbon steel sheet, mechanical properties.

GJRE-J Classification: LCC: TA401-492

Effect of Interlayer Thickness on Mechanical Properties of Steel/Polymer/Steel Laminates Fabricated by Roll Bonding Technique

Payam Maleki [α], Abbas Akbarzadeh [σ] & Mahdi Damghani [ρ]

Abstract- Nowadays, metal/polymer/metal laminates are extensively used in various industries due to their unparalleled properties. In this study, the roll bonding process was employed for lamination of low carbon steel (St14) and semi-melted thermoplastic polyurethane sheets. The T-peel and Single Lap Shear (SLS) tests were conducted to determine the optimal rolling speed to achieve the highest bond strength between the polymer core and the steel skins. Then, with the goal of investigation of the effect of polymer volume fraction on the mechanical properties of laminates, the lamination process was performed at the optimal rolling speed and various thickness reductions. The uniaxial tensile tests were conducted at three directions of 0°, 45°, and 90° with respect to rolling direction for the skin sheet and four different laminates. The results of both T-peel and SLS tests recommend the lowest rolling speed (25 rpm) to acquire maximum bond strength. The results of tensile tests show that the mechanical properties of the laminates depend on the sample direction. It is also observed that as the volume fraction of the polymer in the laminate structure increases, the yield strength, tensile strength and elastic modulus decrease. The bond strength of the metal/ polymer interface is directly related to the ductility behavior of the laminates.

Keywords: metal/polymer/metal laminate sheet, roll bonding, thermoplastic polyurethane, low carbon steel sheet, mechanical properties.

I. Introduction

In recent years, there has been growing research in developing materials that are lightweight and have enhanced mechanical properties compared to traditional and conventional metallic structures such as aluminum, steel, titanium, etc. During the past decades, the widespread use of traditional metallic structures has led to an abundance of readily available design data supported by extensive and expensive experimental testing that makes designing and analyzing such structures safe and more convenient. For instance, the use of aluminum alloys for more than 70 years in the manufacture of aerostructures has led to a plethora of both available design data and past experiences. This makes it convenient and safe for designers and structural analysts to use such materials in the design of aerostructures. Furthermore, the use of optimization techniques, i.e. topology, topography and size optimizations, has enabled structural designers and analysts to make metallic structures more lightweight. The use of modern manufacturing techniques such as Additive Layer Manufacturing (ALM) for metals has also contributed to making components that are lightweight. Whilst these approaches in design and manufacture are valid for single purpose structures, i.e. to be load bearing only, they are not suitable for when the structure has to be multi-functional. For instance, the metallic structures may exhibit desirable structural stiffness and strength but are not well suited for applications where high comparable specific stiffness and strength, improved isolation, superior vibration and sound damping properties and improved ductility are required [1]. Hence, scientists have resorted to alternative material systems and manufacturing methods. Amongst such material systems, hybridization has the potential to provide an economical mean [2], [3] to create material systems that can combine the advantages of miscellaneous materials, i.e. low density, high bending resistance, energy absorption, high load-capacity at low weight and etc., with each other and yield a material system that exploits the advantage of each constituent material meeting the required functions of a structure.

Amongst hybrid structures, three-layered metal/polymer/metal or multi-layer sheets, offer a great potential for the automotive, construction, naval industries and aerostructures. For instance, GLARE, a combination of aluminum layers and a Glass Fiber Reinforced Polymer (GFRP) has been applied in the construction of Airbus A380 double decker aircraft [1]. Another example is the use of Aramid Reinforced ALuminum Laminate (ARALL) for a damage tolerant wing design particularly areas prone to the fatigue loading [4]. It is worth noting that for newly adapted lightweight material systems, such as hybrid structures of metals-polymers, future gains are obtained with respect to environmental protection and sustainability. Metal/polymer/metal laminates as hybrid materials are also an alternative to homogeneous metal sheets that have polymeric properties as well as metallic characteristics. Good formability, excellent mechanical properties, lightweight, and acoustic and vibration

Author α σ: Department of Materials Science and Engineering, Sharif University of Technology, Tehran, Iran.
Author ρ: Department of Engineering, Design and Mathematics (EDM), University of the West of England (UWE), Bristol, UK.
e-mail: mahdi.damghani@uwe.ac.uk

damping are the three-layer sheets characteristics. The usage of these sheets is common in various industries.

Three-layered examples of metal/polymer/metal composites such as HYLITE have been used in automotive industry, due to their high mechanical and formability properties and being lightweight [5]. HYLITE is an aluminum/polypropylene/aluminum with thicknesses $0.2/0.8/0.2mm$ which was used in the construction of Audi A2. Another example is the use of BONDAL, a steel/polypropylene/steel composite known as steel counterpart to HYLITE, with a polymer core having approximate thickness of 50 μm. BONDAL has layer thicknesses of $0.5/0.5/0.5\,mm$ and is used for damping applications such as reducing radiating construction noise. It is worth noting that such composite material systems are being used in the aerospace industry as a result of their excellent compressive strength, high corrosion resistance, high toughness and workability. Furthermore, these sheets are currently being used in home appliances such as dishwashers and lawnmowers, where vibration and sound damping are crucial. Depending on the application of three-layer sandwich sheets in the industry, the ratio of the metal skin thickness to the polymer core, the type of metal and polymer, and the manufacturing and bonding of three-layer sheets are different.

Kim et al. [6] classified metal/polymer/metal three-layer laminates into three categories:

- Laminates with low-density polymeric core, containing 40% to 60% of the total thickness (lightweight).
- Laminates with thin polymeric core, containing 20% of the total thickness (acoustic damper).
- Laminates with very thin polymeric core (or without core) where the thickness and nature of the skins can be different (to take advantage of the different properties of both layers).

The three-layer composites metal skins mostly consist of steel sheets (often stainless steel) [7] or aluminum alloys such as AA5052 [8], AA5754 [9], and AA5182 [10] with different thicknesses. The most important criteria for selecting steel and aluminum sheets are high mechanical and formability properties [11], flexural stiffness, corrosion resistance, joinability, dent resistance, [12] and cost reduction [13]. Considering the superior inherent formability of the steel compared to aluminum, three-layer steel/polymer/steel sheets offer a higher stiffness-to-weight ratio than aluminum and steel monolithic sheets. In the assortment made by Hayashi et al. [14], specifically for laminated steel sheets, these laminates are divided into two categories; (i) vibration-damping sheets, i.e. with thickness composition of core $= 0.03\,mm - 0.1\,mm$ and skin $= 0.15\,mm - 1.6\,mm$, and (ii) lightweight laminate sheets, i.e. with thickness composition of core $= 0.2\,mm - 1\,mm$ and skin $= 0.1\,mm - 0.4\,mm$. Moreover, there are a variety of polymers to be selected as the middle layer. Polypropylene [10], polyethylene [15], polyolefin (PP-PE) [7], and polyamide [16] are the most popular polymers used in three-layer laminates. The chief reasons for choosing these polymers are low density, good mechanical properties, good chemical stability, low cost, and high-temperature resistance [12]. These polymers usually have low wettability and bondability in contact with other surfaces due to their low-polarity behavior. Therefore, various adhesive films are used to attach the polymer core to metal adherends. Common adhesives used in the manufacturing of three-layer laminates are hot-melt polyethylene adhesive film [8], maleic polyethylene adhesive film [9], Ethylene-Vinyl Acetate (EVA) film [10], epoxy resin (koratac FL 201) [17] and PolyproPylene Grafted Maleic Anhydride (PP-G-MA) thin film [18]. Due to the indirect bonding of the metal to the polymer and the presence of an additional layer and subsequently the dependence of metal/ polymer interface strength on adhesive strength, and considering the subsequent mechanical and metallurgical processes, appropriate selection of the adhesive is crucial. In some studies, adhesives have been used directly as an intermediate layer (without the polymer core) between two metals [13]. The results show that the presence of adhesive between the two steel layers, while improving the laminate elongation, and delaying the necking, increases the formability of the three-layer sheet compared to the two-layer sheet without the adhesive. Adhesive bonding (manual lamination) [19], hot [17] and cold roll bonding [20], and hot pressing [9] are well-known processes in the production of metal/polymer/metal laminates. Carrado et al. [1], by comparing the roll bonded and hot-press bonded specimens of the same thickness, showed that the initial crack strength of the rolled sheet was higher than that of the hot-pressed sheet. Kazemi et al. [9] applied three-point bending test on the aluminum/ polyurethan/aluminum three-layer sheet produced by the hot-pressing method. They related the debonding observed in the interface of aluminum/polyethylene to the creation, growth, and connection of micro-voids formed on the polymer surface during the hot pressing. The thickness and physical and mechanical properties of the polymer core and the bond strength affect the mechanical properties, formability, paintability, and weldability of the three-layer laminates sheet. Harhash et al. [7] reported the decrease in density and subsequently weight-saving as a positive and decrease in tensile and yield strength as an adverse effect of increasing the volume fraction of the polymer in the three-layer composite sheets (constant skins thickness). The importance of the polymeric layer shear strength is revealed where the shear force generated between the skin layers during the various forming processes (bending, drawing, etc.) overcomes the shear strength of the polymer and interfacial delamination occurs. It was observed that weak polymer core causes skin sheets to slide on the other layer (lubricant-like behavior), resulting in a premature splitting [21]. By investigating the deep drawing process of the three-layer sheets with different polymer cores, Liu et al. [15] showed that the drawability of three-layer sheets becomes poor as the thickness and strength of the polymeric core increase. Kim et al. [10] attributed the improvement in the formability of the three-layer sheets to the high elongation of the polymer core and the high bond strength of the metal/polymer interface. It is demonstrated that for two laminate sheets of the same thickness and steel skins, the sheet with polypropylene core shows lower springback than the laminate with the Poly Vinyl Chloride (PVC) core [22]. This is attributed to higher strength of the PVC sheet compared to the polypropylene sheet. Since three-layer sheets in the car body are placed in the paint bath (temperature of 200°C for 30 minutes) after the forming stage, the polymeric core must have a melting temperature of more than 200°C to maintain its structure [23]. If the melting temperature of the polymer is less than the painting temperature, the polymer melts, and the flow of the polymer disturbs the structure of the part, and the paint bath becomes contaminated. Saito et al. [24] and Oberle et al. [25] in two separate investigations demonstrated that, since during spot welding process, the polymer core is heated and pressurized by the welding electrode, to improve the weldability of the three-layer sheet and the formation of an ideal weld, the polymer core must flow away from the welded area. As such, the flow properties of the polymeric core should be optimal so that the delamination does not occur in the composite during the welding and painting processes. Studies have shown that the surface treatment of the skin metal sheet such as corona treatment [1] and preheating plus wire brushing [26] effectively improves the surface energy and wettability and produces more contact surfaces. This leads to the enhancement of shear strength and formability of the three-layer sheet.

It is evident from the literature that the manufacture of multilayer composites is challenging because of significant differences in the mechanical properties and adhesion characteristics of polymeric core and metallic face sheets. This unique combination of materials requires advanced joining techniques to ensure a strong bond between the joining layers. Thus far, few studies have been carried out to consider the impact of fabrication methods, core volume fraction and orientation of Steel/Polymer/Steel (S/P/S) laminate sheets on its overall mechanical properties. Subsequently, considering that many parameters are involved in the manufacture and the final properties of this type of composite material systems, an exact evaluation is necessary to identify and achieve the mechanical properties of the composite for each specific application.

The present study holds significant implications for the field of metal/polymer composites and endeavors to bridge the gap in knowledge. It also contributes to advancing the understanding of the direct roll bonding process and provides valuable insights for further optimizing the fabrication process, leading to the development of novel S/P/S composites with improved performance for various applications in automotive, aerospace, and structural engineering.

Thus, in this research, S/P/S laminates are manufactured by the roll-bonding process, without the use of adhesives (or reinforcements) and heated rollers (section 2). The authors attempt to achieve optimal mechanical properties. Three variables are considered:

- The polymer layer thickness (volume fraction of the core material)
- The rolling speed
- The rolling direction

Single Lap Shear (SLS) and T-peel tests were carried out to obtain the best rolling speed value for fabrication of four different laminate thicknesses by comparing the results of shear and bond strength, respectively. The effect(s) of the core volume fraction and rolling direction on the mechanical properties of the S/P/S sheet was studied by performing the uniaxial tensile test. The results were analyzed by examining the obtained data and the Scanning Electron Microscope (SEM) and are presented in section 3. Finally, the findings of the present work are concluded in section 4.

II. Methodology

a) Laminate Manufacturing

The Aluminum Killed (AK) low carbon steel St14 having $0.45\ mm$ thickness was selected as the face sheet of the S/P/S laminate due to its good mechanical properties and excellent formability and weldability. The chemical composition of the St14 steel sheet is illustrated in Table 1. Furthermore, a Thermoplastic Polyurethane (TPU) sheet with an initial thickness of $2\ mm$ was employed as the middle layer (core) of the three-layer sandwich sheet. Selection of the TPU sheet was due to its remarkable tensile and tear strengths, exceptional impact resistance, high chemical and corrosion resistance, excellent ductility over a vast temperature range, low weight and cost, and ultra-high adhesion with various surfaces [27]. Due to the importance of the working temperature of thermo-mechanical processes and changes in the polymer behavior at different temperatures, it is essential to know the rheology of the polymer. Thus, the Differential Scanning Calorimetry (DSC) analysis was performed on the TPU to determine the working temperature. The DSC curve of the TPU shows an endothermic peak at $226°C$ associated with the melting temperature (T_m), as shown in Figure 1. The DSC curve of the TPU usually shows two glass transitions at $-40°C$ and $95°C$ related to the soft and hard segments (T_g^{SS} and T_g^{HS}), respectively [10], [22], [28]. Accordingly, the working temperature of this study was chosen between the highest glass transition (T_g^{HS}) and the melting temperature (T_m).

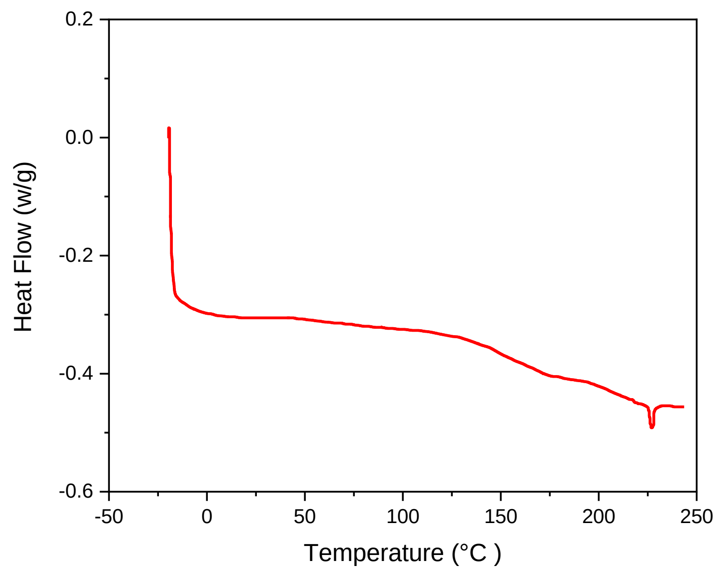

Figure 1: DSC curve of the TPU

Table 1: Chemical composition of the steel sheet

Fe	C *	Si	P	S	Cr	Ni	Mn	Mo	Al
Base	0.090	0.020	0.010	0.005	0.012	0.030	0.300	0.030	0.040

** numbers are in %*

The three-layer S/P/S laminates were manufactured by the roll bonding process, without any adhesive or reinforcement. The following steps were conducted in hierarchal order:

I. To increase the adhesion strength, the inner surfaces of both skin steel sheets were roughened in the rolling direction of sheet using stainless steel wire brush. Surface roughness was perfectly uniform and was measured by the Pocket-Surf®**III** roughness measuring mobile instrument after each brushing step. Post brushing, the average surface roughness of the St14 sheet was $R_a = 3.63\ \mu m$. The optical graph of the brushed steel surface is shown in Figure 2.

II. The contact surfaces (brushed side) of the two skin sheets and both sides of the TPU sheet were washed with acetone. The surfaces were air-dried to remove the surface contaminants and improve the quality of the bond.

III. The TPU sheet was sandwiched between the two skin face sheets. The four corners of the laminated sheet were punched to prevent slipping of the layers during the process.

IV. The unbonded laminate was placed at $200°C$ fixed temperature oven for 5 minutes. The goal was to semi-melt the polymer to ease penetration of the rough surfaces into TPU surfaces leading to enhancement of the bond strength.

V. The sample was rolled immediately after removal from the oven to achieve the desired thickness. Considering the thickness of the unbonded laminate ($2.9\ mm$), the three-layer laminates were fabricated at three rolling speeds and four rolling thickness reductions. The naming of test laminates was based on corresponding rolling speeds and thickness reductions, respectively (see Table 2). The cross-sectional view of four laminates with various thicknesses is presented in Figure 3.

b) Evaluation of the Mechanical Properties of the Base Sheets

To investigate the mechanical properties of metal and polymer sheets and compare them with different laminates, the uniaxial tensile test specimens were prepared according to ASTM E8/E8M and ASTM D638 (type IV) standards for steel and polymer sheets, respectively. Tensile tests of the steel sheet specimens along the rolling (RD), diagonal (DD), and transverse

(TD) directions, were conducted by the Hounsfield H10NKS machine with the test speed of $1\ mm/min$. The mechanical behavior of the TPU sheet was also obtained by the same machine with the test speed of $50\ mm/min$. Repeatability of the results was assured by performing at least three tensile tests for each condition. Due to the importance of the polymer tear strength under tension and shear conditions, the tear strength test was conducted on the TPU sheet according to ASTM D624-00 (type C) standard and with the crosshead speed of $50\ mm/min$. It is worth noting that all tests were performed at room temperature.

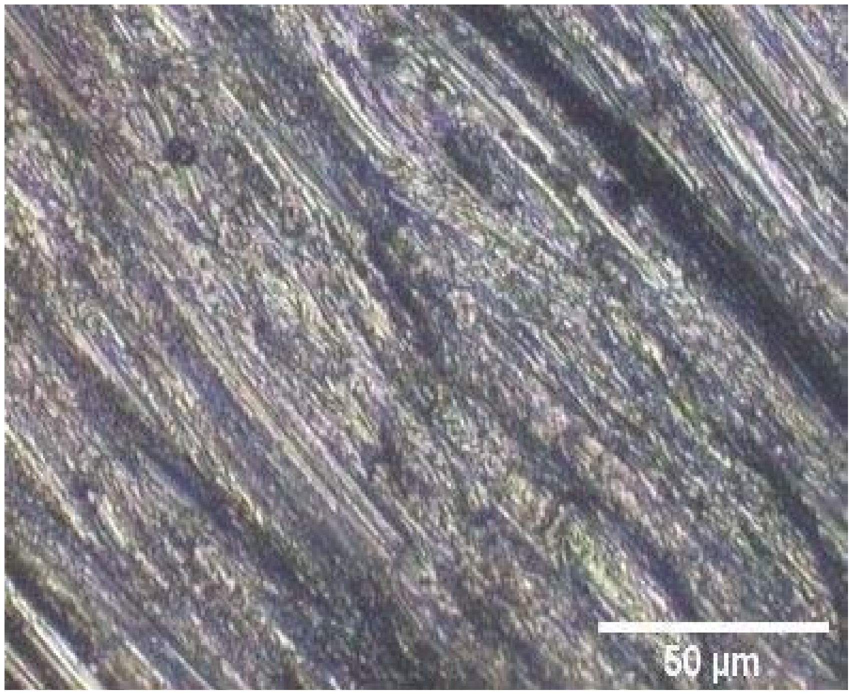

Figure 2: The optical micrograph of the roughened surface

Table 2: The laminates parameters and naming

Thickness Reduction (%)	Total Thickness (mm)	Core Volume Fraction (%)	Rolling Speed (rpm)		
			25	35	40
			Laminate Naming		
30	2.03	55.6	L-25-30	L-35-30	L-40-30
40	1.74	48.2	L-25-40	L-35-40	L-40-40
50	1.45	37.6	L-25-50	L-35-50	L-40-50
60	1.16	22.4	L-25-60	L-35-60	L-40-60

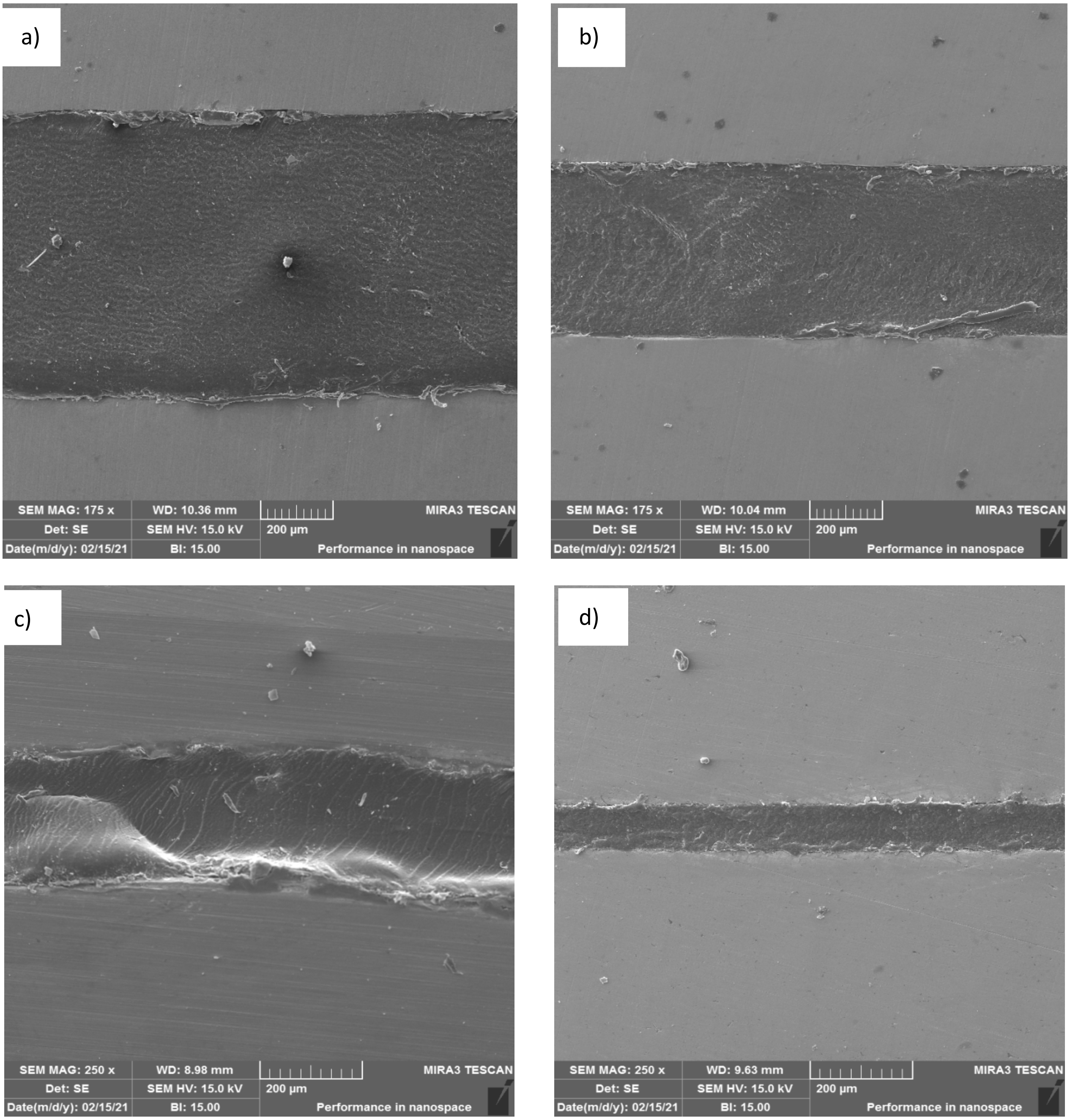

Figure 3: Cross sectional view of various laminates; (a) 30%, (b) 40%, (c) 50%, and (d) 60% thickness reduction

c) Rolling Speed Characterization

The optimal rolling speed is a key factor that has a significant impact on both the interfacial strength and fabrication of the three-layer laminates. Moreover, It can influence the mechanical and physical properties [29]. To determine the optimum rolling speed, bonding evaluation tests were carried out [30]. To evaluate the bond strength at skin-core interface of the different laminates under normal loading conditions, the T-peel and SLS tests were used. The T-peel test was performed according to the ASTM D1876-08 with the test speed of $20\ mm/min$. On the other hand, the SLS test was conducted according to ASTM D-3165-07 with the crosshead speed of $1\ mm/min$ to reflect the shear mechanical properties of the polymer layer. Figure 4 shows the geometric parameters of the T-peel and Lap-shear specimens. The size of specimens was modified in the small range. Due to the sensitivity of the results of these two tests and aiming to assure the accuracy of the results, the tests were repeated five times for each sample and the average values are reported.

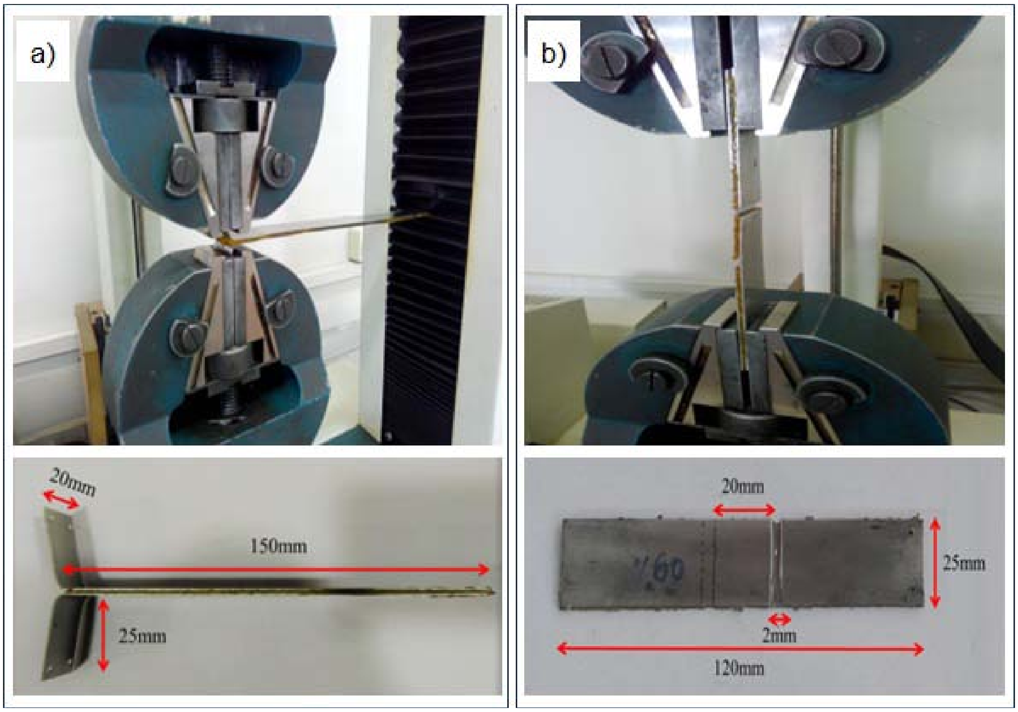

Figure 4: Experimental test set up and size of specimens for a) T-peel test and b) Single Lap Shear (SLS) test

d) Characterization of the Mechanical Properties of the Laminates

To study the impact of the core volume fraction and rolling direction on mechanical properties of three-layer laminates and its comparison with the monolithic steel sheet, the uniaxial tensile test was designed at three directions (RD, DD, and TD). To that end, the ASTM E8/E8M standard test method and constant crosshead speeds of $1\,mm/min$ were chosen. Repeatability of the results was assured by performing at least three tensile tests for each direction, i.e. a total of 9 tensile tests.

e) Analysis of the Results

Due to thickness reduction of the polymeric core during the thermomechanical process and its impact on polymer microstructure, the density of different laminates may be different. Therefore, this property was experimentally investigated using a measuring cylinder and laboratory digital scale.

The experimental results were compared with those predicted using the rule of mixture for laminates [31]:

$$P_{SMS} = P_{Skin} \times V_{Skin} + P_{Core} \times V_{Core} \qquad (1)$$

where P_{SMS} is the specific property of the laminate sheet, P_{Skin} and P_{Core} are that property for the skin sheet and polymeric core, respectively. V_{Skin} and V_{Core} are volume fractions of the skin sheet and polymeric core, respectively.

The bonding interface of the St14/TPU/St14 laminate sheet was investigated by using the Scanning Electron Microscope (SEM). Furthermore, the SEM was utilized to examine the fracture surface of the specimens after performing the T-peel and SLS tests.

III. Results and Discussions

a) Mechanical Properties of the Core Sheet

Since the mechanical properties of the core and the skin face sheets control the mechanical properties of three-layer laminates, a precise study of their mechanical behavior is required. Figure 5 shows the typical true strain-stress curve of the $2\,mm$ thick TPU sheet.

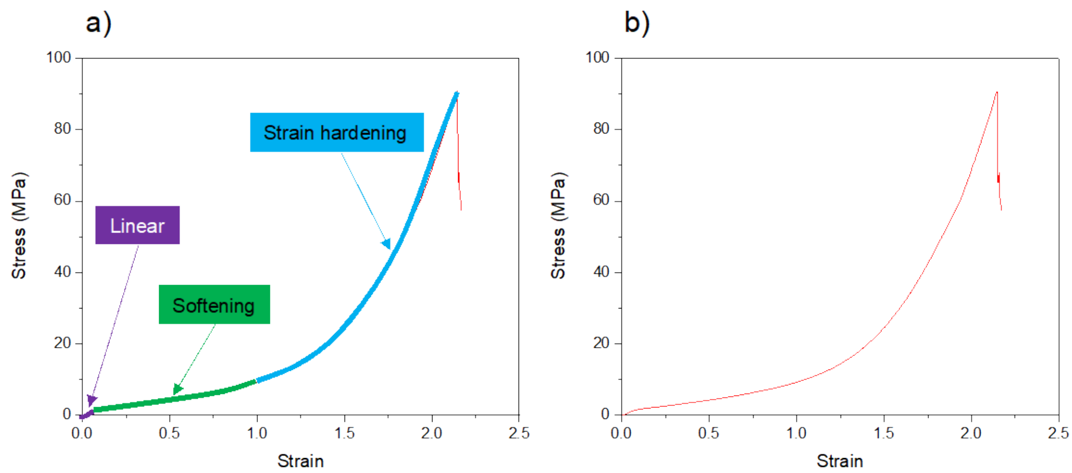

Figure 5: Stress-strain curve of the TPU sheet, a) characteristic areas of the graph, b) true stress-strain curve

The stress-strain behavior of the TPU is divided into three stages [32] as shown in Figure 5a. For the small strains, the curve is almost linear (purple region), and the specimen exhibits relatively stiff behavior. Material softening is the second phenomenon at the medium strain level (green region), and finally, strain hardening evolves progressively due to the strain-induced crystallization phenomenon at the largest strain (blue region). The combination of these three stages leads to the high strength of the polymer while maintaining considerably large elongation up to the point of failure.

The possibility of cutting, necking, and rupturing of the polyurethane sheet under tension or shear loading, increases the importance of the tear strength. The load-extension curve obtained from the tear test which is performed according to ASTM D-624-00 (Type C) is shown in Figure 6.

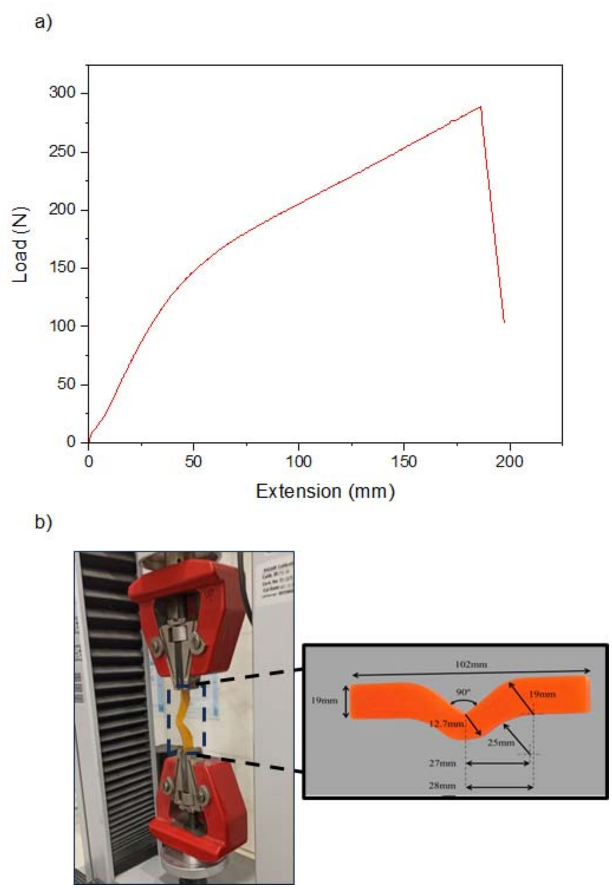

Figure 6: Illustration of tear test set up, a) Tear strength curve of the polymeric sheet, b) the experimental setup, and c) Dimensions of the sample based on ASTM D-624 (type C)

The change in the slope of the curve in the $50\,mm$ extension is due to the change of loading conditions in the torn region of the test specimen. Tear strength of the TPU sheet is defined as the ratio of maximum load ($286\,N$) at fracture point ($\approx 186\,mm$ extension) to the thickness of the specimen ($2\,mm$). Therefore, the tear strength of $\approx 143\,N/mm$ indicates high resistance of the TPU sheet to local deformation, and he extended tearing time (≈ 223 seconds) proves their superior level of stretchability, and excellent elongation.

b) The Optimum Rolling Speed of S/P/S Laminate

T-peel and SLS tests were performed on different laminates to determine the optimal rolling speed. T-peel test and SLS test data reflect the normal and shear mechanical properties of the laminates, respectively. Hence, by evaluating and comparing the results of these tests, it is possible to determine the optimal rolling speed for fabricating the maximum-bond-strength laminates for further experiments. The typical load-extension curves resulted from the T-peel and the SLS tests are illustrated in Figure 7.

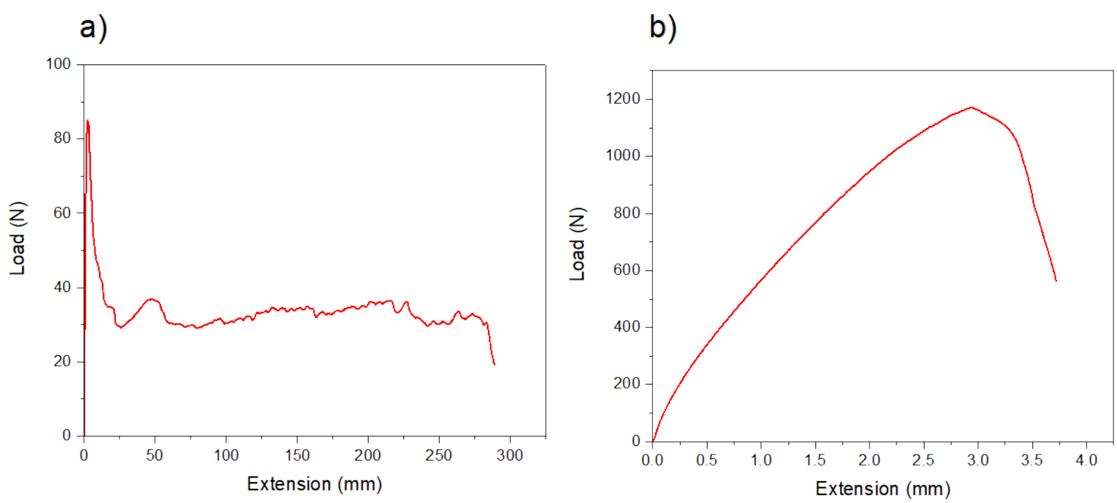

Figure 7: Load versus extension of, a) a T-peel test and b) SLS test

The Average Peel Strength (APS) can be calculated by [26]:

$$APS = {averageload\,(N)}\Big/{bondwidth\,(mm)} \quad (2)$$

where the average load is the average stable peel force after the first peak load.

Figure 8 shows the average peel strength at three various rolling speeds for four different laminates. Based on the figure, the bond strength decreases with increasing the rolling speed. The high bond strength at low rolling speed can be related to the longer time that the sample passes through the rollers. In general, in the rolling process of metallic sheets and composites which consists of two or more metallic sheets, the rolling speed before and after rolling (at the entrance and exit points) is not equal due to the occurrence of thickness reduction in the samples. In S/P/S laminates due to the fact that thickness reduction is only on the semi-melted polymericlayer and the steel sheets pass through the rollers without any reduction in thickness, it can be assumed that in the rolling process of S/P/S laminates, the initial and final velocity of the rollers is equal. Therefore, by converting the angular rolling speed to linear speed, it is possible to obtain the time that the samples pass through the rollers.

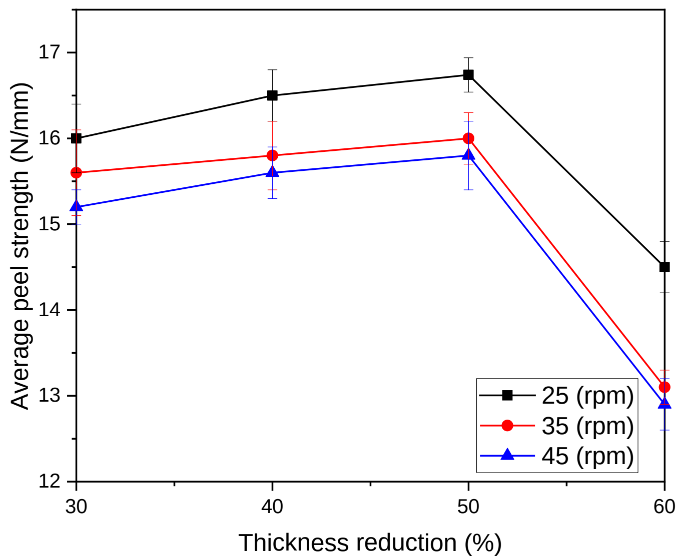

Figure 8: Comparison of the average peel strength at three various rolling speeds for four different laminate

The passage time is calculated by the following equation:

$$T = {}^{L \times 60}/_{V \times P} \tag{3}$$

Where T represents the passage time (s), L is the sample length (mm), V is the angular rolling speed (rpm), and P is the roller perimeter. Figure 9 illustrates the schematic view of the roll bonding process of S/P/S laminates including these parameters.

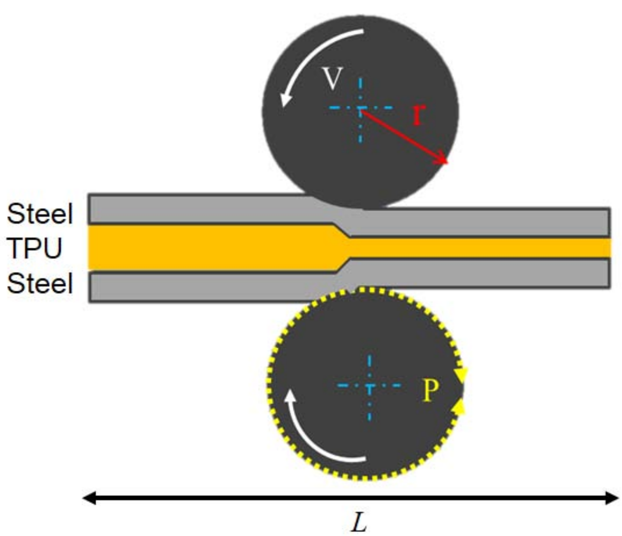

Figure 9: Schematic illustration of the roll bonding process

Therefore, the passage time of a $15\ cm$ long T-peel sample between two rollers with a diameter of $15\ cm$ at rolling speeds of 25, 35 and $45\ rpm$ is 0.76, 0.54, and 0.42 seconds, respectively. This longer passage time guarantees uniform flow of the semi-melted polymer in the rolling direction between the two face sheets. Additionally, the low rolling speed prevents displacement and unwanted sliding of the two face sheets relative to each other and ensures the structural integrity of the laminates. Any sliding and movement of the face sheets relative to each other, which is probable at higher rolling speeds, can prevent the smooth flowing of the semi-melted polymer between them leading to formation of the cavities resulting in weakening of the bond strength. Therefore, the coincidence of brushed surfaces in rolling direction provides ducts for polymer flow in the same direction. This results in more engagement between the polymer and the roughened surfaces of the steel sheets. Consequently, this leads to improvement of the bond strength and minimizes the risk of delamination or separation. Andani et al. [33] have reported that the probability of formation of cavities at metal-polymer interface is higher as the semi-melted polymer flowed outside the laminate structure resulting in decreasing the bond strength. These cavities were formed in samples that were wire brushed first in the rolling direction and then perpendicular to the rolling direction. Therefore, it can be concluded that the smooth flow of the polymer in one direction can prevent the formation of these cavities and promote the cohesion of the bond.

At the exit of the rolling machine, the final temperature of the laminates that rolled at high rolling speed is higher than that of those rolled at low rolling speed. This is due to the short contact time of the preheated sample with the cold rollers. This phenomenon elevates the potential of the generation of interlayer cavities by giving the warm polymer adequate time to undergo a gradual cooling process without the presence of external pressure. Andani et al. [33] demonstrated that at high rolling speed, the high temperature of the sample causes the polymer to become excessively soft, and the removal of the polymer from the sandwich structure is easier. Thus, there is not enough time for the polymer to penetrate the roughened surfaces, and consequently the bond strength decreases.

Furthermore, as Abbasi and Toroghinejad [34] observed, higher rolling speeds lead to shorter bond times to effectively apply pressure on the rolled sheets resulting in a sharp decrease in the adhesion strength. Thus, as the rolling speed decreases, the contact time increases. Increasing the effective pressure of the rollers which is obtained by lowering the rolling speed, facilitates the squeezing, extruding, and penetrating of the semi-melt polyurethane into the brushed surface of skin sheets resulting in effective integration and generation of more mechanical interlocks.

Observation of the T-peel specimens after performing the test revealed both cohesive failure (fracture within the polymeric core) and adhesive failure (fracture along the interface between the polymeric core and skin sheets) modes. Samples with cohesive failure were associated to the result of optimum thickness reduction and low rolling speed, whereas the samples having adhesive failure were the result of suboptimal thickness reduction and high rolling speed (Figure 10).

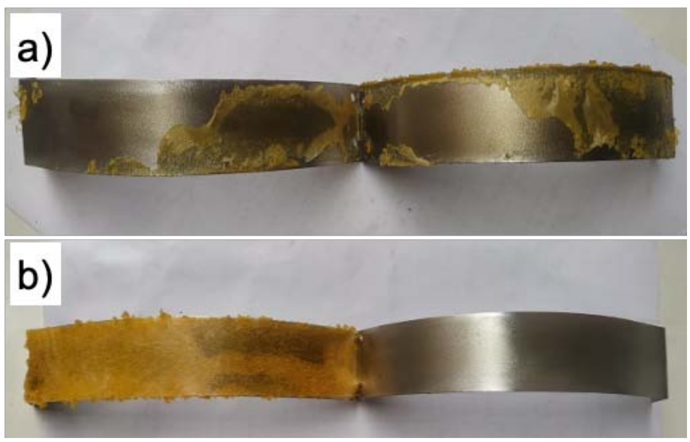

Figure 10: Failure of specimens after T-peel test, a) cohesive failure and (b) adhesive failure

Figure 11 shows the shear strength of S/P/S laminate for various thickness reductions. In this graph, the shear stress is calculated as:

$$\tau = {F_{max}}/{A} \tag{4}$$

Where F_{max} and A are the maximum load and the overlap area ($400\ mm^2$), respectively. As shown in Figure 11, increase in rolling speed leads to reduction in shear strength. Moreover, for all rolling speeds, as the thickness of S/P/S laminates decreases (up to 50% thickness reduction), the single lap shear strength increases. This is attributed to the fact that thinner laminates have smaller load eccentricity. As such, joint bending moment caused by load eccentricity decreases leading to less peel stress at steel-polymer interface. It can be inferred that in S/P/S laminates, the volume fraction of micro pores and cavities and interfacial toughening, contribute to the resistance of the metal-polymer interface against crack initiation and propagation. In laminates with a high polymer volume fraction, the larger volume of micro pores and cavities within the polymer structure surpasses the benefits of interfacial toughening, subsequently reducing the resistance of the metal-polymer interface to crack propagation. Conversely, in laminates with a low volume fraction of core material, although the volume of micro pores and cavities in the polymer structure is smaller, interfacial toughening is minimal, resulting in easier crack propagation. Therefore, achieving the highest level of crack resistance at metal-polymer interface requires optimizing both the volume fraction of micro-pores and the degree of interfacial toughening. Additionally, the optimum thickness of the core acts as a stress-absorbing element, effectively preventing crack initiation and arresting crack propagation at the interface, thereby improving the overall shear strength of the laminate. It is worth noting that laminates with 50% thickness reduction showed higher normal strength in T-peel test (see Figure 8). Hence, it could be inferred that, by striking a balance between interfacial toughening and the volume fraction of micro-cavities, laminates with a 50% thickness reduction exhibit the highest shear strength.

Global Journal of Researches in Engineering (J) Volume XXIII Issue IV Version I Year 2023

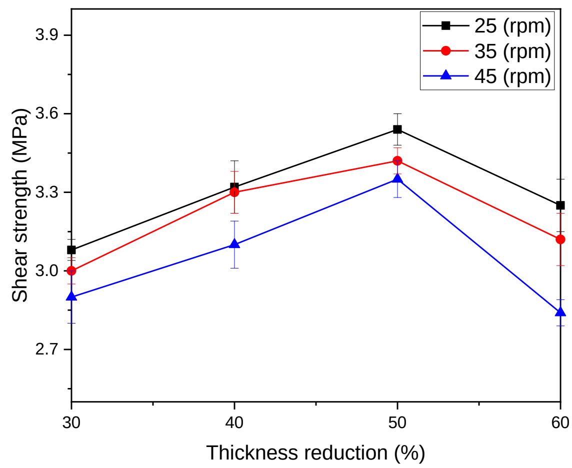

Figure 11: Comparison of the shear strength at three various rolling speeds for four different laminates

Figure 12 shows the fracture surfaces of the two SLS test specimens at the same thickness reduction (40%) at two rolling speeds of $25\ rpm$ and $45\ rpm$. The magnitude of effective pressure applied to the specimen controls the volume fraction of the micro-cavities at the metal-polymer interface. It is suspected that there is an inverse correlation between the volume fraction of the micro-cavities at the metal-polymer interface and the effective contact surface and subsequently the bond strength of the laminates. In other words, the higher metal-polymer interfacial volume fraction leads to low bond strength due to lower effective contact surface. Furthermore, lower rolling speeds are accompanied by higher effective pressure on the specimens, better penetration of the polymer to the rough surfaces of the skins, and thus reduction in volume fraction of the metal-polymer interfacial micro-cavities.

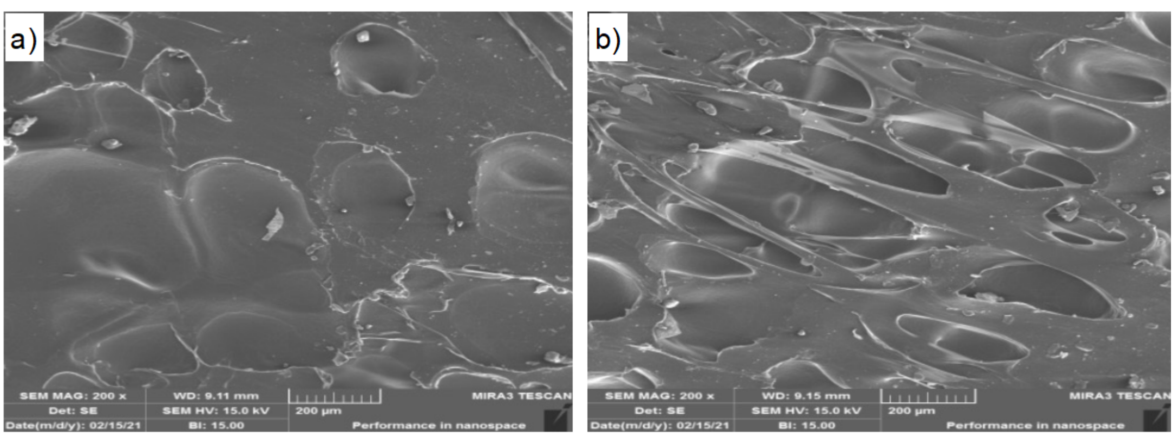

Figure 12: Fracture surfaces of the single lap shear specimens fabricated at rolling speed of: a) $25\ rpm$ and b) $45\ rpm$

c) Mechanical Properties of the Laminate and Monolithic Steel Sheet

In this section, the effects of sample direction and volume fraction on the mechanical properties of laminates are discussed. The results provided hereafter are for steel sheet and four different laminates fabricated at optimum rolling speed of $25\ rpm$ in three directions with respect to the rolling direction.

i. *Effect of the Sample Direction*

Figure 13 compares the typical stress-strain curve of both monolithic steel sheet (0.45 mm) and a specific Steel/Polymer/Steel sheet (0.45/0.26/0.45 mm) under uniaxial tensile loading. Both materials initially display linear elastic behavior. Generally, the stress-strain curve of the laminate displays a more gradual transition from the elastic region to plastic deformation compared to that of a monolithic. As the steel sheet approaches ultimate failure, it exhibits a more abrupt necking behavior, resulting in a relatively sharp drop in stress. This brittle failure is characteristic of metallic materials, where the strong atomic bonds lead to sudden fracture under high strain. In contrast, the presence of the polymer layer in the S/P/S laminate introduces a ductile behavior that enhances toughness and prevents rapid failure. The polymer layer provides additional energy absorption and deformation capacity, resulting in a more gradual and controlled stress reduction prior to failure.

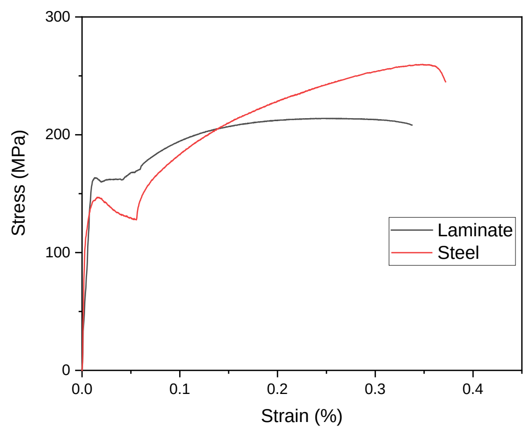

Figure 13: Stress-Strain curve of monolithic and laminated steel sheets

Figure 14 and Figure 15 show the yield and ultimate strength of laminates for various sample orientations with respect to RD and various thickness reductions, respectively.

As shown in the figures, there are considerable differences in the yield and ultimate tensile strengths for all four laminates compared to the monolithic steel sheet. Based on Figure 14, the yield strength of the monolithic steel sheet at all three directions (RD, DD, and TD) is higher than the three laminates L-25-30, L-25-40, and L-25-50. However, the yield strength of L-25-60 laminate is higher than that of the steel sheet. Similarity of the trends of L-25-50 and L-25-60 to the steel sheet curve suggests that the yield behavior of the thinner laminates is closer to that of the skin sheet due to reduced influence of polymer layer. While the polymer layer still contributes to factors such as interfacial adhesion and other mechanical properties of laminate, its influence on the overall yield behavior diminishes as laminate thickness decreases. Increasing the volume fraction of the polymer leads to the same yield behavior in three directions.

Comparison of the results of Figure 15 shows that the tensile strength of the monolithic steel sheet in the DD is higher than that of all other laminates. However, for both RD and TD, the tensile strength of the steel sheet is lower than the L-25-60 and more than L-25-30, L-25-40, and L-25-50 laminates. The same trend of the steel sheet curve and all laminates exhibit the high dependence of the tensile strength of the laminates on the tensile strength of the skin sheets in all three directions. Consequently, this finding suggests that the mechanical properties of the steel face sheets exert a relatively greater impact on the UTS of the laminate compared to the polymeric core.

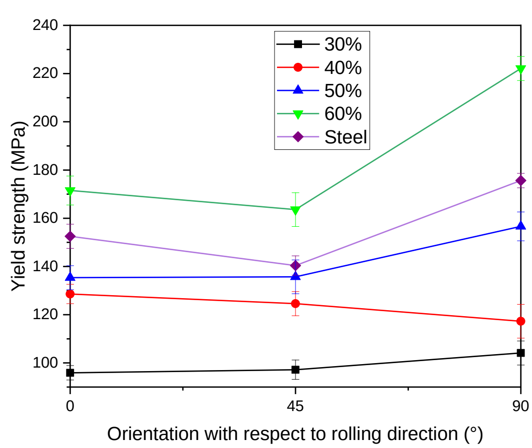

Figure 14: Effect of the angle of the sample axis with respect to RD on the yield strength (for various thickness reductions and bars on data points shows standard deviation of the test samples)

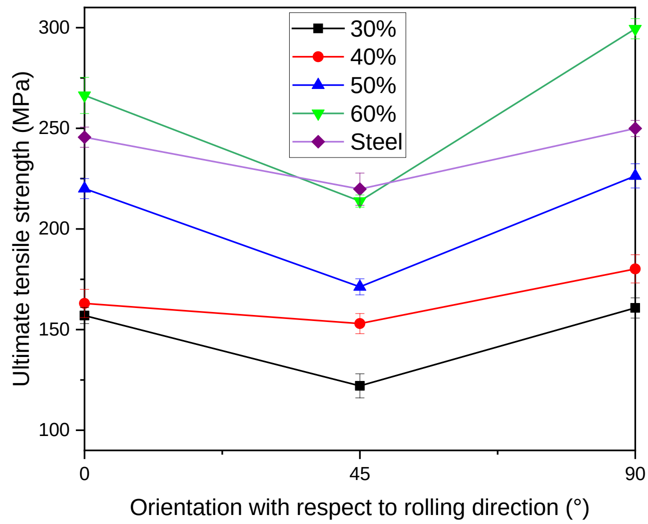

Figure 15: Effect of the angle of the sample axis with respect to RD on the ultimate tensile strength (for various thickness reductions and bars on data points shows standard deviation of the test samples)

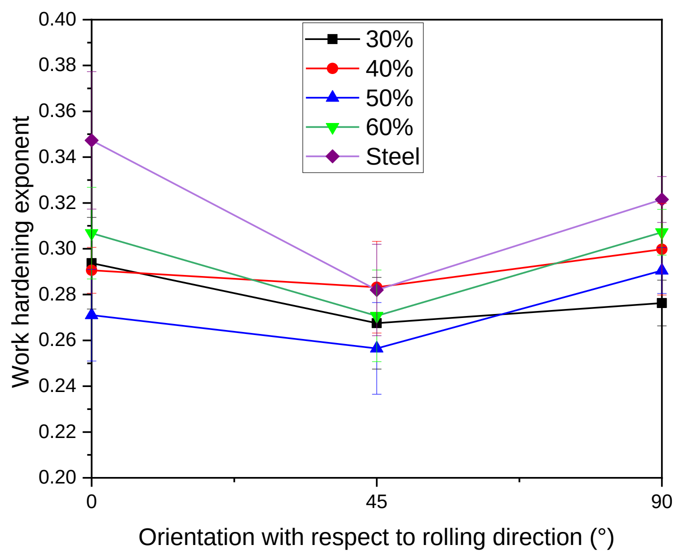

Figure 16: Effect of the angle of the sample axis with respect to RD on the work hardening exponent (for various thickness reductions and bars on data points shows standard deviation of the test samples)

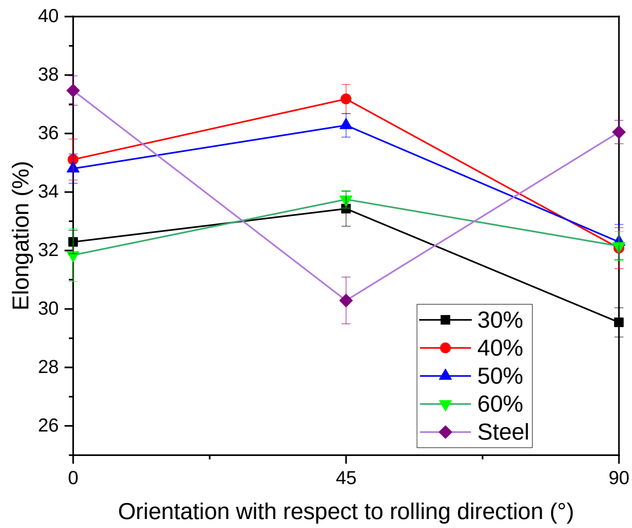

Figure 17: Effect of the angle of the sample axis with respect to RD on the ultimate elongation (for various thickness reductions and bars on data points shows standard deviation of the test samples)

The work hardening exponent measures the extent to which the material (monolithic and laminated steel sheet) undergo work hardening in response to uniaxial tensile load. Based on Considère criterion, the true strain (at maximum force) equates to the strain hardening exponent ($\varepsilon_u = n$) at the onset of localized necking. The work hardening exponent parameter of both monolithic steel and S/P/S laminate is given in Figure 16. Based on the figure, the n value of monolithic steel face sheet in RD and TD directions is higher than that of all S/P/S laminates. Besides, in DD direction, n of monolithic steel face sheet is approximately equal to that of L-25-40 and higher than that of other laminates. It is worth noting that DiCello [35] attributed the low work hardening exponent of the laminate compared to that of skin face sheet to the thermal aging of the metal skin during the lamination process. On the other hand, Harhash et al. [7] and Forcellese and Simoncini [36] attributed such a result to the soft polymer core which negatively affects the strengthening behavior of the laminate sheets. Furthermore, according to the study by Kim et al. [10], the strain hardening exponent of the polypropylene was reported to be lower compared to that of the AA5182 skin. This resulted in the reduction of the overall strain-hardening exponent of the sandwich sheets compared to monolithic aluminum sheet.

By changing the direction of the tensile samples of all laminates from $0°$ to $45°$, the work hardening exponent decreases. Then, the n value increases from $45°$ to $90°$. The same trend of n value at three directions for the monolithic steel sheet indicates that the work hardening exponent of laminates is dependent on the skinsheet.

As shown in Figure 17, by increasing the angular orientation of the tensile samples from $0°$ to $90°$, the elongation of all laminates first increases and then decreases while the skin sheet shows the opposite trend. Because the thicknesses of two skins of a laminate are equal and with same pressure on both sides of the polymer core, the metal-polymer interface strength of both sides is equal. It is suspected that, the occurrence of simultaneous necking of two steel skins in the same place increases the possibility of the premature fracture relative to the monolithic steel sheet. This simultaneous necking indicates a strong interaction between the skin layers, where they undergo a synchronized deformation mechanism. It can be influenced by various factors, such as the properties of the skin and polymer materials, their thicknesses, and the bonding strength between layers. At the DD, there is an improvement of this property for laminates. This can be related to high load bearing capacity (the ability of this specimen in distributing stress throughout the specimen length) of the metal-polymer interface samples at this direction. Forcellese and Simoncini [36] reported highest ultimate elongation value and post-necking deformation at $45°$ and similar elongation values for the $0°$ and $90°$ directions as well as lower post-necking deformation. They related this behavior to the lowest attitude to thinning owing to the highest normal anisotropy of the S/P/S sandwich composite occurring in the $45°$ angular orientation. Consequently, they observed the higher formability of samples at $45°$ orientation in the plane strain and drawing regions of Forming Limit Diagrams (FLD). Due to the significant difference between the elongation of the three-layer laminates and polymeric sheet, it can be concluded that the two skin sheets strongly affect the three-layer sheet ductility behavior.

Figure 18 shows the Young's modulus (E, slope of linear portion of stress-strain curve) of S/P/S laminates and monolithic steel for various rolling directions. Based on the graph, E of S/P/S are lower than that of monolithic steel sheet for all rolling directions. Furthermore, the value of E is insensitive to the rolling direction for all laminates and monolithic steel. This indicates that, in the present study, S/P/S laminates demonstrate an isotropic and macroscopically homogenous behavior.

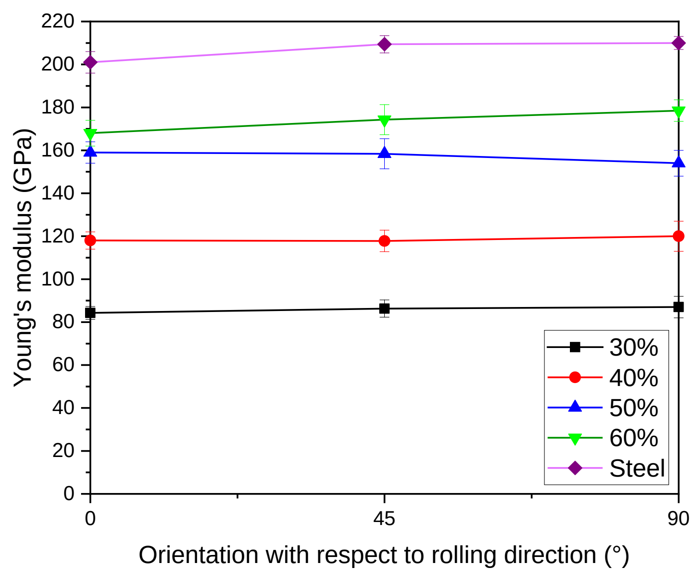

Figure 18: Effect of the angle of the sample axis with respect to RD on the Young's modulus (for various thickness reductions and bars on data points shows standard deviation of the test samples)

ii. *Effect of the Polymer Volume Fraction*

Figure 14 and Figure 15 show the increase in yield and tensile strength by decreasing the volume fraction of the polymer. Such result is in excellent agreement with those observed by Carrado et al. [1] and Harhash et al. [7].

Figure 19 shows the interface micrograph of all four laminates after lamination. According to the figure and the results of T-peel test (Figure 8), the mechanical interlocks have occurred between the rough surface of the skin sheet and the soft surface of the core sheet. This led to high bond strength at metal-polymer interface hindering the formation of delamination under tensile loading. On the other hand, the high tear strength of the polymeric sheet guarantees non-tearing along the width of the core sheet in the laminate structure. Therefore, all four laminates perform as an integrated sandwich structure. According to Figure 20, the ultimate tensile strength obtained from the tensile test (in the rolling direction) for two laminates L-25-50 and L-25-60 is higher than the calculated values obtained by the Rule Of Mixture (ROM). However, for L-25-30 and L-25-40, the experimental tensile strengths are lower than those obtained by ROM. It is observed that as the volume fraction of the polymer increases, the difference between the experimental and predicted tensile strength decreases commensurately.

It should be noted that there is not a clear correlation between the polymer volume fraction and the work hardening exponent (Figure 16).The similarity of results of all four laminates at all three directions to those of the monolithic steel sheet indicates that S/P/S laminates have high strain distribution behavior and consequently possess high formability.

Additionally, the highest elongation at all rolling directions belongs to L-25-40 and L-25-50 (Figure 17). The high bond strength of these laminates can be the reason of high elongation and consequently their delayed fracture. A similar conclusion was reached in [19].

Figure 18 indicates that increasing the thickness of the polymeric core leads to a decrease in the Young's modulus of the S/P/S laminates. As the thickness of the polymeric core increases, the proportion of the steel layers decreases. The polymer layer, which typically has a lower Young's modulus than steel, becomes a larger component of the structure. As a result, the overall Young's modulus of the structure decreases. Young's modulus of S/M/S sandwich sheets are calculated following the rule of mixture based on the Young's modulus of St14 steel and TPU sheets which are

$209.4\,GPa$ and $12.35\,MPa$, respectively. Figure 21 exhibits the difference between experimental and ROM values of young's modulus of S/P/S samples in rolling direction. Since ROM does not account for the interfacial bonding strength, this difference can be attributed to interfacial properties of the laminates along with strain rate dependency of the TPU core.

Comparison of the experimental and predicted ROM results indicates that the higher the volume fraction of the polymer, the larger becomes the difference between the obtained and predicted elongations (Figure 22). Due to the lack of pressure on the laminated sheet during cooling, micro-cavities may form in the polymer structure. Thicker laminates have more microcavities due to their high polymer volume fraction. Increasing the difference between the experimental density and its predicted value by increasing the polymer volume fraction supports this hypothesis (Figure 23). The density of the monolithic steel and polymer sheets is $7.8\ {}^{gr}/_{cm^3}$ and $1.25\ {}^{gr}/_{cm^3}$, respectively.

Figure 24 shows the effect of core volume fraction on the specific stiffness (Young's modulus/ Density) of the S/P/S laminates and compares experimental and estimated (ROM) values. The lower specific stiffness of L25-30 may be due to the thicker core, which might not be as effective in distributing the load, especially when the core material has significantly lower stiffness (0.0096 GPa/g.cm^{-3}) than the skin sheets (26.84 GPa/g.cm^{-3}). L-25-40 and L-25-60 have specific stiffness values close to that of the steel skin sheet, suggesting effective load distribution and potentially good interfacial bonding. The highest specific stiffness of L-25-50 (28.95) could be due to an optimal combination of core thickness and material properties, maximizing the load distribution and minimizing stress concentrations. It can be concluded that L-25-50 is the sample with promising thickness combination, which maintains a reasonable weight saving in addition to higher specific stiffness. Harhash et al. [7] demonstrated that E/D of 316L/PP PE/316L decrease as core volume fraction increase due to dominant effect of the polymeric core.

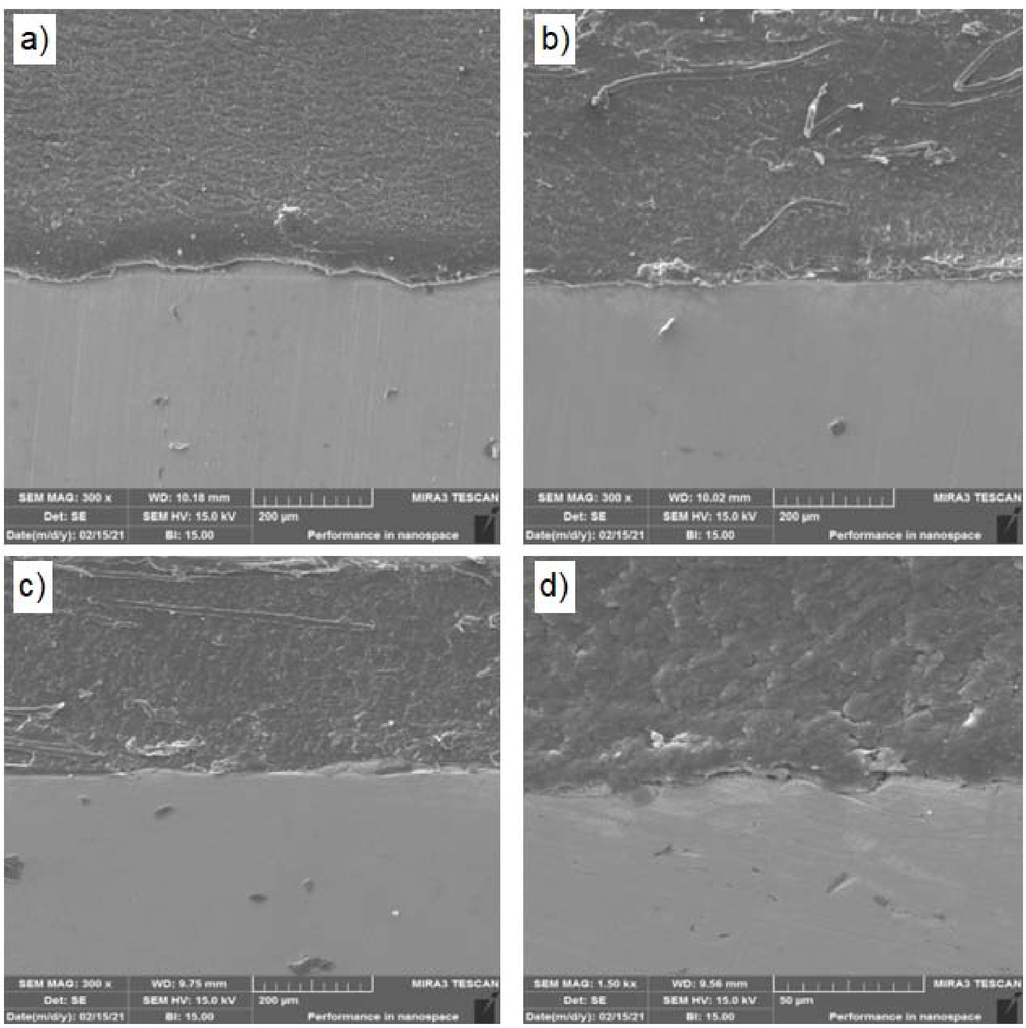

Figure 19: Metal/polymer interface of different laminates: (a) L-25-30, (b) L-25-40, (c) L-25-50, and (d) L-25-60 (Note: due to different thicknesses of specimens' different zooms and scales are used for each sample)

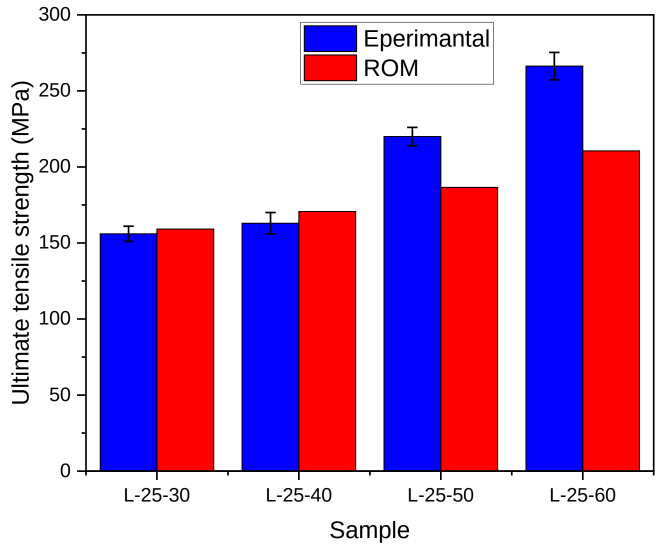

Figure 20: Comparison of the experimental and ROM results of UTS (at RD)

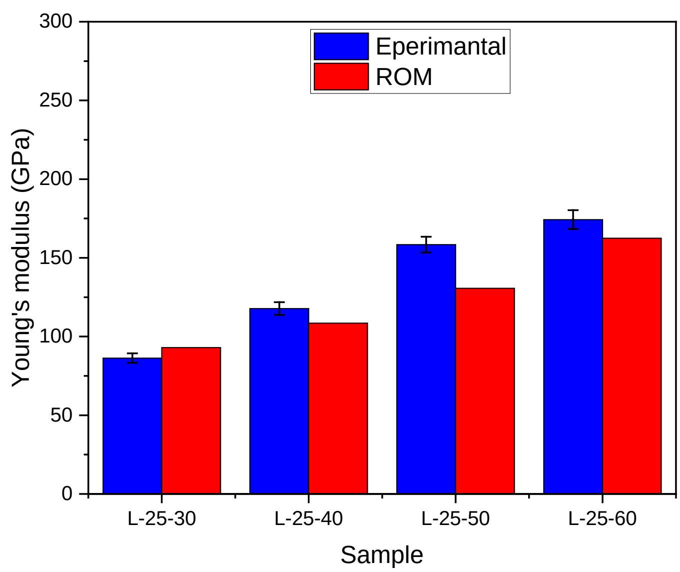

Figure 21: Comparison of the experimental and ROM results of young's modulus (at RD)

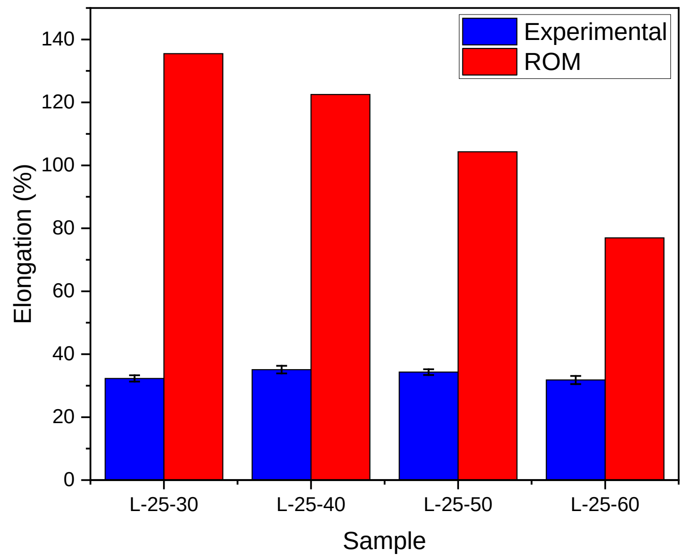

Figure 22: Comparison of the experimental and ROM results of elongation (at RD)

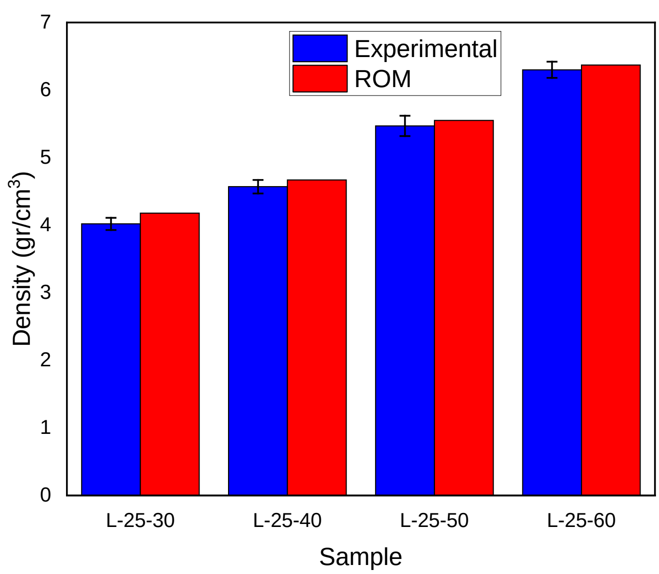

Figure 23: Comparison of the experimental and ROM results of density

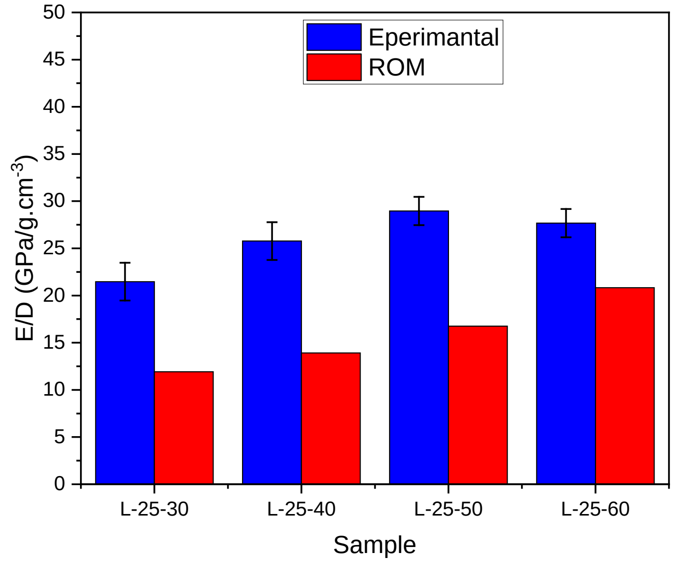

Figure 24: Comparison of the experimental and ROM results of specific stiffness

IV. Conclusions

A comprehensive experimental study was performed to investigate the effect(s) of the core volume fraction and rolling direction on the mechanical properties of the S/P/S composite laminate under uniaxial tensile loading. In the frame of the current study, the following conclusions are made:

1. Due to the higher passing time and consequently the higher effective pressure, the lower rolling speed leads to higher bond strength.
2. By increasing the polymer volume fraction in the laminate structure, the yield behavior becomes the same at RD, DD, and TD. On the other hand, S/P/S Laminates, like monolithic steel sheet exhibit higher ultimate tensile strength at $0°$ and $90°$ orientations, compared to the strength exhibited in a $45°$ orientation. As the volume fraction of the polymer increases, both yield and tensile strengths as well as elastic Young's modulus of laminates decreases.
3. The work hardening exponent (n) of all laminates is almost lower than that of monolithic steel sheet at all directions. Direct correlation between formability and n-value was observed. In other words, similarity of both the value and the trend of results obtained for low carbon steel and S/P/S laminates were indicative of high formability of laminates.
4. Increasing the angular orientation of the tensile samples from $0°$ to $90°$, led too initial increase in the elongation of all laminates. However, the increase was succeeded by decreases in elongation while the skin sheet showed the opposite trend. Moreover high-bond strength laminates have higher elongation than low-bond strength laminates. The difference between the obtained elongations and the calculated ones showed that thicker laminates had a larger volume fraction of micro-cavities that formed after lamination.
5. S/P/S laminates demonstrated homogeneous material behavior. This was the result of consistent stiffness properties in all directions relative to the rolling direction.
6. The likelihood of premature fracture in S/P/S laminates was higher than monolithic steel sheet thanks to occurrence of simultaneous necking of two steel face sheets at the same location.

Conducting experimental and finite element analysis to further understand the effect of interlayer thickness on formability, weldability, and impact resistance of this laminates is essential for improving their properties for various industrial applications. Additionally, the fracture mechanisms of the laminates need to be investigated under various loading conditions.

References Références Referencias

1. A. Carradò, J. Faerber, S. Niemeyer, G. Ziegmann, and H. Palkowski, "Metal/polymer/metal hybrid systems: Towards potential formability applications," *Compos Struct,* vol. 93, no. 2, pp. 715–721, 2011, doi: https://doi.org/10.1016/j.compstruct.2010.07.016
2. M. Damghani, C. Wallis, J. Bakunowicz, and A. Murphy, "Experimental and numerical analysis for postbuckling behaviour of tailored hybrid composite laminates subjected to shear loading," *Compos Struct,* p. Accepted for publication, 2020.

3. M. Damghani, J. Saddler, E. Sammon, G. A. Atkinson, J. Matthews, and A. Murphy, "An experimental investigation of the impact response and Post-impact shear buckling behaviour of hybrid composite laminates," *Compos Struct,* vol. 305, p. 116506, 2023, doi: https://doi.org/10.1016/j.compstruct.2022.116506
4. A. Kwakernaak, J. Hofstede, J. Poulis, and R. Benedictus, "8 - Improvements in bonding metals for aerospace and other applications," in *Woodhead Publishing Series in Welding and Other Joining Technologies,* M. C. B. T.-W. and J. of A. M. Chaturvedi, Ed., Woodhead Publishing, 2012, pp. 235–287. doi: https://doi.org/10.1533/9780857095169.2.235
5. I. Burchitz, R. Boesenkool, S. van der Zwaag, and M. Tassoul, "Highlights of designing with Hylite – a new material concept," *Mater Des,* vol. 26, no. 4, pp. 271–279, 2005, doi: https://doi.org/10.1016/j.matdes.2004.06.021
6. J.-K. Kim and T.-X. Yu, "Forming and failure behaviour of coated, laminated and sandwiched sheet metals: a review," *J Mater Process Technol,* vol. 63, no. 1, pp. 33–42, 1997, doi: https://doi.org/10.1016/S0924-0136(96)02596-4
7. M. Harhash, O. Sokolova, A. Carradó, and H. Palkowski, "Mechanical properties and forming behaviour of laminated steel/polymer sandwich systems with local inlays – Part 1," *Compos Struct,* vol. 118, pp. 112–120, 2014, doi: https://doi.org/10.1016/j.compstruct.2014.07.011
8. J. Liu, W. Liu, and W. Xue, "Forming limit diagram prediction of AA5052/polyethylene/AA5052 sandwich sheets," *Materials & Design (1980-2015),* vol. 46, pp. 112–120, 2013, doi: https://doi.org/10.1016/j.matdes.2012.09.057
9. F. Kazemi, R. Hashemi, and S. A. Niknam, "Formability and fractography of AA5754/polyethylene/AA5754 sandwich composites," *Mechanics Based Design of Structures and Machines,* vol. 50, no. 4, pp. 1253–1267, Apr. 2022, doi: 10.1080/15397734.2020.1747 488
10. K. J. Kim *et al.,* "Formability of AA5182/polypropylene/AA5182 sandwich sheets," *J Mater Process Technol,* vol. 139, no. 1, pp. 1–7, 2003, doi: https://doi.org/10.1016/S0924-0136(03)00173-0
11. K. Logesh and V. K. B. Raja, "Formability analysis for enhancing forming parameters in AA8011/PP/AA1100 sandwich materials," *The International Journal of Advanced Manufacturing Technology,* vol. 93, no. 1, pp. 113–120, 2017, doi: 10.1007/s00170-015-7832-5
12. K. J. Kim *et al.,* "Development of application technique of aluminum sandwich sheets for automotive hood," *International Journal of Precision Engineering and Manufacturing,* vol. 10, no. 4, pp. 71–75, 2009, doi: 10.1007/s12541-009-0073-5
13. V. Satheeshkumar and R. G. Narayanan, "Investigation on the influence of adhesive properties on the formability of adhesive-bonded steel sheets," *Proc Inst Mech Eng C J Mech Eng Sci,* vol. 228, no. 3, pp. 405–425, May 2013, doi: 10.1177/0954406213488727
14. H. Hayashi and T. Nakagawa, "Recent trends in sheet metals and their formability in manufacturing automotive panels," *J Mater Process Technol,* vol. 46, no. 3, pp. 455–487, 1994, doi: https://doi.org/10.1016/0924-0136(94)90128-7
15. J. Liu and L. Zhuang, "Cylindrical cup-drawing characteristics of aluminum-polymer sandwich sheet," *The International Journal of Advanced Manufacturing Technology,* vol. 97, no. 5, pp. 1885–1896, 2018, doi: 10.1007/s00170-018-2077-8
16. M. Nourjani Pourmoghadam, R. Shahrokh Esfahani, M. R. Morovvati, and B. Nekooei Rizi, "Bifurcation analysis of plastic wrinkling formation for anisotropic laminated sheets (AA2024–Polyamide–AA2024)," *Comput Mater Sci,* vol. 77, pp. 35–43, 2013, doi: https://doi.org/10.1016/j.commatsci.2013.03.037
17. M. Harhash, A. Carradó, and H. Palkowski, "DEEP- AND STRETCH-FORMING OF STEEL/POLYMER/STEEL LAMINATES," in *Euro Hybrid Materials and Structures,* Kaiserslautern (Germany), 2016.
18. B. Rezaei Anvar and A. Akbarzadeh, "Roll bonding of AA5052 and polypropylene sheets: Bonding mechanisms, microstructure and mechanical properties," *J Adhes,* vol. 93, no. 7, pp. 550–574, Jun. 2017, doi: 10.1080/00218464.2015.1116067
19. S. Nambu, M. Michiuchi, J. Inoue, and T. Koseki, "Effect of interfacial bonding strength on tensile ductility of multilayered steel composites," *Compos Sci Technol,* vol. 69, no. 11, pp. 1936–1941, 2009, doi: https://doi.org/10.1016/j.compscitech.2009.04.013.
20. H. Park, S.-J. Kim, J. Lee, J. H. Kim, and D. Kim, "Characterization of the Mechanical Properties of a High-Strength Laminated Vibration Damping Steel Sheet and Their Application to Formability Prediction," *Metals and Materials International,* vol. 25, no. 5, pp. 1326–1340, 2019, doi: 10.1007/s12540-019-00281-8
21. R. B. Ruokolainen and D. R. Sigler, "The Effect of Adhesion and Tensile Properties on the Formability of Laminated Steels," *J Mater Eng Perform,* vol. 17, no. 3, pp. 330–339, 2008, doi: 10.1007/s11665-008-9207-7.
22. M. Weiss, B. Rolfe, M. Dingle, and P. Hodgson, "The influence of interlayer thickness and properties on spring-back of SPS- (steel/polymer/steel) laminates.," *Steel grips,* vol. 2, pp. 445–449, 2004, [Online]. Available: https://dro.deakin.edu.au/articlees/journal_contribution/The_influence_of_interlayer_thickness_and_properties_on_spring-back_of_SPS-_steel_polymer_steel_laminates_/20537805

23. F. Avril, R. Rahmé, M. Doux, D. Verchere, D. Sage, and P. Cassagnau, "New Polymer Materials for Steel/Polymer/Steel Laminates in Automotive Applications," *Macromol Mater Eng,* vol. 298, no. 6, pp. 644–652, Jun. 2013, doi: https://doi.org/10.1002/mame.201200058
24. T. Saito and N. Mizuhashi, "Resistance welding of vibration-damped steel sheet," *Welding International,* vol. 4, no. 12, pp. 993–997, Jan. 1990, doi: 10.1080/09507119009453040
25. H. Oberle, C. Commaret, C. Minier, R. Magnaud, and G. Pradere, "Optimizing resistance spot welding parameters for vibration damping steel sheets," *Weld J,* vol. 77, 1998, [Online]. Available: https://api.semanticscholar.org/CorpusID:136653269
26. S. Mousa and G.-Y. Kim, "Direct Adhesion of Warm Roll-Bonded Al1100/Polyurethane/Al1100 Sandwich Composite," in *Proceedings of the ASME 2015 International Manufacturing Science and Engineering Conference,* North Carolina (USA), Jun. 2015. doi: 10.1115/MSEC2015-9467
27. W. Lin, X. Li, W. Dong, Y. Zhao, M. Li, and Y. Wang, "Ultrahigh bonding strength and excellent corrosion resistance of Al-TPU hybrid induced by microstructures and silane layer," *J Mater Process Technol,* vol. 296, p. 117180, 2021, doi: https://doi.org/10.1016/j.jmatprotec.2021.117180
28. M. Yahiaoui, J. Denape, J.-Y. Paris, A. G. Ural, N. Alcalá, and F. J. Martínez, "Wear dynamics of a TPU/steel contact under reciprocal sliding," *Wear,* vol. 315, no. 1, pp. 103–114, 2014, doi: https://doi.org/10.1016/j.wear.2014.04.005
29. J. Liu, Q. Zhang, B. Zhang, and M. Yu, "The Influence of the Roll-Laminating Process on the Bonding Quality of Polymer-Coated Steel Interface," *Coatings,* vol. 11, no. 4. 2021. doi: 10.3390/coatings11040472
30. S. Mousa, N. Scheirer, and G.-Y. Kim, "Roll-bonding of metal-polymer-metal sandwich composites reinforced by glass whiskers at the interface," *J Mater Process Technol,* vol. 255, pp. 463–469, 2018, doi: https://doi.org/10.1016/j.jmatprotec.2017.12.039
31. M. Harhash, R. R. Gilbert, S. Hartmann, and H. Palkowski, "Experimental characterization, analytical and numerical investigations of metal/polymer/metal sandwich composites – Part 1: Deep drawing," *Compos Struct,* vol. 202, pp. 1308–1321, 2018, doi: https://doi.org/10.1016/j.compstruct.2018.06.066
32. A. Frick, M. Borm, N. Kaoud, J. Kolodziej, and J. Neudeck, "Microstructure and thermomechanical properties relationship of segmented thermoplastic polyurethane (TPU)," *AIP Conf Proc,* vol. 1593, no. 1, pp. 520–525, May 2014, doi: 10.1063/1.4873835
33. M. Kamali Andani, H. Daneshmanesh, and S. A. Jenabali Jahromi, "Investigation of the bonding strength of the stainless steel 316L/polyurethane/stainless steel 316L tri-layer composite produced by the warm rolling process," *Journal of Sandwich Structures & Materials,* vol. 22, no. 3, pp. 728–742, Apr. 2018, doi: 10.1177/1099636218770911
34. M. Abbasi and M. R. Toroghinejad, "Effects of processing parameters on the bond strength of Cu/Cu roll-bonded strips," *J Mater Process Technol,* vol. 210, no. 3, pp. 560–563, 2010, doi: https://doi.org/10.1016/j.jmatprotec.2009.11.003
35. J. A. DiCello, "Steel-Polypropylene-Steel Laminate – A New Weight Reduction Material," in *1980 Automotive Engineering Congress and Exposition,* SAE International, Feb. 1980. doi: https://doi.org/10.4271/800078
36. A. Forcellese and M. Simoncini, "Mechanical properties and formability of metal–polymer–metal sandwich composites," *The International Journal of Advanced Manufacturing Technology,* vol. 107, no. 7, pp. 3333–3349, 2020, doi: 10.1007/s00170-020-05245-6

Global Journals Guidelines Handbook 2023

www.GlobalJournals.org

MEMBERSHIPS

FELLOWS/ASSOCIATES OF ENGINEERING RESEARCH COUNCIL

FERC/AERC MEMBERSHIPS

INTRODUCTION

FERC/AERC is the most prestigious membership of Global Journals accredited by Open Association of Research Society, U.S.A (OARS). The credentials of Fellow and Associate designations signify that the researcher has gained the knowledge of the fundamental and high-level concepts, and is a subject matter expert, proficient in an expertise course covering the professional code of conduct, and follows recognized standards of practice. The credentials are designated only to the researchers, scientists, and professionals that have been selected by a rigorous process by our Editorial Board and Management Board.

Associates of FERC/AERC are scientists and researchers from around the world are working on projects/researches that have huge potentials. Members support Global Journals' mission to advance technology for humanity and the profession.

FERC

FELLOW OF ENGINEERING RESEARCH COUNCIL

FELLOW OF ENGINEERING RESEARCH COUNCIL is the most prestigious membership of Global Journals. It is an award and membership granted to individuals that the Open Association of Research Society judges to have made a 'substantial contribution to the improvement of computer science, technology, and electronics engineering.

The primary objective is to recognize the leaders in research and scientific fields of the current era with a global perspective and to create a channel between them and other researchers for better exposure and knowledge sharing. Members are most eminent scientists, engineers, and technologists from all across the world. Fellows are elected for life through a peer review process on the basis of excellence in the respective domain. There is no limit on the number of new nominations made in any year. Each year, the Open Association of Research Society elect up to 12 new Fellow Members.

Benefit

To the institution

Get letter of appreciation

Global Journals sends a letter of appreciation of author to the Dean or CEO of the University or Company of which author is a part, signed by editor in chief or chief author.

Exclusive Network

Get access to a closed network

A FERC member gets access to a closed network of Tier 1 researchers and scientists with direct communication channel through our website. Fellows can reach out to other members or researchers directly. They should also be open to reaching out by other.

Career | Credibility | Exclusive | Reputation

Certificate

Certificate, LoR and Laser-Momento

Fellows receive a printed copy of a certificate signed by our Chief Author that may be used for academic purposes and a personal recommendation letter to the dean of member's university.

Career | Credibility | Exclusive | Reputation

Designation

Get honored title of membership

Fellows can use the honored title of membership. The "FERC" is an honored title which is accorded to a person's name viz. Dr. John E. Hall, Ph.D., FERC or William Walldroff, M.S., FERC.

Career | Credibility | Exclusive | Reputation

Recognition on the Platform

Better visibility and citation

All the Fellow members of FERC get a badge of "Leading Member of Global Journals" on the Research Community that distinguishes them from others. Additionally, the profile is also partially maintained by our team for better visibility and citation. All fellows get a dedicated page on the website with their biography.

Career | Credibility | Reputation

Future Work

Get discounts on the future publications

Fellows receive discounts on the future publications with Global Journals up to 60%. Through our recommendation programs, members also receive discounts on publications made with OARS affiliated organizations.

Career Financial

GJ Account

Unlimited forward of Emails

Fellows get secure and fast GJ work emails with unlimited storage of emails that they may use them as their primary email. For example, john [AT] globaljournals [DOT] org.

Career Credibility Reputation

Premium Tools

Access to all the Premium Tools

To take future researches to the zenith, fellows receive access to all the premium tools that Global Journals have to offer along with the partnership with some of the best marketing leading tools out there.

Financial

Conferences & Events

Organize seminar/conference

Fellows are authorized to organize symposium/seminar/conference on behalf of Global Journal Incorporation (USA). They can also participate in the same organized by another institution as representative of Global Journal. In both the cases, it is mandatory for him to discuss with us and obtain our consent. Additionally, they get free research conferences (and others) alerts.

Career Credibility Financial

Early Invitations

Early invitations to all the symposiums, seminars, conferences

All fellows receive the early invitations to all the symposiums, seminars, conferences and webinars hosted by Global Journals in their subject.

Exclusive

Publishing Articles & Books

Earn 60% of sales proceeds

Fellows can publish articles (limited) without any fees. Also, they can earn up to 70% of sales proceeds from the sale of reference/review books/literature/publishing of research paper. The FERC member can decide its price and we can help in making the right decision.

Exclusive Financial

Reviewers

Get a remuneration of 15% of author fees

Fellow members are eligible to join as a paid peer reviewer at Global Journals Incorporation (USA) and can get a remuneration of 15% of author fees, taken from the author of a respective paper.

Financial

Access to Editorial Board

Become a member of the Editorial Board

Fellows may join as a member of the Editorial Board of Global Journals Incorporation (USA) after successful completion of three years as Fellow and as Peer Reviewer. Additionally, Fellows get a chance to nominate other members for Editorial Board.

Career Credibility Exclusive Reputation

And Much More

Get access to scientific museums and observatories across the globe

All members get access to 5 selected scientific museums and observatories across the globe. All researches published with Global Journals will be kept under deep archival facilities across regions for future protections and disaster recovery. They get 10 GB free secure cloud access for storing research files.

AERC

ASSOCIATE OF ENGINEERING RESEARCH COUNCIL

ASSOCIATE OF ENGINEERING RESEARCH COUNCIL is the membership of Global Journals awarded to individuals that the Open Association of Research Society judges to have made a 'substantial contribution to the improvement of computer science, technology, and electronics engineering.

The primary objective is to recognize the leaders in research and scientific fields of the current era with a global perspective and to create a channel between them and other researchers for better exposure and knowledge sharing. Members are most eminent scientists, engineers, and technologists from all across the world. Associate membership can later be promoted to Fellow Membership. Associates are elected for life through a peer review process on the basis of excellence in the respective domain. There is no limit on the number of new nominations made in any year. Each year, the Open Association of Research Society elect up to 12 new Associate Members.

Benefit

To the Institution

Get letter of appreciation

Global Journals sends a letter of appreciation of author to the Dean or CEO of the University or Company of which author is a part, signed by editor in chief or chief author.

Exclusive Network

Get access to a closed network

A AERC member gets access to a closed network of Tier 1 researchers and scientists with direct communication channel through our website. Associates can reach out to other members or researchers directly. They should also be open to reaching out by other.

Career | Credibility | Exclusive | Reputation

Certificate

Certificate, LoR and Laser-Momento

Associates receive a printed copy of a certificate signed by our Chief Author that may be used for academic purposes and a personal recommendation letter to the dean of member's university.

Career | Credibility | Exclusive | Reputation

Designation

Get honored title of membership

Associates can use the honored title of membership. The “AERC” is an honored title which is accorded to a person’s name viz. Dr. John E. Hall, Ph.D., AERC or William Walldroff, M.S., AERC.

Career | Credibility | Exclusive | Reputation

Recognition on the Platform

Better visibility and citation

All the Associate members of AERC get a badge of "Leading Member of Global Journals" on the Research Community that distinguishes them from others. Additionally, the profile is also partially maintained by our team for better visibility and citation. All associates get a dedicated page on the website with their biography.

Career | Credibility | Reputation

Future Work

Get discounts on the future publications

Associates receive discounts on the future publications with Global Journals up to 60%. Through our recommendation programs, members also receive discounts on publications made with OARS affiliated organizations.

Career | Financial

GJ Account

Unlimited forward of Emails

Associates get secure and fast GJ work emails with unlimited storage of emails that they may use them as their primary email. For example, john [AT] globaljournals [DOT] org..

Career | Credibility | Reputation

Premium Tools

Access to all the premium tools

To take future researches to the zenith, associates receive access to all the premium tools that Global Journals have to offer along with the partnership with some of the best marketing leading tools out there.

Financial

Conferences & Events

Organize seminar/conference

Associates are authorized to organize symposium/seminar/conference on behalf of Global Journal Incorporation (USA). They can also participate in the same organized by another institution as representative of Global Journal. In both the cases, it is mandatory for him to discuss with us and obtain our consent. Additionally, they get free research conferences (and others) alerts.

Career | Credibility | Financial

Early Invitations

Early invitations to all the symposiums, seminars, conferences

All associates receive the early invitations to all the symposiums, seminars, conferences and webinars hosted by Global Journals in their subject.

Exclusive

Publishing Articles & Books

Earn 30-40% of sales proceeds

Associates can publish articles (limited) without any fees. Also, they can earn up to 30-40% of sales proceeds from the sale of reference/review books/literature/publishing of research paper.

Exclusive Financial

Reviewers

Get a remuneration of 15% of author fees

Associate members are eligible to join as a paid peer reviewer at Global Journals Incorporation (USA) and can get a remuneration of 15% of author fees, taken from the author of a respective paper.

Financial

And Much More

Get access to scientific museums and observatories across the globe

All members get access to 2 selected scientific museums and observatories across the globe. All researches published with Global Journals will be kept under deep archival facilities across regions for future protections and disaster recovery. They get 5 GB free secure cloud access for storing research files.

Associate	Fellow	Research Group	Basic
$4800 **lifetime designation**	$6800 **lifetime designation**	$12500.00 **organizational**	APC **per article**
Certificate, LoR and Momento 2 discounted publishing/year **Gradation** of Research 10 research contacts/day 1 **GB** Cloud Storage **GJ** Community Access	**Certificate,** LoR and Momento **Unlimited** discounted publishing/year **Gradation** of Research **Unlimited** research contacts/day 5 **GB** Cloud Storage **Online Presense** Assistance **GJ** Community Access	**Certificates,** LoRs and Momentos **Unlimited** free publishing/year **Gradation** of Research **Unlimited** research contacts/day **Unlimited** Cloud Storage **Online Presense** Assistance **GJ** Community Access	**GJ** Community Access

We accept the manuscript submissions in any standard (generic) format.

We typeset manuscripts using advanced typesetting tools like Adobe In Design, CorelDraw, TeXnicCenter, and TeXStudio. We usually recommend authors submit their research using any standard format they are comfortable with, and let Global Journals do the rest.

Alternatively, you can download our basic template from https://globaljournals.org/Template.zip

Authors should submit their complete paper/article, including text illustrations, graphics, conclusions, artwork, and tables. Authors who are not able to submit manuscript using the form above can email the manuscript department at submit@globaljournals.org or get in touch with chiefeditor@globaljournals.org if they wish to send the abstract before submission.

Before and during Submission

Authors must ensure the information provided during the submission of a paper is authentic. Please go through the following checklist before submitting:

1. Authors must go through the complete author guideline and understand and *agree to Global Journals' ethics and code of conduct,* along with author responsibilities.
2. Authors must accept the privacy policy, terms, and conditions of Global Journals.
3. Ensure corresponding author's email address and postal address are accurate and reachable.
4. Manuscript to be submitted must include keywords, an abstract, a paper title, co-author(s') names and details (email address, name, phone number, and institution), figures and illustrations in vector format including appropriate captions, tables, including titles and footnotes, a conclusion, results, acknowledgments and references.
5. Authors should submit paper in a ZIP archive if any supplementary files are required along with the paper.
6. Proper permissions must be acquired for the use of any copyrighted material.
7. Manuscript submitted *must not have been submitted or published elsewhere* and all authors must be aware of the submission.

Declaration of Conflicts of Interest

It is required for authors to declare all financial, institutional, and personal relationships with other individuals and organizations that could influence (bias) their research.

Policy on Plagiarism

Plagiarism is not acceptable in Global Journals submissions at all.

Plagiarized content will not be considered for publication. We reserve the right to inform authors' institutions about plagiarism detected either before or after publication. If plagiarism is identified, we will follow COPE guidelines:

Authors are solely responsible for all the plagiarism that is found. The author must not fabricate, falsify or plagiarize existing research data. The following, if copied, will be considered plagiarism:

- Words (language)
- Ideas
- Findings
- Writings
- Diagrams
- Graphs
- Illustrations
- Lectures

- Printed material
- Graphic representations
- Computer programs
- Electronic material
- Any other original work

Authorship Policies

Global Journals follows the definition of authorship set up by the Open Association of Research Society, USA. According to its guidelines, authorship criteria must be based on:

1. Substantial contributions to the conception and acquisition of data, analysis, and interpretation of findings.
2. Drafting the paper and revising it critically regarding important academic content.
3. Final approval of the version of the paper to be published.

Changes in Authorship

The corresponding author should mention the name and complete details of all co-authors during submission and in manuscript. We support addition, rearrangement, manipulation, and deletions in authors list till the early view publication of the journal. We expect that corresponding author will notify all co-authors of submission. We follow COPE guidelines for changes in authorship.

Copyright

During submission of the manuscript, the author is confirming an exclusive license agreement with Global Journals which gives Global Journals the authority to reproduce, reuse, and republish authors' research. We also believe in flexible copyright terms where copyright may remain with authors/employers/institutions as well. Contact your editor after acceptance to choose your copyright policy. You may follow this form for copyright transfers.

Appealing Decisions

Unless specified in the notification, the Editorial Board's decision on publication of the paper is final and cannot be appealed before making the major change in the manuscript.

Acknowledgments

Contributors to the research other than authors credited should be mentioned in Acknowledgments. The source of funding for the research can be included. Suppliers of resources may be mentioned along with their addresses.

Declaration of funding sources

Global Journals is in partnership with various universities, laboratories, and other institutions worldwide in the research domain. Authors are requested to disclose their source of funding during every stage of their research, such as making analysis, performing laboratory operations, computing data, and using institutional resources, from writing an article to its submission. This will also help authors to get reimbursements by requesting an open access publication letter from Global Journals and submitting to the respective funding source.

Preparing your Manuscript

Authors can submit papers and articles in an acceptable file format: MS Word (doc, docx), LaTeX (.tex, .zip or .rar including all of your files), Adobe PDF (.pdf), rich text format (.rtf), simple text document (.txt), Open Document Text (.odt), and Apple Pages (.pages). Our professional layout editors will format the entire paper according to our official guidelines. This is one of the highlights of publishing with Global Journals—authors should not be concerned about the formatting of their paper. Global Journals accepts articles and manuscripts in every major language, be it Spanish, Chinese, Japanese, Portuguese, Russian, French, German, Dutch, Italian, Greek, or any other national language, but the title, subtitle, and abstract should be in English. This will facilitate indexing and the pre-peer review process.

The following is the official style and template developed for publication of a research paper. Authors are not required to follow this style during the submission of the paper. It is just for reference purposes.

Manuscript Style Instruction (Optional)

- Microsoft Word Document Setting Instructions.
- Font type of all text should be Swis721 Lt BT.
- Page size: 8.27" x 11'", left margin: 0.65, right margin: 0.65, bottom margin: 0.75.
- Paper title should be in one column of font size 24.
- Author name in font size of 11 in one column.
- Abstract: font size 9 with the word "Abstract" in bold italics.
- Main text: font size 10 with two justified columns.
- Two columns with equal column width of 3.38 and spacing of 0.2.
- First character must be three lines drop-capped.
- The paragraph before spacing of 1 pt and after of 0 pt.
- Line spacing of 1 pt.
- Large images must be in one column.
- The names of first main headings (Heading 1) must be in Roman font, capital letters, and font size of 10.
- The names of second main headings (Heading 2) must not include numbers and must be in italics with a font size of 10.

Structure and Format of Manuscript

The recommended size of an original research paper is under 15,000 words and review papers under 7,000 words. Research articles should be less than 10,000 words. Research papers are usually longer than review papers. Review papers are reports of significant research (typically less than 7,000 words, including tables, figures, and references)

A research paper must include:

a) A title which should be relevant to the theme of the paper.
b) A summary, known as an abstract (less than 150 words), containing the major results and conclusions.
c) Up to 10 keywords that precisely identify the paper's subject, purpose, and focus.
d) An introduction, giving fundamental background objectives.
e) Resources and techniques with sufficient complete experimental details (wherever possible by reference) to permit repetition, sources of information must be given, and numerical methods must be specified by reference.
f) Results which should be presented concisely by well-designed tables and figures.
g) Suitable statistical data should also be given.
h) All data must have been gathered with attention to numerical detail in the planning stage.

Design has been recognized to be essential to experiments for a considerable time, and the editor has decided that any paper that appears not to have adequate numerical treatments of the data will be returned unrefereed.

i) Discussion should cover implications and consequences and not just recapitulate the results; conclusions should also be summarized.
j) There should be brief acknowledgments.
k) There ought to be references in the conventional format. Global Journals recommends APA format.

Authors should carefully consider the preparation of papers to ensure that they communicate effectively. Papers are much more likely to be accepted if they are carefully designed and laid out, contain few or no errors, are summarizing, and follow instructions. They will also be published with much fewer delays than those that require much technical and editorial correction.

The Editorial Board reserves the right to make literary corrections and suggestions to improve brevity.

Format Structure

It is necessary that authors take care in submitting a manuscript that is written in simple language and adheres to published guidelines.

All manuscripts submitted to Global Journals should include:

Title

The title page must carry an informative title that reflects the content, a running title (less than 45 characters together with spaces), names of the authors and co-authors, and the place(s) where the work was carried out.

Author details

The full postal address of any related author(s) must be specified.

Abstract

The abstract is the foundation of the research paper. It should be clear and concise and must contain the objective of the paper and inferences drawn. It is advised to not include big mathematical equations or complicated jargon.

Many researchers searching for information online will use search engines such as Google, Yahoo or others. By optimizing your paper for search engines, you will amplify the chance of someone finding it. In turn, this will make it more likely to be viewed and cited in further works. Global Journals has compiled these guidelines to facilitate you to maximize the web-friendliness of the most public part of your paper.

Keywords

A major lynchpin of research work for the writing of research papers is the keyword search, which one will employ to find both library and internet resources. Up to eleven keywords or very brief phrases have to be given to help data retrieval, mining, and indexing.

One must be persistent and creative in using keywords. An effective keyword search requires a strategy: planning of a list of possible keywords and phrases to try.

Choice of the main keywords is the first tool of writing a research paper. Research paper writing is an art. Keyword search should be as strategic as possible.

One should start brainstorming lists of potential keywords before even beginning searching. Think about the most important concepts related to research work. Ask, "What words would a source have to include to be truly valuable in a research paper?" Then consider synonyms for the important words.

It may take the discovery of only one important paper to steer in the right keyword direction because, in most databases, the keywords under which a research paper is abstracted are listed with the paper.

Numerical Methods

Numerical methods used should be transparent and, where appropriate, supported by references.

Abbreviations

Authors must list all the abbreviations used in the paper at the end of the paper or in a separate table before using them.

Formulas and equations

Authors are advised to submit any mathematical equation using either MathJax, KaTeX, or LaTeX, or in a very high-quality image.

Tables, Figures, and Figure Legends

Tables: Tables should be cautiously designed, uncrowned, and include only essential data. Each must have an Arabic number, e.g., Table 4, a self-explanatory caption, and be on a separate sheet. Authors must submit tables in an editable format and not as images. References to these tables (if any) must be mentioned accurately.

Figures

Figures are supposed to be submitted as separate files. Always include a citation in the text for each figure using Arabic numbers, e.g., Fig. 4. Artwork must be submitted online in vector electronic form or by emailing it.

Preparation of Eletronic Figures for Publication

Although low-quality images are sufficient for review purposes, print publication requires high-quality images to prevent the final product being blurred or fuzzy. Submit (possibly by e-mail) EPS (line art) or TIFF (halftone/ photographs) files only. MS PowerPoint and Word Graphics are unsuitable for printed pictures. Avoid using pixel-oriented software. Scans (TIFF only) should have a resolution of at least 350 dpi (halftone) or 700 to 1100 dpi (line drawings). Please give the data for figures in black and white or submit a Color Work Agreement form. EPS files must be saved with fonts embedded (and with a TIFF preview, if possible).

For scanned images, the scanning resolution at final image size ought to be as follows to ensure good reproduction: line art: >650 dpi; halftones (including gel photographs): >350 dpi; figures containing both halftone and line images: >650 dpi.

Color charges: Authors are advised to pay the full cost for the reproduction of their color artwork. Hence, please note that if there is color artwork in your manuscript when it is accepted for publication, we would require you to complete and return a Color Work Agreement form before your paper can be published. Also, you can email your editor to remove the color fee after acceptance of the paper.

Tips for Writing a Good Quality Engineering Research Paper

Techniques for writing a good quality engineering research paper:

1. Choosing the topic: In most cases, the topic is selected by the interests of the author, but it can also be suggested by the guides. You can have several topics, and then judge which you are most comfortable with. This may be done by asking several questions of yourself, like "Will I be able to carry out a search in this area? Will I find all necessary resources to accomplish the search? Will I be able to find all information in this field area?" If the answer to this type of question is "yes," then you ought to choose that topic. In most cases, you may have to conduct surveys and visit several places. Also, you might have to do a lot of work to find all the rises and falls of the various data on that subject. Sometimes, detailed information plays a vital role, instead of short information. Evaluators are human: The first thing to remember is that evaluators are also human beings. They are not only meant for rejecting a paper. They are here to evaluate your paper. So present your best aspect.

2. Think like evaluators: If you are in confusion or getting demotivated because your paper may not be accepted by the evaluators, then think, and try to evaluate your paper like an evaluator. Try to understand what an evaluator wants in your research paper, and you will automatically have your answer. Make blueprints of paper: The outline is the plan or framework that will help you to arrange your thoughts. It will make your paper logical. But remember that all points of your outline must be related to the topic you have chosen.

3. Ask your guides: If you are having any difficulty with your research, then do not hesitate to share your difficulty with your guide (if you have one). They will surely help you out and resolve your doubts. If you can't clarify what exactly you require for your work, then ask your supervisor to help you with an alternative. He or she might also provide you with a list of essential readings.

4. Use of computer is recommended: As you are doing research in the field of research engineering then this point is quite obvious. Use right software: Always use good quality software packages. If you are not capable of judging good software, then you can lose the quality of your paper unknowingly. There are various programs available to help you which you can get through the internet.

5. Use the internet for help: An excellent start for your paper is using Google. It is a wondrous search engine, where you can have your doubts resolved. You may also read some answers for the frequent question of how to write your research paper or find a model research paper. You can download books from the internet. If you have all the required books, place importance on reading, selecting, and analyzing the specified information. Then sketch out your research paper. Use big pictures: You may use encyclopedias like Wikipedia to get pictures with the best resolution. At Global Journals, you should strictly follow here.

6. Bookmarks are useful: When you read any book or magazine, you generally use bookmarks, right? It is a good habit which helps to not lose your continuity. You should always use bookmarks while searching on the internet also, which will make your search easier.

7. Revise what you wrote: When you write anything, always read it, summarize it, and then finalize it.

8. Make every effort: Make every effort to mention what you are going to write in your paper. That means always have a good start. Try to mention everything in the introduction—what is the need for a particular research paper. Polish your work with good writing skills and always give an evaluator what he wants. Make backups: When you are going to do any important thing like making a research paper, you should always have backup copies of it either on your computer or on paper. This protects you from losing any portion of your important data.

9. Produce good diagrams of your own: Always try to include good charts or diagrams in your paper to improve quality. Using several unnecessary diagrams will degrade the quality of your paper by creating a hodgepodge. So always try to include diagrams which were made by you to improve the readability of your paper. Use of direct quotes: When you do research relevant to literature, history, or current affairs, then use of quotes becomes essential, but if the study is relevant to science, use of quotes is not preferable.

10. Use proper verb tense: Use proper verb tenses in your paper. Use past tense to present those events that have happened. Use present tense to indicate events that are going on. Use future tense to indicate events that will happen in the future. Use of wrong tenses will confuse the evaluator. Avoid sentences that are incomplete.

11. Pick a good study spot: Always try to pick a spot for your research which is quiet. Not every spot is good for studying.

12. Know what you know: Always try to know what you know by making objectives, otherwise you will be confused and unable to achieve your target.

13. Use good grammar: Always use good grammar and words that will have a positive impact on the evaluator; use of good vocabulary does not mean using tough words which the evaluator has to find in a dictionary. Do not fragment sentences. Eliminate one-word sentences. Do not ever use a big word when a smaller one would suffice.

Verbs have to be in agreement with their subjects. In a research paper, do not start sentences with conjunctions or finish them with prepositions. When writing formally, it is advisable to never split an infinitive because someone will (wrongly) complain. Avoid clichés like a disease. Always shun irritating alliteration. Use language which is simple and straightforward. Put together a neat summary.

14. Arrangement of information: Each section of the main body should start with an opening sentence, and there should be a changeover at the end of the section. Give only valid and powerful arguments for your topic. You may also maintain your arguments with records.

15. Never start at the last minute: Always allow enough time for research work. Leaving everything to the last minute will degrade your paper and spoil your work.

16. Multitasking in research is not good: Doing several things at the same time is a bad habit in the case of research activity. Research is an area where everything has a particular time slot. Divide your research work into parts, and do a particular part in a particular time slot.

17. Never copy others' work: Never copy others' work and give it your name because if the evaluator has seen it anywhere, you will be in trouble. Take proper rest and food: No matter how many hours you spend on your research activity, if you are not taking care of your health, then all your efforts will have been in vain. For quality research, take proper rest and food.

18. Go to seminars: Attend seminars if the topic is relevant to your research area. Utilize all your resources.

19. Refresh your mind after intervals: Try to give your mind a rest by listening to soft music or sleeping in intervals. This will also improve your memory. Acquire colleagues: Always try to acquire colleagues. No matter how sharp you are, if you acquire colleagues, they can give you ideas which will be helpful to your research.

20. Think technically: Always think technically. If anything happens, search for its reasons, benefits, and demerits. Think and then print: When you go to print your paper, check that tables are not split, headings are not detached from their descriptions, and page sequence is maintained.

21. Adding unnecessary information: Do not add unnecessary information like "I have used MS Excel to draw graphs." Irrelevant and inappropriate material is superfluous. Foreign terminology and phrases are not apropos. One should never take a broad view. Analogy is like feathers on a snake. Use words properly, regardless of how others use them. Remove quotations. Puns are for kids, not grunt readers. Never oversimplify: When adding material to your research paper, never go for oversimplification; this will definitely irritate the evaluator. Be specific. Never use rhythmic redundancies. Contractions shouldn't be used in a research paper. Comparisons are as terrible as clichés. Give up ampersands, abbreviations, and so on. Remove commas that are not necessary. Parenthetical words should be between brackets or commas. Understatement is always the best way to put forward earth-shaking thoughts. Give a detailed literary review.
22. Report concluded results: Use concluded results. From raw data, filter the results, and then conclude your studies based on measurements and observations taken. An appropriate number of decimal places should be used. Parenthetical remarks are prohibited here. Proofread carefully at the final stage. At the end, give an outline to your arguments. Spot perspectives of further study of the subject. Justify your conclusion at the bottom sufficiently, which will probably include examples.
23. Upon conclusion: Once you have concluded your research, the next most important step is to present your findings. Presentation is extremely important as it is the definite medium though which your research is going to be in print for the rest of the crowd. Care should be taken to categorize your thoughts well and present them in a logical and neat manner. A good quality research paper format is essential because it serves to highlight your research paper and bring to light all necessary aspects of your research.

Informal Guidelines of Research Paper Writing

Key points to remember:

- Submit all work in its final form.
- Write your paper in the form which is presented in the guidelines using the template.
- Please note the criteria peer reviewers will use for grading the final paper.

Final points:

One purpose of organizing a research paper is to let people interpret your efforts selectively. The journal requires the following sections, submitted in the order listed, with each section starting on a new page:

The introduction: This will be compiled from reference matter and reflect the design processes or outline of basis that directed you to make a study. As you carry out the process of study, the method and process section will be constructed like that. The results segment will show related statistics in nearly sequential order and direct reviewers to similar intellectual paths throughout the data that you gathered to carry out your study.

The discussion section:

This will provide understanding of the data and projections as to the implications of the results. The use of good quality references throughout the paper will give the effort trustworthiness by representing an alertness to prior workings.

Writing a research paper is not an easy job, no matter how trouble-free the actual research or concept. Practice, excellent preparation, and controlled record-keeping are the only means to make straightforward progression.

General style:

Specific editorial column necessities for compliance of a manuscript will always take over from directions in these general guidelines.

To make a paper clear: Adhere to recommended page limits.

Mistakes to avoid:

- Insertion of a title at the foot of a page with subsequent text on the next page.
- Separating a table, chart, or figure—confine each to a single page.
- Submitting a manuscript with pages out of sequence.
- In every section of your document, use standard writing style, including articles ("a" and "the").
- Keep paying attention to the topic of the paper.

- Use paragraphs to split each significant point (excluding the abstract).
- Align the primary line of each section.
- Present your points in sound order.
- Use present tense to report well-accepted matters.
- Use past tense to describe specific results.
- Do not use familiar wording; don't address the reviewer directly. Don't use slang or superlatives.
- Avoid use of extra pictures—include only those figures essential to presenting results.

Title page:

Choose a revealing title. It should be short and include the name(s) and address(es) of all authors. It should not have acronyms or abbreviations or exceed two printed lines.

Abstract: This summary should be two hundred words or less. It should clearly and briefly explain the key findings reported in the manuscript and must have precise statistics. It should not have acronyms or abbreviations. It should be logical in itself. Do not cite references at this point.

An abstract is a brief, distinct paragraph summary of finished work or work in development. In a minute or less, a reviewer can be taught the foundation behind the study, common approaches to the problem, relevant results, and significant conclusions or new questions.

Write your summary when your paper is completed because how can you write the summary of anything which is not yet written? Wealth of terminology is very essential in abstract. Use comprehensive sentences, and do not sacrifice readability for brevity; you can maintain it succinctly by phrasing sentences so that they provide more than a lone rationale. The author can at this moment go straight to shortening the outcome. Sum up the study with the subsequent elements in any summary. Try to limit the initial two items to no more than one line each.

Reason for writing the article—theory, overall issue, purpose.

- Fundamental goal.
- To-the-point depiction of the research.
- Consequences, including definite statistics—if the consequences are quantitative in nature, account for this; results of any numerical analysis should be reported. Significant conclusions or questions that emerge from the research.

Approach:

- o Single section and succinct.
- o An outline of the job done is always written in past tense.
- o Concentrate on shortening results—limit background information to a verdict or two.
- o Exact spelling, clarity of sentences and phrases, and appropriate reporting of quantities (proper units, important statistics) are just as significant in an abstract as they are anywhere else.

Introduction:

The introduction should "introduce" the manuscript. The reviewer should be presented with sufficient background information to be capable of comprehending and calculating the purpose of your study without having to refer to other works. The basis for the study should be offered. Give the most important references, but avoid making a comprehensive appraisal of the topic. Describe the problem visibly. If the problem is not acknowledged in a logical, reasonable way, the reviewer will give no attention to your results. Speak in common terms about techniques used to explain the problem, if needed, but do not present any particulars about the protocols here.

The following approach can create a valuable beginning:

- o Explain the value (significance) of the study.
- o Defend the model—why did you employ this particular system or method? What is its compensation? Remark upon its appropriateness from an abstract point of view as well as pointing out sensible reasons for using it.
- o Present a justification. State your particular theory(-ies) or aim(s), and describe the logic that led you to choose them.
- o Briefly explain the study's tentative purpose and how it meets the declared objectives.

Approach:

Use past tense except for when referring to recognized facts. After all, the manuscript will be submitted after the entire job is done. Sort out your thoughts; manufacture one key point for every section. If you make the four points listed above, you will need at least four paragraphs. Present surrounding information only when it is necessary to support a situation. The reviewer does not desire to read everything you know about a topic. Shape the theory specifically—do not take a broad view.

As always, give awareness to spelling, simplicity, and correctness of sentences and phrases.

Procedures (methods and materials):

This part is supposed to be the easiest to carve if you have good skills. A soundly written procedures segment allows a capable scientist to replicate your results. Present precise information about your supplies. The suppliers and clarity of reagents can be helpful bits of information. Present methods in sequential order, but linked methodologies can be grouped as a segment. Be concise when relating the protocols. Attempt to give the least amount of information that would permit another capable scientist to replicate your outcome, but be cautious that vital information is integrated. The use of subheadings is suggested and ought to be synchronized with the results section.

When a technique is used that has been well-described in another section, mention the specific item describing the way, but draw the basic principle while stating the situation. The purpose is to show all particular resources and broad procedures so that another person may use some or all of the methods in one more study or referee the scientific value of your work. It is not to be a step-by-step report of the whole thing you did, nor is a methods section a set of orders.

Materials:

Materials may be reported in part of a section or else they may be recognized along with your measures.

Methods:

- Report the method and not the particulars of each process that engaged the same methodology.
- Describe the method entirely.
- To be succinct, present methods under headings dedicated to specific dealings or groups of measures.
- Simplify—detail how procedures were completed, not how they were performed on a particular day.
- If well-known procedures were used, account for the procedure by name, possibly with a reference, and that's all.

Approach:

It is embarrassing to use vigorous voice when documenting methods without using first person, which would focus the reviewer's interest on the researcher rather than the job. As a result, when writing up the methods, most authors use third person passive voice.

Use standard style in this and every other part of the paper—avoid familiar lists, and use full sentences.

What to keep away from:

- Resources and methods are not a set of information.
- Skip all descriptive information and surroundings—save it for the argument.
- Leave out information that is immaterial to a third party.

Results:

The principle of a results segment is to present and demonstrate your conclusion. Create this part as entirely objective details of the outcome, and save all understanding for the discussion.

The page length of this segment is set by the sum and types of data to be reported. Use statistics and tables, if suitable, to present consequences most efficiently.

You must clearly differentiate material which would usually be incorporated in a study editorial from any unprocessed data or additional appendix matter that would not be available. In fact, such matters should not be submitted at all except if requested by the instructor.

Content:

- Sum up your conclusions in text and demonstrate them, if suitable, with figures and tables.
- In the manuscript, explain each of your consequences, and point the reader to remarks that are most appropriate.
- Present a background, such as by describing the question that was addressed by creation of an exacting study.
- Explain results of control experiments and give remarks that are not accessible in a prescribed figure or table, if appropriate.
- Examine your data, then prepare the analyzed (transformed) data in the form of a figure (graph), table, or manuscript.

What to stay away from:

- Do not discuss or infer your outcome, report surrounding information, or try to explain anything.
- Do not include raw data or intermediate calculations in a research manuscript.
- Do not present similar data more than once.
- A manuscript should complement any figures or tables, not duplicate information.
- Never confuse figures with tables—there is a difference.

Approach:

As always, use past tense when you submit your results, and put the whole thing in a reasonable order.

Put figures and tables, appropriately numbered, in order at the end of the report.

If you desire, you may place your figures and tables properly within the text of your results section.

Figures and tables:

If you put figures and tables at the end of some details, make certain that they are visibly distinguished from any attached appendix materials, such as raw facts. Whatever the position, each table must be titled, numbered one after the other, and include a heading. All figures and tables must be divided from the text.

Discussion:

The discussion is expected to be the trickiest segment to write. A lot of papers submitted to the journal are discarded based on problems with the discussion. There is no rule for how long an argument should be.

Position your understanding of the outcome visibly to lead the reviewer through your conclusions, and then finish the paper with a summing up of the implications of the study. The purpose here is to offer an understanding of your results and support all of your conclusions, using facts from your research and generally accepted information, if suitable. The implication of results should be fully described.

Infer your data in the conversation in suitable depth. This means that when you clarify an observable fact, you must explain mechanisms that may account for the observation. If your results vary from your prospect, make clear why that may have happened. If your results agree, then explain the theory that the proof supported. It is never suitable to just state that the data approved the prospect, and let it drop at that. Make a decision as to whether each premise is supported or discarded or if you cannot make a conclusion with assurance. Do not just dismiss a study or part of a study as "uncertain."

Research papers are not acknowledged if the work is imperfect. Draw what conclusions you can based upon the results that you have, and take care of the study as a finished work.

- You may propose future guidelines, such as how an experiment might be personalized to accomplish a new idea.
- Give details of all of your remarks as much as possible, focusing on mechanisms.
- Make a decision as to whether the tentative design sufficiently addressed the theory and whether or not it was correctly restricted. Try to present substitute explanations if they are sensible alternatives.
- One piece of research will not counter an overall question, so maintain the large picture in mind. Where do you go next? The best studies unlock new avenues of study. What questions remain?
- Recommendations for detailed papers will offer supplementary suggestions.

Approach:

When you refer to information, differentiate data generated by your own studies from other available information. Present work done by specific persons (including you) in past tense.

Describe generally acknowledged facts and main beliefs in present tense.

The Administration Rules

Administration Rules to Be Strictly Followed before Submitting Your Research Paper to Global Journals Inc.

Please read the following rules and regulations carefully before submitting your research paper to Global Journals Inc. to avoid rejection.

Segment draft and final research paper: You have to strictly follow the template of a research paper, failing which your paper may get rejected. You are expected to write each part of the paper wholly on your own. The peer reviewers need to identify your own perspective of the concepts in your own terms. Please do not extract straight from any other source, and do not rephrase someone else's analysis. Do not allow anyone else to proofread your manuscript.

Written material: You may discuss this with your guides and key sources. Do not copy anyone else's paper, even if this is only imitation, otherwise it will be rejected on the grounds of plagiarism, which is illegal. Various methods to avoid plagiarism are strictly applied by us to every paper, and, if found guilty, you may be blacklisted, which could affect your career adversely. To guard yourself and others from possible illegal use, please do not permit anyone to use or even read your paper and file.

Criterion for Grading a Research Paper (Compilation) by Global Journals

Please note that following table is only a Grading of "Paper Compilation" and not on "Performed/Stated Research" whose grading solely depends on Individual Assigned Peer Reviewer and Editorial Board Member. These can be available only on request and after decision of Paper. This report will be the property of Global Journals.

Topics	Grades		
	A-B	**C-D**	**E-F**
Abstract	Clear and concise with appropriate content, Correct format. 200 words or below	Unclear summary and no specific data, Incorrect form Above 200 words	No specific data with ambiguous information Above 250 words
Introduction	Containing all background details with clear goal and appropriate details, flow specification, no grammar and spelling mistake, well organized sentence and paragraph, reference cited	Unclear and confusing data, appropriate format, grammar and spelling errors with unorganized matter	Out of place depth and content, hazy format
Methods and Procedures	Clear and to the point with well arranged paragraph, precision and accuracy of facts and figures, well organized subheads	Difficult to comprehend with embarrassed text, too much explanation but completed	Incorrect and unorganized structure with hazy meaning
Result	Well organized, Clear and specific, Correct units with precision, correct data, well structuring of paragraph, no grammar and spelling mistake	Complete and embarrassed text, difficult to comprehend	Irregular format with wrong facts and figures
Discussion	Well organized, meaningful specification, sound conclusion, logical and concise explanation, highly structured paragraph reference cited	Wordy, unclear conclusion, spurious	Conclusion is not cited, unorganized, difficult to comprehend
References	Complete and correct format, well organized	Beside the point, Incomplete	Wrong format and structuring

Index

A

Acceleration · 1, 4
Afforestation · 20
Aforementioned · 24

C

Colloidal · 23
Consequences · 8, 19

E

Elaborated · 17
Embolization · 25
Epirubicin · 24, 25

M

Mitoxantrone · 25

N

Nanoparticles · 22, 27, 28, 29

O

Obtained · 13, 17, 27

R

Radionuclides · 25

S

Savannah · 8, 12, 13, 17, 19, 20
Sedimentation · 8, 9, 20, 22
Superparamagnetic · 23

save our planet

Global Journal of Researches in Engineering

Visit us on the Web at www.GlobalJournals.org | www.EngineeringResearch.org
or email us at helpdesk@globaljournals.org

ISSN 9755861